

EUROPEAN ORGANISATION FOR NUCLEAR RESEARCH (CERN)



JHEP 04 (2019) 046

DOI: [DOI:10.1007/JHEP04\(2019\)046](https://doi.org/10.1007/JHEP04(2019)046)



CERN-EP-2018-276

17th April 2019

Measurements of inclusive and differential fiducial cross-sections of $t\bar{t}$ production with additional heavy-flavour jets in proton–proton collisions at $\sqrt{s} = 13$ TeV with the ATLAS detector

The ATLAS Collaboration

This paper presents measurements of $t\bar{t}$ production in association with additional b -jets in pp collisions at the LHC at a centre-of-mass energy of 13 TeV. The data were recorded with the ATLAS detector and correspond to an integrated luminosity of 36.1 fb^{-1} . Fiducial cross-section measurements are performed in the dilepton and lepton-plus-jets $t\bar{t}$ decay channels. Results are presented at particle level in the form of inclusive cross-sections of $t\bar{t}$ final states with three and four b -jets as well as differential cross-sections as a function of global event properties and properties of b -jet pairs. The measured inclusive fiducial cross-sections generally exceed the $t\bar{t}b\bar{b}$ predictions from various next-to-leading-order matrix element calculations matched to a parton shower but are compatible within the total uncertainties. The experimental uncertainties are smaller than the uncertainties in the predictions. Comparisons of state-of-the-art theoretical predictions with the differential measurements are shown and good agreement with data is found for most of them.

Contents

1	Introduction	2
2	ATLAS detector	5
3	Monte Carlo simulation	5
4	Object reconstruction and identification	9
4.1	Detector-level object reconstruction	9
4.2	Particle-level object definitions	10
5	Event selection and definition of the fiducial phase space	10
5.1	Data event selection	10
5.2	Fiducial phase-space definition	11
6	Background estimation	11
6.1	Background from single-top, Z/γ^* + jets and $W+$ jets events	12
6.2	Background from non-prompt and fake leptons	12
6.3	Data and prediction comparison of baseline selection	15
7	Extraction of the fiducial cross-sections	15
7.1	Data-driven correction factors for flavour composition of additional jets in $t\bar{t}$ events	15
7.2	Unfolding	17
8	Systematic uncertainties	20
8.1	Experimental uncertainties	20
8.2	Modelling systematic uncertainties	21
8.3	Uncertainty in $t\bar{t}c$ and $t\bar{t}l$ background	22
8.4	Uncertainty in non- $t\bar{t}$ background estimation	22
8.5	Propagation of uncertainties	23
9	Inclusive and differential fiducial cross-section results	23
10	Summary	34

1 Introduction

Measurements of the production cross-section of top-antitop quark pairs ($t\bar{t}$) with additional jets provide important tests of quantum chromodynamics (QCD) predictions. Among these, the process of $t\bar{t}$ produced in association with jets originating from b -quarks (b -jets) is particularly important to measure, as there are many uncertainties in the calculation of the process. For example, calculating the amplitude for the process shown in Figure 1(a) is a challenge due to the non-negligible mass of the b -quark. It is therefore important to compare the predictions with both inclusive and differential experimental cross-section measurements of $t\bar{t}$ production with additional b -jets. State-of-the-art QCD calculations give predictions for the $t\bar{t}$ production cross-section with up to two additional massless partons at next-to-leading order (NLO) in perturbation theory matched to a parton shower [1], and the QCD production of $t\bar{t}bb$ is calculated at NLO matched to a

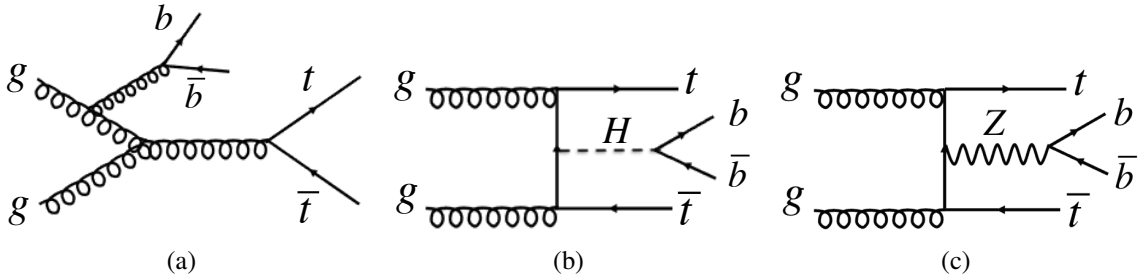


Figure 1: Example Feynman diagrams of processes leading to a $t\bar{t}b\bar{b}$ final state, including (a) QCD $t\bar{t}b\bar{b}$ production, (b) $t\bar{t}H(H \rightarrow b\bar{b})$, and (c) $t\bar{t}Z(Z \rightarrow b\bar{b})$.

parton shower [2–5].

Moreover, since the discovery of the Higgs boson [6, 7], the determination of the Higgs coupling to the heaviest elementary particle, the top quark, is a crucial test of the Standard Model (SM). Direct measurements of the top-quark Yukawa coupling are performed in events where a Higgs boson is produced in association with a top-quark pair ($t\bar{t}H$) [8, 9]. The Higgs branching ratios are dominated by the $H \rightarrow b\bar{b}$ decay [10, 11], and therefore the $t\bar{t}H$ process can be measured with the best statistical precision using events where the Higgs boson decays in this manner, leading to a $t\bar{t}b\bar{b}$ final state as shown in Figure 1(b). However, this channel suffers from a large background from QCD $t\bar{t}b\bar{b}$ production indicated in Figure 1(a) [12, 13].

Measurements of $t\bar{t}H(H \rightarrow b\bar{b})$ would benefit from a better understanding of the QCD production of $t\bar{t}b\bar{b}$ as predicted by the SM and, in particular, improved Monte Carlo (MC) modelling. The measurements presented in this paper were chosen in order to provide data needed to improve the QCD MC modelling of the $t\bar{t}b\bar{b}$ process. The differential observables are particularly interesting as they are sensitive to the relative contribution of events from $t\bar{t}$ -associated Higgs production ($t\bar{t}H$) with $H \rightarrow b\bar{b}$ decays to QCD-produced $t\bar{t}b\bar{b}$ events in various phase space regions. Even though the aim is to improve the modelling of QCD production of additional b -jets in $t\bar{t}$ events, this analysis measures their production without separating the different production channels such as $t\bar{t}H$ or $t\bar{t}$ in association with a vector boson ($t\bar{t}V$), for example the $t\bar{t}Z$ process shown in Figure 1(c).

In this paper, measurements of fiducial cross-sections are presented using data recorded by the ATLAS detector during 2015 and 2016 in proton–proton (pp) collisions at a centre-of-mass energy $\sqrt{s} = 13$ TeV, corresponding to a total integrated luminosity of 36.1 fb^{-1} . In addition, differential measurements at this centre-of-mass energy are presented as a function of various observables. Previous measurements of $t\bar{t}$ production with additional heavy-flavour jets have been reported by ATLAS at $\sqrt{s} = 7$ TeV [14] and both CMS and ATLAS at $\sqrt{s} = 8$ TeV [15–17]. CMS has also reported a measurement of the inclusive $t\bar{t}b\bar{b}$ cross-section using 2.3 fb^{-1} at $\sqrt{s} = 13$ TeV [18].

Since the top quark decays into a b -quark and W boson nearly 100% of the time, $t\bar{t}$ events are typically classified according to how the two W bosons decay. In this analysis, two channels are considered: the $e\mu$ channel, in which both W bosons decay leptonically, one into a muon and muon neutrino and the other into an electron and electron neutrino, and the lepton-plus-jets channel (lepton + jets), in which one W boson decays into an isolated charged lepton (an electron or muon) and corresponding neutrino and the other W boson decays into a pair of quarks. Electrons and muons produced either directly in the decay of the W boson or via an intermediate τ -lepton are included in both channels.

The decay of a top-quark pair results in two b -quarks and therefore a final state which includes the

production of two additional b -quarks may contain up to four b -jets. The inclusive fiducial cross-sections are presented for events with at least three b -jets and for events with at least four b -jets. The differential cross-sections are presented for events with at least three b -jets in the $e\mu$ channel and with at least four b -jets in the lepton + jets channel. The results are obtained as a function of the transverse momentum (p_T)¹ of each of the b -jets, the scalar sum of the p_T of the lepton(s) and jets in the events (H_T) and of only jets in the events (H_T^{had}) and as a function of the b -jet multiplicity ($N_{b\text{-jets}}$).

This analysis does not attempt to identify the origin of the b -jets, i.e. it does not distinguish between additional b -jets and b -jets that come from the top-quark decays. This is to avoid using simulation-based information to attribute b -jets to a particular production process, which would lead to significant modelling uncertainties. Instead, differential cross-sections are measured as a function of kinematic distributions of pairs of b -jets. The reported distributions could be used to distinguish the contribution of specific production mechanisms: the pair made from the two b -jets closest in angular distance is expected to be formed by b -jets from gluon splitting and the pair made from the two highest- p_T b -jets is expected to be dominated by top-pair production. For each of these pairs, the distributions are measured for the angular separation between the b -jets ($\Delta R(b, b)$), the invariant mass (m_{bb}) and transverse momentum ($p_{T,bb}$). It should be noted that for events with at least three b -jets, it is likely that one of the two closest b -jets originates from the top quark. Hence the simple picture that the two closest b -jets are usually from gluon splitting may not apply. However, ΔR , m_{bb} and $p_{T,bb}$ are used for reconstruction of the final state in analyses with multiple b -jets and therefore probing the modelling of these observables is important.

The cross-sections are obtained by subtracting the estimated number of non- $t\bar{t}$ background events from the data distributions. At detector level, jets are identified as containing b -hadrons (“ b -tagging”) by a multivariate algorithm [19]. The $t\bar{t}$ background resulting from additional light-flavour and charm-quark jets wrongly identified as b -jets is evaluated using a template fit, in which the templates are constructed from the output discriminant of the b -tagging algorithm. The background-subtracted distributions are corrected for acceptance and detector effects using an unfolding technique that includes corrections for the $t\bar{t}$ -related backgrounds.

This paper is laid out as follows. The experimental set-up for the collected data is described in Section 2. Details of the simulation used in this analysis are provided in Section 3. The reconstruction and identification of leptons and jets, the b -tagging of jets at detector level, and the definitions of objects at particle level are described in Section 4. The selection of reconstructed events and the definition of the fiducial phase space are given in Section 5. Estimation of the background from non- $t\bar{t}$ processes is described in Section 6. The method to estimate the $t\bar{t}$ background with additional jets misidentified as b -jets and the unfolding procedure to correct the data to particle level for fiducial cross-section measurements are explained in Section 7. Sources of systematic uncertainties and their propagation to the measured cross-sections are described in Section 8. The measured inclusive and normalised differential fiducial cross-sections and the comparison with various theoretical predictions are presented in Section 9. Finally, the results are summarised in Section 10.

¹ ATLAS uses a right-handed coordinate system with its origin at the nominal interaction point (IP) in the centre of the detector and the z -axis along the beam pipe. The x -axis points from the IP to the centre of the LHC ring, and the y -axis points upward. Cylindrical coordinates (r, ϕ) are used in the transverse plane, ϕ being the azimuthal angle around the z -axis. The pseudorapidity is defined in terms of the polar angle θ as $\eta = -\ln \tan(\theta/2)$. The angular separation between two points in η and ϕ is defined as $\Delta R = \sqrt{(\Delta\eta)^2 + (\Delta\phi)^2}$.

2 ATLAS detector

The ATLAS detector [20] at the LHC covers nearly the entire solid angle around the collision point. It consists of an inner-tracking detector surrounded by a thin superconducting solenoid, electromagnetic and hadronic calorimeters, and a muon spectrometer incorporating three large superconducting toroidal magnets.

The inner detector (ID) system is immersed in a 2 T axial magnetic field and provides charged-particle tracking in the pseudorapidity range $|\eta| < 2.5$. The ID is composed of silicon detectors and the transition radiation tracker. The high-granularity silicon pixel detector covers the interaction region and is followed by the silicon microstrip tracker. The innermost silicon pixel layer, added to the inner detector before the start of Run-2 data taking [21, 22], improves the identification of b -jets. The tracking capabilities of the silicon detectors are augmented by the transition radiation tracker, which is located at a larger radius and enables track reconstruction up to $|\eta| = 2.0$. It also provides signals used to separate electrons from pions.

The calorimeter system covers the range $|\eta| < 4.9$. Within the region $|\eta| < 3.2$, electromagnetic calorimetry is provided by barrel and endcap high-granularity lead/liquid-argon (LAr) electromagnetic calorimeters, with an additional thin LAr presampler covering $|\eta| < 1.8$ to correct for energy loss in material upstream of the calorimeters. Hadronic calorimetry is provided by the steel/scintillating-tile calorimeter, segmented into three barrel structures within $|\eta| < 1.7$, and two copper/LAr hadronic endcap calorimeters. The solid angle coverage is completed with forward copper/LAr and tungsten/LAr calorimeter modules optimised for electromagnetic and hadronic measurements, respectively.

The muon spectrometer (MS) comprises separate trigger and high-precision tracking chambers measuring the deflection of muons in a magnetic field generated by the superconducting air-core toroids. The field integral of the toroids ranges between 2.0 and 6.0 T m across most of the detector. A set of precision chambers covers the region $|\eta| < 2.7$ with three layers of drift tubes, complemented by cathode strip chambers in the forward region, where the background is highest. The muon trigger system covers the range $|\eta| < 2.4$ with resistive plate chambers in the barrel, and thin gap chambers in the endcap regions.

A two-level trigger system is used for event selection [23, 24]. The first trigger level is implemented in hardware and uses a subset of detector information to reduce the event rate to a design value of at most 100 kHz. This is followed by a software-based trigger that reduces the event rate to about 1 kHz.

3 Monte Carlo simulation

Monte Carlo simulations are used in three ways in this analysis: to estimate the signal and background composition of the selected data samples, to determine correction factors for detector and acceptance effects for unfolding, and finally to estimate systematic uncertainties. In addition, theoretical predictions are compared with the unfolded data. The computer codes used to generate the samples and how they were configured are described in the following. The signal MC samples used in the analysis are listed in Table 1.

The nominal $t\bar{t}$ sample was generated using the PowHEG-Box generator (version 2, r3026) [25–28] at next-to-leading-order (NLO) in α_s with the NNPDF3.0NLO set of parton distribution functions (PDF) in the matrix element calculation. The parton shower, fragmentation, and the underlying event were

Table 1: Summary of the MC sample set-ups used for modelling the signal processes ($t\bar{t} + t\bar{t}V + t\bar{t}H$) for the data analysis and for comparisons with the measured cross-sections and differential distributions. All samples used the NNPDF3.0NLO PDF set with the exception of the two SHERPA samples, which used NNPDF3.0NNLO. The different blocks indicate from top to bottom the samples used as nominal MC (nom.), systematic variations (syst.) and for comparison only (comp.). For details see Section 3.

Generator sample	Process	Matching	Tune	Use
POWHEG-Box v2 + PYTHIA 8.210	$t\bar{t}$ NLO	POWHEG $h_{\text{damp}} = 1.5m_t$	A14	nom.
MADGRAPH5_aMC@NLO + PYTHIA 8.210	$t\bar{t} + V/H$ NLO	MC@NLO	A14	nom.
POWHEG-Box v2 + PYTHIA 8.210 RadLo	$t\bar{t}$ NLO	POWHEG $h_{\text{damp}} = 1.5m_t$	A14Var3cDown	syst.
POWHEG-Box v2 + PYTHIA 8.210 RadHi	$t\bar{t}$ NLO	POWHEG $h_{\text{damp}} = 3.0m_t$	A14Var3cUp	syst.
POWHEG-Box v2 + HERWIG 7.01	$t\bar{t}$ NLO	POWHEG $h_{\text{damp}} = 1.5m_t$	H7UE	syst.
SHERPA 2.2.1 $t\bar{t}$	$t\bar{t}$ +0,1 parton at NLO +2,3,4 partons at LO	MEPs@NLO	SHERPA	syst.
MADGRAPH5_aMC@NLO + PYTHIA 8.210	$t\bar{t}$ NLO	MC@NLO	A14	comp.
SHERPA 2.2.1 $t\bar{t}bb$ (4FS)	$t\bar{t}bb$ NLO	MC@NLO	SHERPA	comp.
PowHEL + PYTHIA 8.210 (5FS)	$t\bar{t}bb$ NLO	POWHEG $h_{\text{damp}} = H_T/2$	A14	comp.
PowHEL + PYTHIA 8.210 (4FS)	$t\bar{t}bb$ NLO	POWHEG $h_{\text{damp}} = H_T/2$	A14	comp.
POWHEG-Box v2 + PYTHIA 8.210 $t\bar{t}bb$ (4FS)	$t\bar{t}bb$ NLO	POWHEG $h_{\text{damp}} = H_T/2$	A14	comp.

simulated using PYTHIA 8.210 [29] with the NNPDF2.3LO PDF sets [30, 31] and the corresponding A14 set of tuned parameters [32]. The h_{damp} parameter, which controls the p_T of the hardest additional parton emission beyond the Born configuration, was set to $1.5m_t$ [33], where m_t denotes the top-quark mass. The POWHEG hardness criterion used in the matching (POWHEG:pTdef) is set to 2 following a study in Ref. [33]. The renormalisation and factorisation scales were set to $\mu = \sqrt{m_t^2 + p_{T,t}^2}$, where $p_{T,t}$ is the transverse momentum of the top quark. Additional jets, including b -jets, were generated by the hardest additional parton emission and from parton showering. This sample is called PowHEG+PYTHIA 8 in the following.

Processes involving the production of a W , Z or Higgs boson in addition to a $t\bar{t}$ pair were simulated using the MADGRAPH5_aMC@NLO generator [34, 35] at NLO in α_s in the matrix element calculation. The parton shower, fragmentation and underlying event were simulated using PYTHIA 8 with the A14 parton shower tune. A dynamic renormalisation and factorisation scale set to $H_T/2$ was used, where H_T is defined as the scalar sum of the transverse mass, $m_T = \sqrt{m^2 + p_T^2}$, of all partons in the partonic final state. The NNPDF3.0NLO PDF set was used in the matrix element calculation while the NNPDF2.3LO PDF set was used in the parton shower. In the case of $t\bar{t}H$, the Higgs boson mass was set to 125 GeV and all possible Higgs decay modes were allowed, with the branching fractions calculated with HDECAY [36, 37]. The $t\bar{t}W$ and $t\bar{t}Z$ samples are normalised to cross-sections calculated to NLO in α_s with MADGRAPH5_aMC@NLO. The $t\bar{t}H$ sample is normalised to a cross-section calculated to NLO accuracy in QCD, including NLO electroweak corrections [36].

Alternative $t\bar{t}$ samples were generated to assess the uncertainties due to a particular choice of QCD MC model for the production of the additional b -jets and to compare with unfolded data, as listed in Table 1. In order to investigate the effects of initial- and final-state radiation, two samples were generated using PowHEG+PYTHIA 8 with the renormalisation and factorisation scales varied by a factor of 2 (0.5) and using low-radiation (high-radiation) variations of the A14 tune and an h_{damp} value of $1.5m_t$ ($3.0m_t$), corresponding

to less (more) parton shower radiation [33]. These samples are called PowHEG+PYTHIA 8 (RadLo) and PowHEG+PYTHIA 8 (RadHi) in the following. To estimate the effect of the choice of parton shower and hadronisation algorithms, a MC sample was generated by interfacing PowHEG with HERWIG 7 [38, 39] (v7.01) using the H7UE set of tuned parameters [39].

In order to estimate the effects of QCD scales, and matching and merging algorithms used in the NLO $t\bar{t}$ matrix element calculation and the parton shower to predict additional b -jets, events were generated with the SHERPA 2.2.1 generator [40], which models the zero and one additional-parton process at NLO accuracy and up to four additional partons at LO accuracy, using the MEps@NLO prescription [41]. Additional b -quarks were treated as massless and the NNPDF3.0NNLO PDF set was used. The calculation uses its own parton shower tune. This sample is referred to as SHERPA 2.2 $t\bar{t}$.

In addition to the $t\bar{t}$ samples described above, a $t\bar{t}$ sample was generated using the MADGRAPH5_aMC@NLO [34] (v2.3.3) generator, interfaced to PYTHIA 8.210 and is referred to as MADGRAPH5_aMC@NLO+PYTHIA 8 hereafter. As with the nominal PowHEG+PYTHIA 8 $t\bar{t}$ sample, the NNPDF3.0NLO PDF set was used in the matrix element calculation and the NNPDF2.3LO PDF set was used in the parton shower. This sample is used to calculate the fraction of $t\bar{t} + V/H$ events in $t\bar{t}$ events and to compare with the data. The A14 set of tuned parameters was used for PYTHIA.

The $t\bar{t}$ samples are normalised to a cross-section of $\sigma_{t\bar{t}} = 832^{+46}_{-51}$ pb as calculated with the Top++2.0 program to next-to-next-to-leading order (NNLO) in perturbative QCD, including soft-gluon resummation to next-to-next-to-leading-log (NNLL) order (see Ref. [42] and references therein), and assuming $m_t = 172.5$ GeV. The uncertainty in the theoretical cross-section comes from independent variations of the factorisation and renormalisation scales and variations in the PDF and α_S , following the PDF4LHC prescription with the MSTW 2008 NNLO, CT10 NNLO and NNPDF2.3 5f FFN PDF sets (see Ref. [43] and references therein, and Refs. [44–46]).

Four more predictions were calculated only for comparisons with data and are all based on $t\bar{t}b\bar{b}$ matrix element calculations. These predictions all use the same renormalisation and factorisation scale definitions as the study presented in Ref. [36]. The renormalisation scale, μ_R , is set to $\mu_R = \prod_{i=t,\bar{t},b,\bar{b}} E_{T,i}^{1/4}$, where $E_{T,i}$ refers to the transverse energy of the parton i in the partonic final state, and the factorisation scale, μ_F , is set to $H_T/2$ which is defined as

$$\mu_F = H_T/2 = \frac{1}{2} \sum_{i=t,\bar{t},b,\bar{b},j} E_{T,i},$$

where j refers to the additional QCD-radiated partons at NLO.

Three of the four predictions are based on the PowHEG method, and use the PYTHIA 8 parton shower with the same parton shower tune and the same matching settings as the nominal PowHEG+PYTHIA 8 sample, with the exception of the h_{damp} parameter, which is set to the same value as the factorisation scale, i.e. $H_T/2$. In the $t\bar{t}b\bar{b}$ matrix element calculations with massive b -quarks, the b -quark mass is set to $m_b = 4.75$ GeV. The set-up of the four dedicated samples are described below.

A sample of $t\bar{t}b\bar{b}$ events was generated using SHERPA+OPENLOOPS [2]. The $t\bar{t}b\bar{b}$ matrix elements were calculated with massive b -quarks at NLO, using the COMIX [47] and OPENLOOPS [48] matrix element generators, and merged with the SHERPA parton shower, tuned by the authors [49]. The four-flavour NNLO NNPDF3.0 PDF set was used. The resummation scale, μ_Q , was set to the same value as μ_F . This sample is referred to as SHERPA 2.2 $t\bar{t}b\bar{b}$ (4FS). A sample of $t\bar{t}b\bar{b}$ events was generated using the PowHEL generator [3], where the matrix elements were calculated at NLO assuming massless b -quarks and using

the five-flavour NLO NNPDF3.0 PDF set. Events were required to have the invariant mass, m_{bb} , of the $b\bar{b}$ system to be larger than 9.5 GeV and the p_T of the b -quark larger than 4.75 GeV as described in Ref. [36]. These events were matched to the PYTHIA 8 parton shower using the POWHEG method. This sample is referred to as PowHEL+PYTHIA 8 $t\bar{t}b\bar{b}$ (5FS).

A sample of $t\bar{t}b\bar{b}$ events using the PowHEL generator where the matrix elements were calculated at NLO with massive b -quarks and using the four-flavour NLO NNPDF3.0 PDF set [4]. Events were matched to the PYTHIA 8 parton shower using the POWHEG method. This sample is referred to as PowHEL+PYTHIA 8 $t\bar{t}b\bar{b}$ (4FS).

A sample of $t\bar{t}b\bar{b}$ events using the POWHEG generator where $t\bar{t}b\bar{b}$ matrix elements were calculated at NLO with massive b -quarks and using the four-flavour NLO NNPDF3.0 PDF set [5]. Events were matched to the PYTHIA 8 parton shower using the POWHEG method. This sample is referred to as POWHEG+PYTHIA 8 $t\bar{t}b\bar{b}$ (4FS) to distinguish it from the nominal PowHEL+PYTHIA 8 sample mentioned above.

For all samples involving top quarks, m_t was set to 172.5 GeV and the EvtGEN v1.2.0 program [50] was used for properties of the bottom and charm hadron decays except for the SHERPA samples. To preserve the spin correlation information, top quarks were decayed following the method of Ref. [51] which is implemented in PowHEG-Box and by MADSPIN [52] in the MADGRAPH5_aMC@NLO+PYTHIA 8 samples. SHERPA performs its own calculation for spin correlation. Both of the PowHEL+PYTHIA 8 $t\bar{t}b\bar{b}$ samples used PYTHIA to decay the top quarks, with a top-quark decay width of 1.33 GeV, and hence these predictions do not include $t\bar{t}$ spin correlations.

The production of single top-quarks in the tW - and s -channels was simulated using the POWHEG-Box (v2, r2819) NLO generator with the CT10 PDF set in the matrix element calculations. Electroweak t -channel single-top-quark events were generated using the POWHEG-Box (v1, r2556) generator. This generator uses the four-flavour scheme for the NLO matrix elements calculation together with the fixed four-flavour PDF set CT10f4. For all top processes, top-quark spin correlations are preserved (in the case of the t -channel, top quarks were decayed using MADSPIN). The interference between $t\bar{t}$ and tW production is accounted for using the diagram-removal scheme [53]. The parton shower, fragmentation, and the underlying event were simulated using PYTHIA 6.428 [54] with the CTEQ6L1 PDF sets and the Perugia 2012 tune (P2012) [55, 56]. The single-top MC samples for the t - and s -channels are normalised to cross-sections from NLO predictions [57, 58], while the tW -channel MC sample is normalised to approximate NNLO [59].

Events containing W or Z bosons with associated jets were simulated using the SHERPA 2.2.1 generator. Matrix elements were calculated for up to two partons at NLO and up to four partons at leading order (LO) using the COMIX and OPENLOOPS matrix element generators and merged with the SHERPA parton shower using the MEPS@NLO prescription. The NNPDF3.0NNLO PDF set was used in conjunction with parton shower tuning developed by the SHERPA authors. The $W/Z+jets$ events are normalised to NNLO cross-sections, computed using FEWZ [60] with the MSTW 2008 NNLO PDF set.

Diboson processes were simulated using the SHERPA 2.1.1 generator. Matrix elements were calculated using the COMIX and OPENLOOPS matrix element generators and merged with the SHERPA parton shower using the MEPS@NLO prescription. In the case of both bosons decaying leptonically, matrix elements contain all diagrams with four electroweak vertices and were calculated for up to one (four charged leptons or two charged leptons and two neutrinos) or zero partons (three charged leptons and one neutrino) at NLO, and up to three partons at LO. In the cases where one of the bosons decays hadronically and the other leptonically, matrix elements were calculated with up to one (ZZ) or zero (WW, WZ) additional partons at NLO and up to three additional partons at LO. The CT10 PDF set was used in conjunction with parton shower tuning developed by the SHERPA authors.

In all MC simulation samples, the effect of multiple pp interactions per bunch crossing (pile-up) was modelled by adding multiple minimum-bias events simulated with PYTHIA 8.186 [29], the A2 set of tuned parameters [61] and the MSTW2008LO set of PDFs [62]. The MC simulation samples are re-weighted to reproduce the distribution of the mean number of interactions per bunch crossing observed in the data.

4 Object reconstruction and identification

4.1 Detector-level object reconstruction

A description of the main reconstruction and identification criteria applied for electrons, muons, jets and b -jets is given below.

Electrons are reconstructed [63] by matching ID tracks to clusters in the electromagnetic calorimeter. Electrons must satisfy the *tight* identification criterion, based on a likelihood discriminant combining observables related to the shower shape in the calorimeter and to the track matching the electromagnetic cluster, and are required to be isolated in both the ID and the EM calorimeter using the p_T -dependent isolation working point. Electrons are required to have $p_T > 25$ GeV and $|\eta_{\text{cluster}}| < 2.47$. Electrons that fall in the transition region between the barrel and endcap calorimeters ($1.37 < |\eta_{\text{cluster}}| < 1.52$) are poorly measured and are therefore not considered in this analysis.

Muon candidates are reconstructed [64] by matching ID tracks to tracks in the muon spectrometer. Track reconstruction is performed independently in the ID and MS before a combined track is formed with a global re-fit to hits in the ID and MS. Muon candidates are required to have $p_T > 25$ GeV and $|\eta| < 2.5$, must satisfy the *medium* identification criteria and are required to be isolated using the p_T -dependent isolation working point.

Electron and muon tracks are required to be associated with the primary vertex. This association requires the electron (muon) track to have $|d_0|/\sigma_{d_0} < 5$ (3) and $|\Delta z_0 \sin \theta| < 0.5$ mm, where d_0 and z_0 are the transverse and longitudinal impact parameters of the electron (muon) track, respectively, σ_{d_0} is the uncertainty in the measurement of d_0 , and θ is the angle of the track relative to the axis parallel to the beamline.

Reconstruction, identification and isolation efficiencies of electrons (muons) are corrected in simulation to match those observed in data using $Z \rightarrow e^+e^- (\mu^+\mu^-)$ events, and the position and width of the observed Z boson peak is used to calibrate the electron (muon) energy (momentum) scale and resolution.

The anti- k_t algorithm [65] with a radius parameter of $R = 0.4$ is used to reconstruct jets with a four-momentum recombination scheme, using energy deposits in topological clusters in the calorimeter as inputs [66]. Jets are calibrated using a series of simulation-based corrections and *in situ* techniques [67]. Calibrated jets are required to have $p_T > 25$ GeV and $|\eta| < 2.5$ so that data from the ID is available for determining whether they contain b -hadrons. Jets with $p_T < 60$ GeV and $|\eta| < 2.4$ are required to be identified as originating from the primary vertex using a jet-vertex tagger (JVT) algorithm [68].

Jets containing b -hadrons are identified exploiting the lifetimes of b -hadrons and their masses. A multivariate algorithm, MV2c10, that combines track and secondary-vertex information is used to distinguish b -jets from other jets [69]. Four working points are defined by different b -tagging discriminant output thresholds corresponding to efficiencies of 85%, 77%, 70% and 60% in simulated $t\bar{t}$ events for b -jets with $p_T > 20$ GeV and rejection factors ranging from 3–35 for c -jets and 30–1500 for light-flavour jets [19, 69].

After selecting electrons, muons and jets as defined above, several criteria are applied to ensure that objects

do not overlap. If a selected electron and muon share a track then the electron is rejected. If an electron is within $\Delta R = 0.2$ of one or more jets then the closest jet to the electron is removed. If there are remaining jets within $\Delta R = 0.4$ of an electron then the electron is removed. When a jet is within $\Delta R = 0.4$ of a muon, it is removed if it has fewer than three tracks, otherwise the muon is removed.

4.2 Particle-level object definitions

Particle-level objects are selected in simulated events using definitions that closely match the detector-level objects defined in Section 4.1. Particle-level objects are defined using stable particles having a proper lifetime greater than 30 ps.

This analysis considers electrons and muons that do not come from hadron decays for the fiducial definition.² In order to take into account final-state photon radiation, the four-momentum of each lepton is modified by adding to it the four-momenta of all photons, not originating from a hadron, that are located within a $\Delta R = 0.1$ cone around the lepton. Electrons and muons are required to have $p_T > 25$ GeV and $|\eta| < 2.5$.

Jets are clustered using the anti- k_t algorithm with a radius parameter of 0.4. All stable particles are included except those identified as electrons and muons, and the photons added to them, using the definition above and neutrinos not from hadron decays. These jets do not include particles from pile-up events but do include those from the underlying event. The decay products of hadronically decaying τ -leptons are therefore included. Jets are required to have $p_T > 25$ GeV and $|\eta| < 2.5$.

Jets are identified as b -jets by requiring that at least one b -hadron with $p_T > 5$ GeV is matched to the jet by ghost association [70]. Here, the ghost-association procedure includes b -hadrons in the jet clustering after scaling their p_T to a negligible value. A similar procedure is followed to define c -jets, with the b -jet definition taking precedence, i.e. a jet containing one b -hadron and one c -hadron is defined as a b -jet. Jets that do not contain either a b -hadron or a c -hadron are considered to be light-flavour jets.

Electrons and muons that meet the selection criteria defined above are required to be separated from selected jets by $\Delta R(\text{lepton}, \text{jet}) > 0.4$. This ensures compatibility with the detector-level selection defined in Section 4.1.

5 Event selection and definition of the fiducial phase space

5.1 Data event selection

The data analysed were collected by the ATLAS detector in 2015 and 2016 during stable pp collisions at $\sqrt{s} = 13$ TeV while all components of the ATLAS detector were fully operational. The total integrated luminosity recorded in this period is 36.1 fb^{-1} .

In order to ensure events originate from pp collisions, events are required to have at least one primary vertex with at least two tracks. The primary vertex is defined as the vertex with the highest $\sum p_T^2$ of tracks assigned to it.

Single-electron or single-muon triggers are used to select the events. They require a p_T of at least 20 (26) GeV for muons and 24 (26) GeV for electrons for the 2015 (2016) data set and also include requirements

² Electrons and muons from τ decays are thus included.

on the lepton quality and isolation. These triggers are complemented by others with higher p_T requirements but loosened isolation requirements to ensure maximum efficiencies at higher lepton p_T .

In the $e\mu$ channel, events are required to have exactly one electron and one muon of $p_T > 27$ GeV and with opposite electric charge. At least one of the two leptons must be matched in flavour and angle to a trigger object. In the lepton + jets channel, exactly one selected lepton of $p_T > 27$ GeV is required and must be matched to the trigger object that triggered the event.

In the $e\mu$ channel, at least two jets are required and at least two of these must be b -tagged at the 77% efficiency b -tagging working point for the baseline selection. The measurement of the fiducial cross-section with one (two) additional b -jets requires at least three (at least four) jets to be b -tagged. For the measurement of the b -jet multiplicity distribution, at least two jets are required and at least two of them must be b -tagged. All other differential cross-section measurements in the $e\mu$ channel require at least three jets and at least three of these must be b -tagged.

In the lepton + jets channel, at least five jets are required and at least two of these must be b -tagged for the baseline selection. For the measurement of the fiducial cross-section with one (two) additional b -jets, five (six) jets are required, of which at least three (at least four) must be b -tagged. For the measurement of the differential cross-sections, at least six jets, at least four of which are b -tagged, are required. In this channel, b -jets are identified using the tighter 60% efficiency b -tagging working point to better suppress c -jets from $W^- \rightarrow \bar{c}s$ or $W^+ \rightarrow c\bar{s}$ decays.

5.2 Fiducial phase-space definition

The phase space in which the fiducial cross-section is measured is defined using particle-level objects with kinematic requirements similar to those placed on reconstructed objects in the event selection. The definitions of the fiducial phase spaces used for the cross-sections measurements are given below. The data are corrected to particle level using slightly different definitions of the fiducial phase space depending on the top-pair decay channel and on the observable.

In the $e\mu$ channel, fiducial cross-sections are determined by requiring exactly one electron and one muon with opposite-sign charge at particle level and at least three (at least four) b -jet(s) for the fiducial cross-section with one (two) additional b -jets. The normalised differential cross-sections are measured in the fiducial volume containing the leptons and at least two b -jets for the distribution differential in number of b -jets and at least three b -jets for all other differential measurements.

In the lepton + jets channel, the fiducial phase space for the measurement of the integrated cross-section with one (two) additional b -jet(s) is defined as containing exactly one particle-level electron or muon and five (six) jets, at least three (four) of which are b -jets. Differential cross-sections are measured in a fiducial volume containing at least six jets and where at least four of them are required to be b -jets.

6 Background estimation

The baseline selection with at least two b -tagged jets results in a sample with only small backgrounds from processes other than $t\bar{t}$ production. As mentioned before, events with additional b -jets produced in $t\bar{t}V$ or $t\bar{t}H$ production are treated as signal. The estimation of $t\bar{t}$ production in association with additional light-flavour jets or c -jets is described in Section 7.1 and is performed simultaneously with the extraction

of fiducial cross-sections.

The remaining background events are classified into two types: those with prompt leptons from single top, W or Z decays (including those produced via leptonic τ decays), which are discussed in Section 6.1, and those where at least one of the reconstructed lepton candidates is non-prompt or “fake” (NP & fake lep.), i.e. a non-prompt lepton from the decay of a b - or c -hadron, an electron from a photon conversion, hadronic jet activity misidentified as an electron, or a muon produced from an in-flight decay of a pion or kaon. This is estimated using a combined data-driven and simulation-based approach in the $e\mu$ channel, and a data-driven approach in the lepton + jets channel, both of which are described in Section 6.2.

6.1 Background from single-top, Z/γ^* + jets and W + jets events

The background from single top-quark production is estimated from the MC simulation predictions in both the $e\mu$ and lepton + jets channels. This background contributes 3% of the event yields in both channels, with slightly smaller contributions in the four b -jets selections.

In the $e\mu$ channel, a very small number of events from Drell–Yan production and $Z/\gamma^*(\rightarrow \tau\tau)$ +jets fulfil the selection criteria. This background is estimated from MC simulation scaled to the data with separate scale factors for the two- b -tagged jets and three- b -tagged jets cases. The scale factors are derived from data events that have a reconstructed mass of the dilepton system corresponding to the Z boson mass and that fulfil the standard selection except that the lepton flavour is ee or $\mu\mu$. The fraction of background events from $Z/\gamma^*(\rightarrow \tau\tau)$ +jets is below two per mill for all b -tagged jet multiplicities. A small number of Z/γ^* +jets events, where the Z/γ^* is decaying into any lepton flavour pair, can enter in the lepton + jets channel and is estimated from MC simulation.

In the lepton + jets channel, a small background from W + jets remains after the event selection; however, this contribution is below 2% in events that have at least three b -tagged jets. This background is estimated directly from MC simulation.

6.2 Background from non-prompt and fake leptons

In the $e\mu$ channel, the normalisation of this background is estimated from data using events in which the electron and muon have the same-sign electric charge. The method is described in Ref. [71]. Known sources of same-sign prompt leptons are subtracted from the data and the non-prompt and fake background is extracted by scaling the remaining data events by a transfer factor determined from MC simulation. This transfer factor is defined as the ratio of predicted opposite-sign to predicted same-sign non-prompt and fake leptons.

In the lepton + jets channel, the background from non-prompt and fake leptons is estimated using the *matrix method* [72]. A sample enriched in non-prompt and fake leptons is obtained by removing the isolation and impact parameter requirements on the lepton selections defined in Section 4. The efficiency for these leptons, hereafter referred to as *loose* leptons, to meet the identification criteria defined in Section 4.1 is then measured separately for prompt and fake leptons.³ For both electrons and muons the efficiency for a prompt loose lepton to pass the identification criteria defined in Section 4.1 is measured using a sample of Z boson decays. The efficiency for fake loose leptons to pass the identification criteria is measured using events that have low missing transverse momentum for electrons and high lepton impact-parameter

³ Here fake leptons also include non-prompt leptons.

Table 2: Predicted and observed $e\mu$ channel event yields in $2b$, $\geq 3b$ and $\geq 4b$ selections. The quoted errors are symmetrised and indicate total statistical and systematic uncertainties in predictions due to experimental sources.

Process	$2b$		$\geq 3b$		$\geq 4b$	
Signal ($t\bar{t} + t\bar{t}H + t\bar{t}V$)	74 400	± 2900	3 200	± 310	210	± 29
$t\bar{t}$	74 200	± 2900	3 100	± 310	190	± 29
$t\bar{t}H$	45.3	± 6.6	36.5	± 7.0	9.4	± 3.3
$t\bar{t}V$	190	± 16	33.5	± 6.7	4.4	± 2.2
Background	3 150	± 810	140	± 53	9.2	± 5.6
Single top	2 460	± 540	96	± 32	4.1	± 2.5
NP and fake lep.	600	± 600	43	± 43	5.1	± 5.1
Z/γ^*+jets	53	± 13	1.3	± 0.3	0.07	± 0.02
Diboson	38	± 20	1.0	± 1.1	< 0.01	
Expected	77 600	± 3000	3 320	± 320	216	± 30
Observed	76 425		3 809		267	

Table 3: Predicted and observed lepton + jets event yields in the $\geq 5j \geq 2b$, $\geq 5j \geq 3b$, $\geq 5j = 3b$, and $\geq 6j \geq 4b$ selections. The quoted uncertainties are symmetrised and indicate total statistical and systematic uncertainties in predictions due to experimental sources.

Process	$\geq 5j, \geq 2b$	$\geq 5j, \geq 3b$	$\geq 5j, = 3b$	$\geq 6j, \geq 4b$				
Signal ($t\bar{t} + t\bar{t}H + t\bar{t}V$)	$429\,000 \pm 42\,000$	23 700	$\pm 2\,200$	22 300	$\pm 2\,100$	1 130	± 110	
$t\bar{t}$	$426\,000 \pm 42\,000$	23 000	$\pm 2\,200$	21 700	$\pm 2\,100$	1 030	± 110	
$t\bar{t}H$	1 250	± 58	437	± 23	351	± 18	68.3	± 5.8
$t\bar{t}V$	2 020	± 110	250	± 16	215	± 14	28.3	± 2.8
Background	39 500	$\pm 7\,900$	2 230	± 470	2 110	± 450	87	± 23
Single top	16 400	$\pm 2\,000$	856	± 99	803	± 94	35.7	± 6.5
NP and fake lep.	11 000	$\pm 5\,500$	740	± 380	710	± 360	32	± 21
$W+jets$	8 600	$\pm 5\,300$	440	± 270	410	± 260	11.0	± 6.9
Z/γ^*+jets	2 960	± 480	164	± 26	155	± 26	5.9	± 1.5
Diboson	529	± 80	34.0	± 5.6	32.0	± 5.5	1.79	± 0.58
Expected	$469\,000 \pm 42\,000$	26 000	$\pm 2\,300$	24 400	$\pm 2\,200$	1 220	± 110	
Observed	469 793		28 167		26 389		1 316	

significance for muons. These efficiencies allow the number of fake leptons selected in the signal region to be estimated.

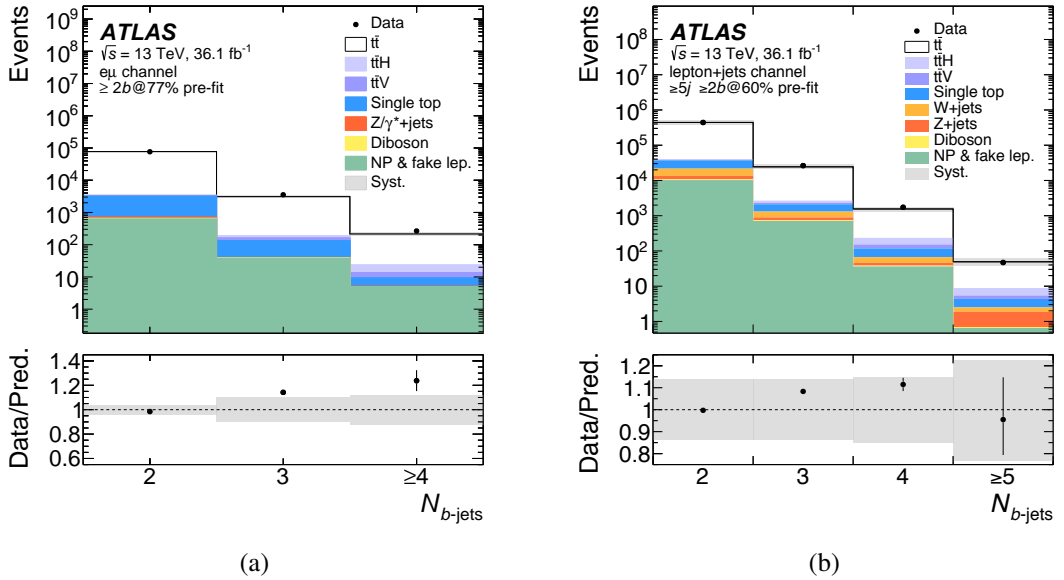


Figure 2: Comparison of the data distributions with predictions for the number of b -tagged jets, in events with at least 2 b -tagged jets, in the (a) $e\mu$ and (b) lepton + jets channels. The systematic uncertainty band, shown in grey, includes all uncertainties from experimental sources.

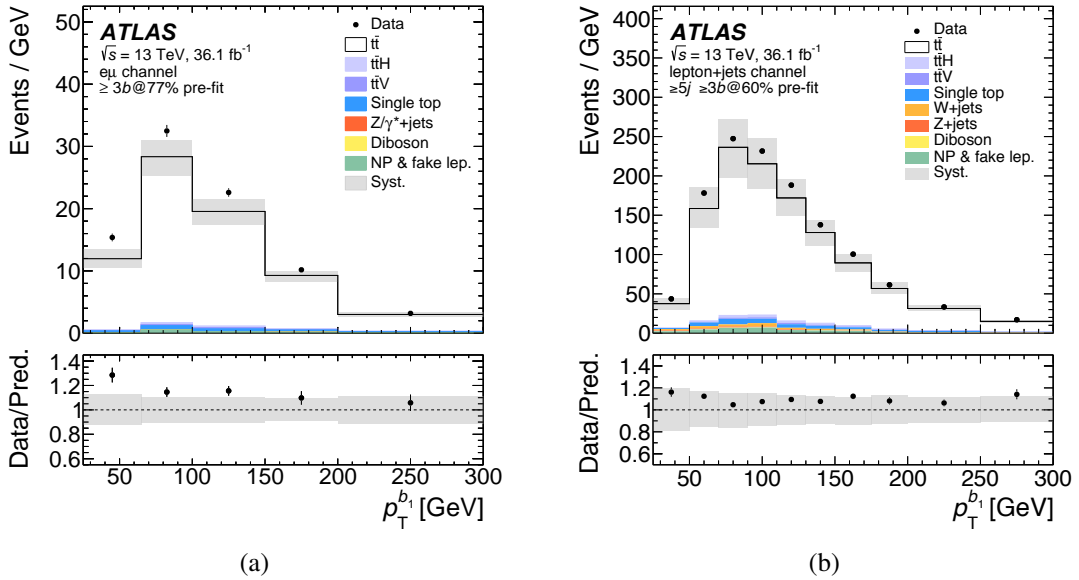


Figure 3: Comparison of the data distributions with predictions for the leading b -tagged jet p_T , in events with at least 3 b -tagged jets, in the (a) $e\mu$ and (b) lepton + jets channels. The systematic uncertainty band, shown in grey, includes all uncertainties from experimental sources. Events that fall outside of the range of the x -axis are not included in the plot.

6.3 Data and prediction comparison of baseline selection

The overall number of events fulfilling the baseline selection is well described by the prediction in both channels, as seen in Tables 2 and 3 and Figure 2, where b and j denote a b -jet and a jet of any flavour, respectively. However, the number of events with more than two b -tagged jets is slightly underestimated, as shown in Figures 2 and 3. Therefore, data-driven scale factors are derived to correct the predictions of additional c -jets or light jets in the $t\bar{t}$ MC simulation, as described in the next section.

7 Extraction of the fiducial cross-sections

Fiducial cross-sections in the phase spaces defined in Section 5.2 for the different observables are extracted from detector-level distributions obtained after the event selections described in Section 5.1 and subtracting the number of background events produced by the non- $t\bar{t}$ processes described in Section 6. After the subtraction of non- $t\bar{t}$ background, the data suffer from backgrounds from $t\bar{t}$ events with additional light-flavour jets ($t\bar{l}l$) or c -jets ($t\bar{t}c$) that are misidentified as b -jets by the b -tagging algorithm. The correction factors for these backgrounds are measured in data, as presented in Section 7.1. The data are then unfolded using the corrected MC simulation as described in Section 7.2.

7.1 Data-driven correction factors for flavour composition of additional jets in $t\bar{t}$ events

The measurement of $t\bar{t} + b$ -jets production is dependent on the determination of the background from other $t\bar{t}$ processes. For example, according to simulation studies in the $e\mu$ channel, only about 50% of the events selected at detector level with at least three b -tagged jets at the 77% efficiency working point and within the fiducial phase space of the analysis, also have at least three b -jets at particle level. The other events contain at least one c -jet or light-flavour jet which is misidentified as a b -jet. The cross-section of $t\bar{t}$ with additional jet production has been measured with 10% (16%) uncertainty for events with two (three) additional jets [73]. However, these measurements did not determine the flavours of the additional jets. Due to the lack of precise measurements of these processes, template fits to data are performed to extract the $t\bar{t}b$ signal yields and estimate the $t\bar{t}c$ and $t\bar{l}l$ backgrounds as described in the following. The templates are constructed from $t\bar{t}$, $t\bar{t}H$ and $t\bar{t}V$ MC simulated samples, as the signal includes the contributions from $t\bar{t}V$ and $t\bar{t}H$.

The events in the $e\mu$ channel are selected within an analysis region consisting of at least three b -tagged jets at the 77% b -tagging working point as specified in Section 5.1. This avoids extrapolation of the background shapes determined outside the selected region into the analysis region. The fit in the lepton + jets channel is performed on a sample with at least five jets, at least two of which are b -tagged with a b -tagging efficiency of 60%. While this means that the MC simulation is needed to extrapolate the results of the fit into the signal regions, it allows the $t\bar{l}l$ background to be extracted in what is effectively a control region. The lepton + jets channel suffers from an additional background due to $W^+ \rightarrow c\bar{s}$ or corresponding W^- decays in the inclusive $t\bar{t}$ process, where the c -jet is misidentified as a b -jet. In order to separate this background from $t\bar{t}+c$ -jets events, events containing only one particle-level c -jet are attributed to this background and grouped into a $t\bar{l}l$ class, while those with two particle-level c -jets are placed into a $t\bar{t}c$ class, as summarised in Table 4. In this sample, 85% of the events with exactly one particle-level c -jet are found to contain $W \rightarrow c\bar{s}(c\bar{s})$ decays, according to $t\bar{t}$ MC simulation. Templates are created for events in the different categories described in Table 4 using the b -tagging discriminant value of the jet with the

Table 4: Event categorisation (for the definition of the MC templates) based on the particle-level selections of b -jets, c -jets and light-flavour jets.

Category	$e\mu$	lepton + jets
$t\bar{t}b$	≥ 3 b -jets	≥ 3 b -jets
$t\bar{t}c$	< 3 b -jets and ≥ 1 c -jet	< 3 b -jets and ≥ 2 c -jets
$t\bar{t}l$	events that do not meet above criteria	events that do not meet above criteria

third-highest b -tagging discriminant in the $e\mu$ channel, and the two jets with the third- and fourth-highest b -tagging discriminant values in the lepton + jets channel. The discriminant values are divided into five b -tagging discriminant bins such that each bin corresponds to a certain range of b -tagging efficiencies defined by the working points. The bins range from 1 to 5, corresponding to efficiencies of 100%–85%, 85%–77%, 77%–70%, 70%–60%, and $< 60\%$ respectively. In the $e\mu$ channel, one-dimensional templates with three bins are formed corresponding to b -tagging efficiencies between 77% and 0% for the jet with the third highest b -tagging discriminant value. In the lepton + jets channel, two-dimensional templates are created using the b -tagging discriminant values of the two jets with the third- and fourth-highest b -tagging discriminant values, corresponding to b -tagging efficiencies between 100% and 0% for the two jets.

In both channels, one template is created from the sum of all backgrounds described in Section 6 and three templates are created from $t\bar{t}$, $t\bar{t}V$ and $t\bar{t}H$ MC simulations, to account for $t\bar{t}b$, $t\bar{t}c$ and $t\bar{t}l$ events, as detailed in Table 4. These templates are then fitted to the data using a binned maximum-likelihood fit, with a Poisson likelihood

$$\mathcal{L}(\vec{\alpha}|x_1, \dots, x_n) = \prod_k^n \frac{e^{-\nu_k(\vec{\alpha})} \nu_k(\vec{\alpha})^{x_k}}{x_k!},$$

where x_k is the number of events in bin k of the data template and $\nu_k(\vec{\alpha})$ is the expected number of events, and depends upon a number of free parameters, $\vec{\alpha}$.

In the $e\mu$ channel, two free parameters are used, such that the expected number of events in bin k is

$$\nu_k(\alpha_b, \alpha_{cl}) = \alpha_b N_{t\bar{t}b}^k + \alpha_{cl} \left(N_{t\bar{t}c}^k + N_{t\bar{t}l}^k \right) + N_{\text{non-}t\bar{t}}^k,$$

where $N_{t\bar{t}b}^k$, $N_{t\bar{t}c}^k$, $N_{t\bar{t}l}^k$ and $N_{\text{non-}t\bar{t}}^k$ are the numbers of events in bin k of the $t\bar{t}b$, $t\bar{t}c$, $t\bar{t}l$ and non- $t\bar{t}$ background templates, respectively. The scale factors obtained from the fit are $\alpha_b = 1.37 \pm 0.06$ and $\alpha_{cl} = 1.05 \pm 0.04$, where the quoted uncertainties are statistical only. Figure 4(a) shows the distributions of the templates before and after scaling the templates by these scale factors.

In the lepton + jets channel, three free parameters, α_b , α_c and α_l , are used in the maximum-likelihood fit, such that the expected number of events in bin k is

$$\nu_k(\alpha_b, \alpha_c, \alpha_l) = \alpha_b N_{t\bar{t}b}^k + \alpha_c N_{t\bar{t}c}^k + \alpha_l N_{t\bar{t}l}^k + N_{\text{non-}t\bar{t}}^k. \quad (1)$$

The best-fit values of the free parameters are $\alpha_b = 1.11 \pm 0.02$, $\alpha_c = 1.59 \pm 0.06$ and $\alpha_l = 0.962 \pm 0.003$ where the quoted uncertainties are statistical only. Including systematic uncertainties, the values of α_b extracted in the $e\mu$ and lepton + jets channels are found to be compatible at a level better than 1.5 standard deviations. Some of the dominant common systematic uncertainties have small correlations between the

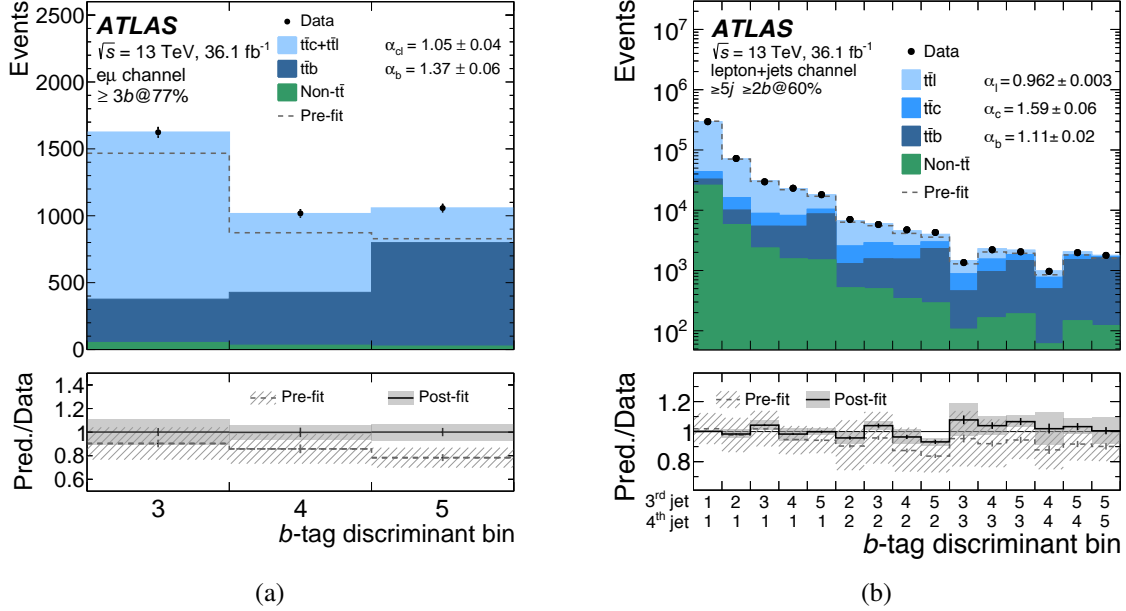


Figure 4: The b -tagging distribution of the third-highest b -tagging discriminant-ranked jet for the (a) $e\mu$ channel, and of the third and fourth b -tagging discriminant-ranked jet for the (b) lepton + jets channel. For clarity, the two-dimensional lepton + jets templates have been flattened into one dimension. The ratios of total predictions before and after the fit to the data are shown in the lower panel. The vertical bar in each ratio represents only the statistical uncertainty, and the grey bands represent the total error including systematic uncertainties from experimental sources. The extracted scale factors α_b , α_c , α_l , α_{cl} are given considering only statistical uncertainties.

two channels, while the uncertainty in α_b due to the modelling of the $t\bar{t}c$ template in the $e\mu$ channel, as discussed in Section 8.3 is uncorrelated between the two channels. Taking only this uncertainty as uncorrelated, the values of α_b extracted from the two channels are found to be compatible at a level better than 1.7 standard deviations. Figure 4(b) shows the distribution of the b -tagging discriminant before and after the fit. For clarity, the two-dimensional lepton + jets templates are flattened into a single dimension. Figures 5 and 6 show the comparison of data and predictions for the b -tagged jet multiplicity and the leading b -tagged jet p_T in the $e\mu$ and lepton + jets channels after the $t\bar{t}b$ signal, and the $t\bar{t}c$ and $t\bar{t}l$ backgrounds, are scaled by the extracted scale factors. The data are described much better by the prediction after the scaling is applied.

7.2 Unfolding

The measured distributions at detector level are unfolded to the particle level. The unfolding procedure corrects for resolution effects and for detector efficiencies and acceptances.

First, the number of non- $t\bar{t}$ background events in bin j ($N_{\text{non-}t\bar{t}\text{-bkg}}^j$), described in Section 6, is subtracted from the data distribution at the detector level in bin j (N_{data}^j). This retains a mixture of signal and $t\bar{t}$ -related backgrounds, the latter coming from mis-tagged events as described in Section 7.1. A series of corrections are then applied, with all corrections derived from simulated $t\bar{t}$, $t\bar{t}H$ and $t\bar{t}V$ events. Following the subtraction of non- $t\bar{t}$ background, the data are first corrected for mis-tagged events by applying a

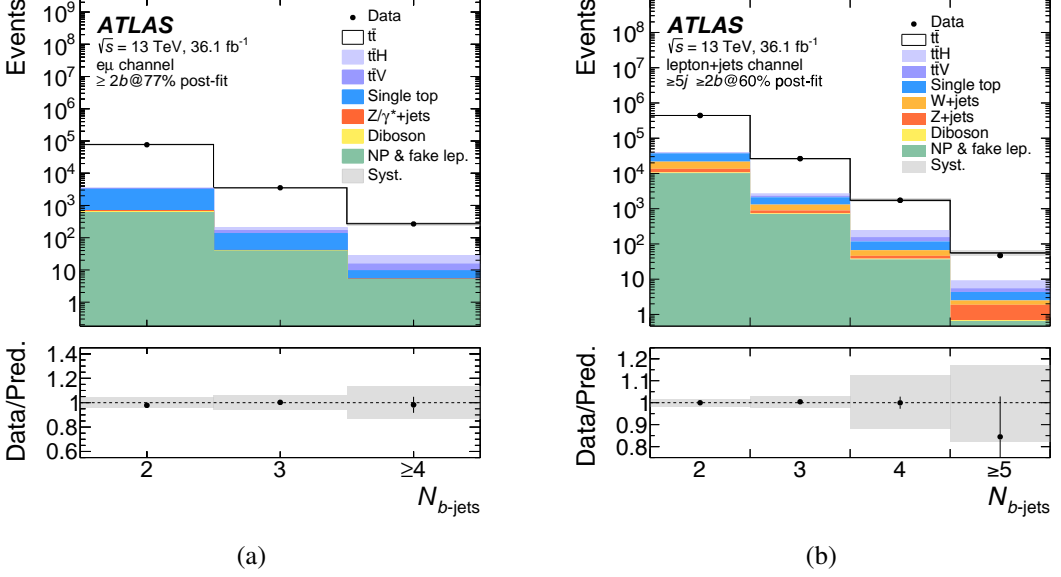


Figure 5: Comparison of the data distributions with predictions, after applying scale factors, for the number of b -tagged jets, in events with at least 2 b -tagged jets, in the (a) $e\mu$ and (b) lepton + jets channels. The systematic uncertainty band, shown in grey, includes all uncertainties from experimental sources.

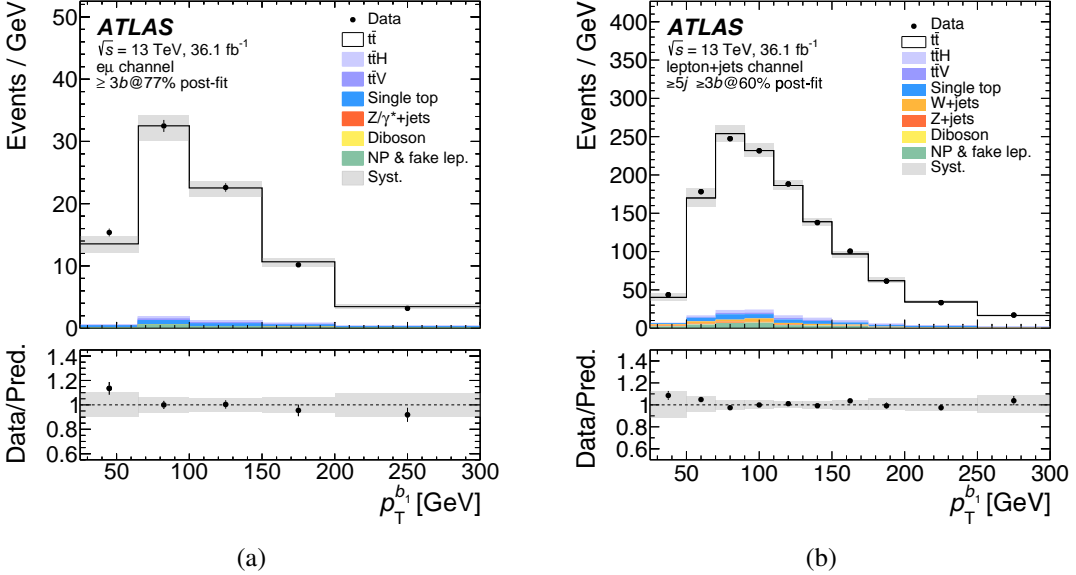


Figure 6: Comparison of the data distributions with predictions for the leading b -tagged jet p_T , after applying scale factors, in events with at least 3 b -tagged jets, in the (a) $e\mu$ and (b) lepton + jets channels. The systematic uncertainty band, shown in grey, includes all uncertainties from experimental sources. Events that fall outside of the range of the x -axis are not included in the plot.

correction

$$f_{t\bar{b}}^j = \frac{\alpha_b N_{t\bar{b},\text{reco}}^j}{\alpha_b N_{t\bar{b},\text{reco}}^j + \mathcal{B}^j},$$

where α_b is defined in the previous section, $N_{t\bar{b},\text{reco}}^j$ is the number of detector-level $t\bar{b}$ events predicted by MC simulation, and \mathcal{B}^j is the number of detector-level $t\bar{c}$ and $t\bar{l}$ events in bin j , after being scaled by the fit parameters, α_{cl} or α_c and α_l , defined in the previous section. In the $e\mu$ channel,

$$\mathcal{B}^j = \alpha_{cl} \left(N_{t\bar{c},\text{reco}}^j + N_{t\bar{l},\text{reco}}^j \right),$$

and in the lepton + jets channel,

$$\mathcal{B}^j = \alpha_c N_{t\bar{c},\text{reco}}^j + \alpha_l N_{t\bar{l},\text{reco}}^j,$$

where $N_{t\bar{c},\text{reco}}^j$ and $N_{t\bar{l},\text{reco}}^j$ are the numbers of reconstructed $t\bar{c}$ and $t\bar{l}$ events in bin j , as predicted by MC simulation, respectively. Next, an acceptance correction, f_{accept}^j , is applied, which corrects for the fiducial acceptance and is defined as the probability of a $t\bar{b}$ event passing the detector-level selection in a given bin j ($N_{t\bar{b},\text{reco}}^j$) to also fall within the fiducial particle-level phase space ($N_{t\bar{b},\text{reco}\wedge\text{part}}^j$). It is estimated as

$$f_{\text{accept}}^j = \frac{N_{t\bar{b},\text{reco}\wedge\text{part}}^j}{N_{t\bar{b},\text{reco}}^j}.$$

The detector-level objects are required to be matched within $\Delta R = 0.4$ to the corresponding particle-level objects. This requirement leads to a better correspondence between the particle and detector levels and improves the unfolding performance. The matching factor f_{matching}^j is defined as

$$f_{\text{matching}}^j = \frac{N_{t\bar{b},\text{reco}\wedge\text{part}\wedge\text{matched}}^j}{N_{t\bar{b},\text{reco}\wedge\text{part}}^j},$$

where $N_{t\bar{b},\text{reco}\wedge\text{part}\wedge\text{matched}}^j$ is the subset of reconstructed events falling in the particle-level fiducial volume which are matched to the corresponding particle-level objects.

The remaining part of the unfolding procedure consists of effectively inverting the migration matrix \mathcal{M} to correct for the resolution effects and subsequently correcting for detector inefficiencies. An iterative Bayesian unfolding technique [74], as implemented in the RooUNFOLD software package [75], is used. The matrix, \mathcal{M} , represents the probability for a particle-level event in bin i to be reconstructed in bin j . The chosen binning is optimised for each distribution to have a migration matrix with a large fraction of events on the diagonal and a sufficient number of events in each bin. The Bayesian unfolding technique performs the effective matrix inversion, \mathcal{M}_{ij}^{-1} , iteratively. Four iterations are used for all measured distributions.

Finally, the factor f_{eff}^i corrects for the reconstruction efficiency and is defined as

$$f_{\text{eff}}^i = \frac{N_{t\bar{b},\text{part}\wedge\text{reco}\wedge\text{matched}}^i}{N_{t\bar{b},\text{part}}^i},$$

where $N_{t\bar{b},\text{part}}^i$ is the number of $t\bar{b}$ events passing the particle-level selection in bin i and $N_{t\bar{b},\text{part}\wedge\text{reco}\wedge\text{matched}}^i$ is the number of $t\bar{b}$ events at particle level in bin i that also pass the detector-level selection, containing matched objects.

The unfolding procedure for an observable X at particle level can be summarised by the following expression

$$\frac{d\sigma^{\text{fid}}}{dX^i} = \frac{N_{\text{unfold}}^i}{\mathcal{L} \Delta X^i} = \frac{1}{\mathcal{L} \Delta X^i f_{\text{eff}}^i} \sum_j \mathcal{M}_{ij}^{-1} f_{\text{matching}}^j f_{\text{accept}}^j f_{t\bar{t}b}^j (N_{\text{data}}^j - N_{\text{non-}t\bar{t}\text{-bkg}}^j),$$

where ΔX^i is the bin width, N_{unfold}^i is the number of events in bin i of the unfolded distribution and \mathcal{L} is the integrated luminosity. In this paper, the integrated fiducial cross-section σ^{fid} is obtained from

$$\sigma^{\text{fid}} = \int \frac{d\sigma^{\text{fid}}}{dX} dX = \frac{\sum N_{\text{unfold}}^i}{\mathcal{L}}$$

and is used as a normalisation factor such that results are presented in terms of a relative differential cross-section as $1/\sigma^{\text{fid}} \cdot d\sigma^{\text{fid}}/dX^i$.

8 Systematic uncertainties

In this section, the statistical and systematic uncertainties considered in this analysis are described. Experimental sources of uncertainty are described in Section 8.1, sources of uncertainty due to $t\bar{t}$ modelling are described in Section 8.2 and uncertainties due to the treatment of the $t\bar{t}$ ($t\bar{t}c$ and $t\bar{t}l$) and non- $t\bar{t}$ background processes are described in Sections 8.3 and 8.4, respectively. The method used to propagate the effects of systematics uncertainties to the final results are described in Section 8.5. The impact of these uncertainties on the fiducial and differential cross-section measurements are discussed in Section 9.

8.1 Experimental uncertainties

The uncertainty in the combined 2015+2016 integrated luminosity is 2.1%. It is derived, following a methodology similar to that detailed in Ref. [76], and using the LUCID-2 detector for the baseline luminosity measurements [77], from a calibration of the luminosity scale using x - y beam-separation scans.

The uncertainty in the pile-up reweighting of the reconstructed events in the MC simulation is estimated by comparing the distribution of the number of primary vertices in the MC simulation with the one in data as a function of the instantaneous luminosity. Differences between these distributions are adjusted by scaling the mean number of pp interactions per bunch crossing in the MC simulation and the $\pm 1\sigma$ uncertainties are assigned to these scaling factors. The pile-up weights are recalculated after varying the scale factors within their uncertainties.

As discussed in Section 4, scale factors to correct differences seen in the lepton reconstruction, identification and trigger efficiency between the data and MC simulation are derived using a tag-and-probe technique in $Z \rightarrow e^+e^-$ and $Z \rightarrow \mu^+\mu^-$ events [63, 64, 78]. The electron (muon) momentum scale and resolution are determined using the measurement of the position and width of the Z boson peak in $Z \rightarrow e^+e^- (\mu^+\mu^-)$ events [63, 64, 78]. The lepton uncertainties considered in this analysis are considerably smaller than the jet and flavour-tagging uncertainties.

The JVT is calibrated using $Z (\rightarrow \mu\mu) +$ jet events where the jet balances the p_T of the Z boson. Scale factors binned in jet p_T are applied to each event in order to correct for small differences in the JVT efficiency

between the data and MC simulation. The scale factors are 0.963 ± 0.006 for jets with $20 < p_T < 30$ GeV, getting closer to one with smaller uncertainties as the jet p_T increases. The uncertainty in the efficiency to pass the JVT requirement is evaluated by varying the scale factors within their uncertainties [79].

Jets are calibrated using a series of simulation-based corrections and *in situ* techniques [67]. The uncertainties due to the jet energy scale (JES) are estimated using a combination of simulations, test-beam data and *in situ* measurements. Contributions from the jet-flavour composition, η -intercalibration, leakage of the hadron showers beyond the extent of the hadronic calorimeters (punch-through), single-particle response, calorimeter response to different jet flavours, and pile-up are taken into account, resulting in 21 orthogonal uncertainty components. The total uncertainty due to the JES is one of the dominant uncertainties in this analysis.

The jet energy resolution (JER) is measured using both data and simulation. First, the “true” resolution is measured by comparing the particle and reconstructed jet p_T in MC simulation as a function of the jet p_T and η . Second, an *in situ* measurement of the JER is made using the *bisector* method in dijet events [80]. The resolution in data and MC simulation are compared and the energies of jets in the MC simulation are smeared to match the resolution observed in data. The uncertainties in the JER stem from uncertainties in both the modelling and the data-driven method.

Differences in the b -tagging and c -jet mis-tag efficiencies between the data and MC simulation are corrected using scale factors derived from dilepton $t\bar{t}$ events and lepton + jets $t\bar{t}$ events, respectively. A negative-tag method is used to calibrate mis-tagged light-flavour (u, d, s) jets [81]. The scale factors are measured for different b -tagging working points and as a function of jet kinematics, namely the jet p_T for the b -tagging efficiency and c -jet mis-tag scale factors, and the jet p_T and η for the light-flavour jet mis-tag scale factors. The c -jet and light-jet mis-tag scale factors are known to a precision of 6–22% [82] and 15–75% [81], respectively. The associated flavour-tagging uncertainties, split into eigenvector components, are computed by varying the scale factors within their uncertainties. In total, there are 30 components related to the b -tagging efficiencies and 15 (80) components related to the mis-tag rates of c -jets (light-flavour jets). Due to the large number of b -tagged jets in each event used in this analysis, the total uncertainty due to b -tagging is one of the dominant uncertainties in this analysis.

8.2 Modelling systematic uncertainties

Uncertainties due to the choice of $t\bar{t}$ MC generator are evaluated by unfolding alternative $t\bar{t}$ samples, described in Section 3 and presented in Table 1, with the nominal unfolding set-up. Uncertainties related to the choice of matrix element generator (labelled “generator” uncertainty) are evaluated using the SHERPA 2.2 $t\bar{t}$ sample. This generator comes with its own parton shower and hadronisation model; hence these are included in the variation. Uncertainties due to the choice of parton shower and hadronisation model are evaluated using the PowHEG+HERWIG 7 sample, in which only the parton shower and hadronisation model is varied relative to the nominal PowHEG+PYTHIA 8 sample. Additionally, two MC samples are used to evaluate an uncertainty in the modelling of initial- and final-state radiation, namely the RadHi and RadLo samples described in Section 3.

The uncertainty due to the choice of PDF is evaluated following the PDF4LHC prescription [83] using event weights that are available in the nominal PowHEG+PYTHIA 8 sample. The uncertainty in the $t\bar{t}H$ cross-section is evaluated by scaling the $t\bar{t}H$ component of the prediction by factors of zero and two, with the nominal values being taken from theoretical predictions. A factor of two is chosen as this is the current 95% confidence-level upper limit on the $t\bar{t}H \rightarrow b\bar{b}$ signal strength as measured by ATLAS [12].

The uncertainty in the $t\bar{t}V$ cross-section is evaluated by varying the $t\bar{t}V$ component of the prediction up and down by 30% to cover the measured uncertainty in this process [84].

8.3 Uncertainty in $t\bar{t}c$ and $t\bar{t}l$ background

Since the $t\bar{t}c$ and $t\bar{t}l$ backgrounds in the $e\mu$ channel are determined within a single fit, the uncertainty in this result is determined by changing the sample composition. This is achieved by loosening the b -tagging requirement on the jet with the third-highest b -tagging discriminant value, such that it is tagged at the 85% b -tagging efficiency working point or not required to be b -tagged at all. This results in the templates having more bins and allows the likelihood to be modified such that three free parameters are used in the fit. The number of expected events is then given by Eq. (1). With these looser selections the values of α_c vary by about 40% and this is used as a systematic uncertainty in the $t\bar{t}c$ template. The validity of this uncertainty is checked by investigating the variations in the values of the $t\bar{t}c$ scale factors after fitting to pseudo-data from alternative MC samples and it is found to cover the uncertainties in the $t\bar{t}c$ template modelling. The values of α_l remain consistent within the statistical uncertainty in fits with looser selections. After propagating the uncertainty in the $t\bar{t}c$ template through the nominal fit set-up, by varying the input $t\bar{t}c$ template by $\pm 40\%$ before performing the fit, the value of α_b is found to change by $\pm 11\%$, while the value of α_{cl} changes by $\pm 7\%$. When evaluating systematic uncertainties related to the choice of $t\bar{t}$ model in the $e\mu$ channel, double counting of these uncertainties with uncertainties associated with the difference of $t\bar{t}b$, $t\bar{t}c$ and $t\bar{t}l$ fractions in the alternative MC samples is avoided by repeating the flavour-composition fits for each systematic model.

In the lepton + jets channel uncertainties in the flavour composition are taken directly from the samples used to evaluate systematic uncertainties in the modelling, as described in Section 8.2.

8.4 Uncertainty in non- $t\bar{t}$ background estimation

The uncertainty in the single-top background is evaluated by comparing the nominal single-top tW sample (with overlap with $t\bar{t}$ removed via the diagram-removal scheme) with an alternative sample generated using the diagram-subtraction scheme [53]. Potential effects of QCD radiation on the single-top background are estimated using MC simulation predictions where the renormalisation and factorisation scales were varied by factors of 0.5 and 2. The uncertainty in the inclusive single-top cross-section [59] is taken to be $^{+5\%}_{-4\%}$.

The uncertainty attributed to the W +jets background normalisation is evaluated by varying the renormalisation and factorisation scales in the MC simulation prediction by a factor of two up and down. Furthermore, the uncertainty due to PDFs is estimated by using a set of 100 different PDF eigenvectors recommended in Ref. [83]. An additional uncertainty of 30% is assumed for the normalisation of the W +heavy-flavour jets cross-section, based on MC simulation comparisons performed in the context of Ref. [12].

The uncertainty in the non-prompt or fake lepton background is obtained by varying the estimate of this background by a factor of $\pm 50\%$ ($\pm 100\%$) in the lepton + jets ($e\mu$) channel. No shape uncertainty is applied, as this background is small in both channels.

The uncertainty in the Drell–Yan background normalisation is evaluated by varying the estimate of this background by $\pm 25\%$. It accounts for the impact of the reconstructed-mass resolution of the Z boson in the $Z \rightarrow ee$ and $Z \rightarrow \mu\mu$ events, for the background contribution of the $t\bar{t}$ events in the Z + jets selection, and for differences in the scale factors obtained from each of the individual $Z \rightarrow ee$ and $Z \rightarrow \mu\mu$ decay

channels relative to the nominal scale factor obtained from the combined $Z \rightarrow ee$ and $Z \rightarrow \mu\mu$ sample.

8.5 Propagation of uncertainties

Pseudo-experiments based on 10 000 histogram replicas are performed to evaluate statistical uncertainties for each distribution considered. Each entry for every event is given a random weight drawn from a Poisson distribution with a mean of one. Each of these histograms is then unfolded using the unfolding procedure described in Section 7.2. The standard deviation of each bin across all unfolded histogram replicas is then taken as the statistical uncertainty in that bin. This procedure is similar to simply obtaining pseudo-experiments by directly Poisson-fluctuating the measured data distributions, but has the added advantage that correlations between bins of different distributions are conserved.

This procedure is extended to include all experimental systematic uncertainties. For each systematic uncertainty effect considered, the relative variation due to that uncertainty is obtained at the detector level, using the nominal MC sample. Rather than unfolding each shifted histogram individually, each Poisson-fluctuated data distribution is smeared by all experimental systematic uncertainties simultaneously. For each pseudo-experiment, and for each uncertainty considered, the size of the shift applied is obtained randomly from a Gaussian distribution with a mean of zero and width equal to the relative shift at detector level in each bin due to that uncertainty, producing a new detector-level distribution. The same procedure that is followed for the statistical uncertainty alone is then followed to get the sum of the statistical and experimental systematic uncertainty. When evaluating the systematic uncertainties in this way, the data-driven correction factors are not extracted for each individual pseudo-experiment and instead the values obtained in Section 7.1 are used.

In the case of $t\bar{t}$ modelling systematic uncertainties, detector-level distributions from alternative MC samples are unfolded using the unfolding procedure described in Section 7.2, with the unfolding corrections derived from the nominal PowHEG+PYTHIA 8 sample. The unfolded distributions are compared with the particle-level distribution from the alternative sample and the relative difference in each bin is taken as the systematic uncertainty.

9 Inclusive and differential fiducial cross-section results

The unfolded results are presented in this section as inclusive fiducial cross-sections and as normalised differential fiducial cross-sections as a function of the b -jet multiplicity, global event properties and kinematic variables. Table 5 lists the measured fiducial cross-sections for $t\bar{t}$ production in association with additional at least one and at least two b -jets and Table 6 lists the contributions to the uncertainty in these cross-sections. The most precise cross-section measurements are for the $\geq 3b$ phase space in the $e\mu$ channel, which has an uncertainty of 13%, and the $\geq 6j$, $\geq 4b$ phase space in the lepton + jets channel, which has an uncertainty of 17%. The uncertainties are dominated by systematic uncertainties, which are mainly caused by the uncertainties due to $t\bar{t}$ modelling and the uncertainties related to b -tagging and the jet energy scale. In the $e\mu$ channel, the uncertainty due to the $t\bar{t}c$ fit variations is also significant. This measurement is more precise than the uncertainties in the theoretical predictions of the inclusive cross-section for this process, which are 20%–30% [36]. The results are summarised in Figure 7 after subtracting the MADGRAPH5_aMC@NLO+PYTHIA 8 predicted values of $t\bar{t}H$ and $t\bar{t}V$ cross-sections from the measured fiducial $t\bar{t}b\bar{b}$ cross-section, and compared with $t\bar{t}b\bar{b}$ predictions from SHERPA 2.2 $t\bar{t}b\bar{b}$, PowHEG+PYTHIA 8

and PowHEL+PYTHIA 8 $t\bar{t}b\bar{b}$. This procedure of $t\bar{t}H$ and $t\bar{t}V$ subtraction is also employed for all following figures showing the normalised differential distributions.

Table 5: Measured and predicted fiducial cross-section results for additional b -jet production in the $e\mu$ and the lepton + jets decay channels.

	$e\mu$ [fb]		lepton + jets [fb]	
	$\geq 3b$	$\geq 4b$	$\geq 5j, \geq 3b$	$\geq 6j, \geq 4b$
Measured	181 ± 5 (stat) ± 24 (syst)	27 ± 3 (stat) ± 7 (syst)	2450 ± 40 (stat) ± 690 (syst)	359 ± 11 (stat) ± 61 (syst)
$t\bar{t}X(X = H, V)$ MC	4	2	80	28
Measured – $t\bar{t}X$	177	25	2370	331
SHERPA 2.2 $t\bar{t}b\bar{b}$ (4FS)	103 ± 30	17.3 ± 4.2	1600 ± 530	270 ± 70
POWHEG+PYTHIA 8 $t\bar{t}b\bar{b}$ (4FS)	104	16.5	1520	260
PowHEL+PYTHIA 8 $t\bar{t}b\bar{b}$ (5FS)	152	18.7	1360	290
PowHEL+PYTHIA 8 $t\bar{t}b\bar{b}$ (4FS)	105	18.2	1690	300

Figure 8 shows the normalised fiducial cross-section as a function of the b -jet multiplicity compared with predictions from various MC generator set-ups. A quantitative assessment of the level of agreement between data and the various predictions is performed by calculating a χ^2 for each prediction. The χ^2 is defined as

$$\chi^2 = S_{b-1}^T V^{-1} S_{b-1},$$

where V^{-1} is the inverse of the covariance matrix V , calculated for each variable including all statistical and systematic uncertainties and S_{b-1} is a vector of the differences between the measured and predicted cross-sections being tested. The resulting value of the χ^2 calculation is converted into a p -value using the number of degrees of freedom for each variable, which is the number of bins minus one in the case of the normalised differential cross-sections to reflect the normalisation constraint.

As normalised distributions are used, one element of S_{b-1} is discarded in the calculation along with the corresponding row and column of the covariance matrix. The resulting χ^2 does not depend on the element of S_{b-1} or the row and column of the covariance matrix that is discarded. The resulting χ^2 values are shown in Table 7, where the second column is for the normalised b -jets multiplicity distribution with $N_{b\text{-jets}} \geq 2$ and the last column is for the normalised b -jets multiplicity distribution with $N_{b\text{-jets}} \geq 3$. All MC predictions that calculate the top-quark pair production matrix element at NLO, but rely on the parton shower for high jet multiplicities, predict too few events with three or four b -jets. This suggests that the b -jet production by the parton shower is not optimal in these set-ups. The situation does not improve significantly when the renormalisation and factorisation scales in the matrix element calculation and in the parton shower are changed by factors of 0.5 and 2, as shown in the middle ratio panel of Figure 8. SHERPA 2.2 $t\bar{t}$, which models one additional-parton process at NLO accuracy and up to four additional partons at LO accuracy, is the only one of the presented generators that describes the b -jet production well over the full phase space.

Predictions that include additional massive b -quarks in the matrix element calculation (SHERPA 2.2 $t\bar{t}b\bar{b}$ (4FS), PowHEL+PYTHIA 8 $t\bar{t}b\bar{b}$ (4FS), POWHEG+PYTHIA 8 $t\bar{t}b\bar{b}$ (4FS)) do not provide top-pair production without

Table 6: Main systematic uncertainties in percentage for particle-level measurement of inclusive cross-sections in ≥ 3 b and ≥ 4 b phase space.

Source	Fiducial cross-section phase space			
	$e\mu$		lepton + jets	
	$\geq 3b$ unc. [%]	$\geq 4b$ unc. [%]	$\geq 5j, \geq 3b$ unc. [%]	$\geq 6j, \geq 4b$ unc. [%]
Data statistics	2.7	9.0	1.7	3.0
Luminosity	2.1	2.1	2.3	2.3
Jet	2.6	4.3	3.6	7.2
b -tagging	4.5	5.2	17	8.6
Lepton	0.9	0.8	0.8	0.9
Pile-up	2.1	3.5	1.6	1.3
$t\bar{t}c$ fit variation	5.9	11	-	-
Non- $t\bar{t}$ bkg	0.8	2.0	1.7	1.8
Detector+background total syst.	8.5	14	18	12
Parton shower	9.0	6.5	12	6.3
Generator	0.2	18	16	8.7
ISR/FSR	4.0	3.9	6.2	2.9
PDF	0.6	0.4	0.3	0.1
$t\bar{t}V/t\bar{t}H$	0.7	1.4	2.2	0.3
MC sample statistics	1.8	5.3	1.2	4.3
$t\bar{t}$ modelling total syst.	10	20	21	12
Total syst.	13	24	28	17
Total	13	26	28	17

additional b -jets and cannot be compared with the region with less than three b -jets. Table 7 therefore also includes χ^2 values where the total additional b -jet production has been adjusted through the normalisation to $N_{b\text{-jets}} \geq 3$. The relative rate of one, two and more than two additional b -jets is described well by all predictions. It is also interesting to note that parton shower generators predict the relative rate of one and two additional b -jets well once the total additional b -jet production has also been adjusted through the normalisation to $N_{b\text{-jets}} \geq 3$.

The comparison of the predictions from various MC generators with the data are made after subtracting the simulation-estimated contributions of $t\bar{t}V$ and $t\bar{t}H$ production from the data. The third ratio panel of Figure 8 shows the ratio of predictions of normalised differential cross-sections from **MADGRAPH5_aMC@NLO+PYTHIA 8** including (numerator) and not including (denominator) the contributions from the $t\bar{t}V$ and $t\bar{t}H$ processes. The impact of including these processes in the prediction increases with b -jet multiplicity, resulting in a change of about 10% relative to the QCD $t\bar{t}$ prediction alone in the inclusive four- b -jet bin.

Observables sensitive to the details of the QCD modelling of additional b -jet production are studied in events with at least three b -jets in the $e\mu$ channel and in events with at least four b -jets in the lepton + jets channel. While the sample with at least four b -jets has high signal purity, leading to smaller dependence on

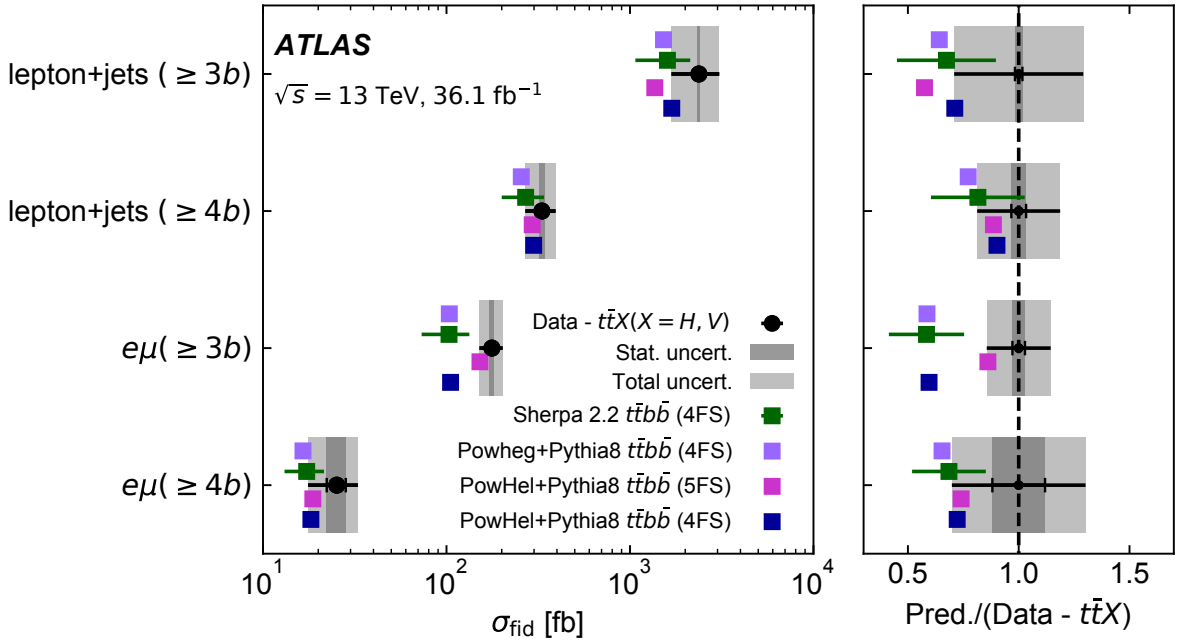


Figure 7: The measured fiducial cross-sections, with $t\bar{t}H$ and $t\bar{t}V$ contributions subtracted from data, compared with $t\bar{t}bb$ predictions obtained using SHERPA 2.2 $t\bar{t}bb$ with uncertainties obtained by varying the renormalisation and factorisation scales by factors of 0.5 and 2.0 and including PDF uncertainties. Comparisons with the central values of the predictions of PowHEG+PYTHIA 8 and PowHEL+PYTHIA 8 $t\bar{t}bb$ are also made. No uncertainties are included in the subtraction of the $t\bar{t}H$ or $t\bar{t}V$ predictions.

Table 7: Values of χ^2 per degree of freedom and p -values between the unfolded normalised cross-section and the predictions for b -jet multiplicity measurements in the $e\mu$ channel. The number of degrees of freedom is equal to the number of bins minus one. Calculations are performed after subtracting estimated contributions from $t\bar{t}H$ and $t\bar{t}V$ from the data. In the two right columns, data and predictions are normalised to cross-section for $N_{b\text{-jets}} \geq 3$ before calculating χ^2 per degree of freedom and p -values.

Generators	$N_{b\text{-jets}} : [2, 3, \geq 4b]$		$N_{b\text{-jets}} : [3, \geq 4b]$	
	χ^2 / NDF	$p\text{-value}$	χ^2 / NDF	$p\text{-value}$
$e\mu$ channel				
POWHEG+PYTHIA 8	18.1 / 2	< 0.01	< 0.01 / 1	1.0
MADGRAPH5_aMC@NLO+PYTHIA 8	14.1 / 2	< 0.01	0.05 / 1	0.83
SHERPA 2.2 $t\bar{t}$	0.85 / 2	0.65	0.06 / 1	0.80
SHERPA 2.2 $t\bar{t}bb$ (4FS)	-	-	0.37 / 1	0.54
PowHEL+PYTHIA 8 $t\bar{t}bb$ (5FS)	-	-	0.33 / 1	0.56
PowHEL+PYTHIA 8 $t\bar{t}bb$ (4FS)	-	-	0.76 / 1	0.38
POWHEG+HERWIG 7	39.4 / 2	< 0.01	0.26 / 1	0.61
POWHEG+PYTHIA 8 $t\bar{t}bb$ (4FS)	-	-	0.28 / 1	0.60
POWHEG+PYTHIA 8 (RadHi)	9.2 / 2	0.01	0.08 / 1	0.77
POWHEG+PYTHIA 8 (RadLo)	27.0 / 2	< 0.01	0.01 / 1	0.92

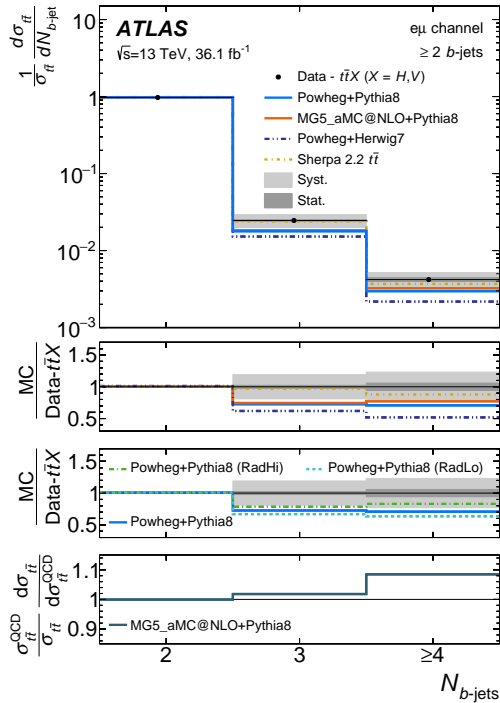


Figure 8: The relative differential cross-section as a function of the b -jet multiplicity in events with at least two b -jets in the $e\mu$ channel compared with various MC generators. The $t\bar{t}H$ and $t\bar{t}V$ contributions are subtracted from data. Three ratio panels are shown, the first two of which show the ratios of various predictions to data. The third panel shows the ratio of predictions of normalised differential cross-sections from **MADGRAPH5_aMC@NLO+PYTHIA 8** including (numerator) and not including (denominator) the contributions from $t\bar{t}V$ and $t\bar{t}H$ production. Uncertainty bands represent the statistical and total systematic uncertainties as described in Section 8.

the MC models, the $e\mu$ channel benefits from an order of magnitude larger size of the sample containing at least three b -jets.

Distributions for H_T and H_T^{had} are shown in Figures 9 and 10. Assessments of the level of agreement between data and the various MC predictions are presented in Table 8. The data are well described by all MC models in both channels within uncertainties of 10%–30%, except for **MADGRAPH5_aMC@NLO+PYTHIA 8**, which shows poor agreement in the lepton + jets channel. Major contributions of systematics uncertainties in the measurement from various sources are illustrated in Figure 11. Parton shower modelling is the dominant uncertainty in most regions of H_T^{had} . Similar uncertainties are found in the measurement of H_T , where the low H_T region has relatively larger uncertainties due to QCD radiation scale variations because of softer jets contributing to this region.

The p_T distributions of the p_T -ordered b -jets are shown in Figure 12 and Figure 13 for events with ≥ 3 b -jets in the $e\mu$ channel and ≥ 4 b -jets in the lepton + jets channel, respectively, with quantitative assessments of the level of data–MC agreement shown in Table 9. Most MC predictions describe the data well, except **PowHEG+PYTHIA 8** $t\bar{t}bb$ (5FS) for the leading and third-highest p_T b -jets in events with ≥ 3 b -jets in the $e\mu$ channel. As the b -jets from the top-quark decays have a tendency to be harder than the b -jets from additional b -quark production via gluon splitting, the leading and sub-leading b -jet distributions have relatively higher probability to contain the b -jets from the top-quark decays, while the third and the fourth

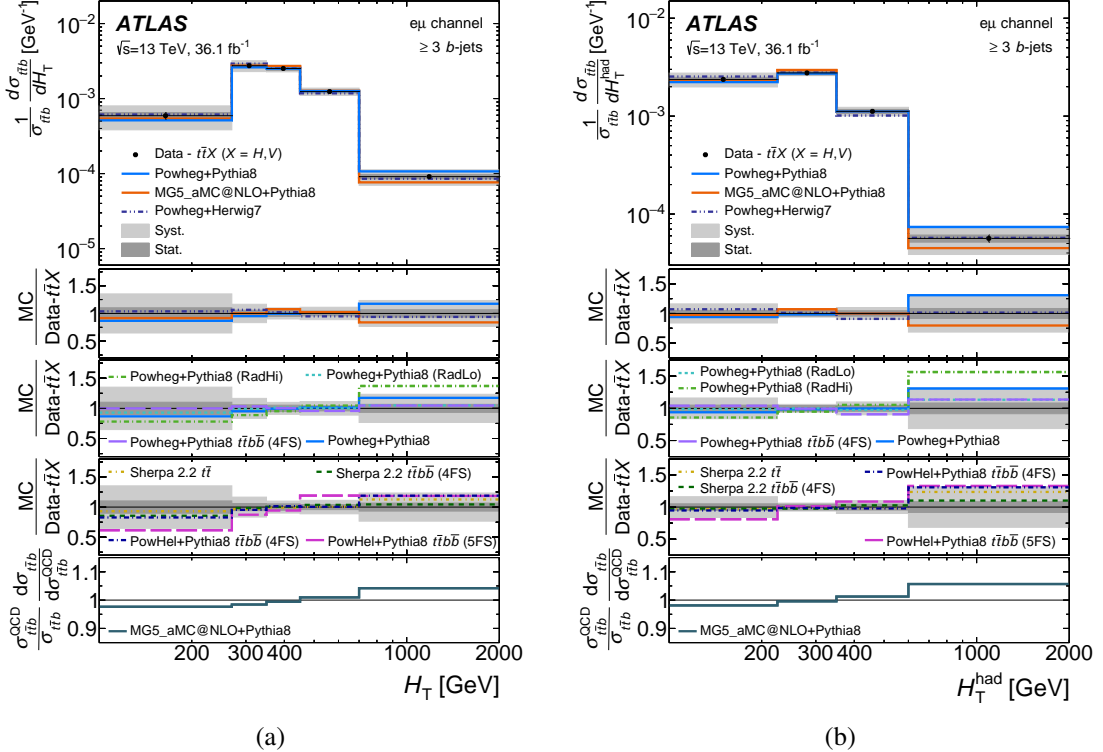


Figure 9: Relative differential cross-sections as a function of (a) H_T , (b) H_T^{had} in events with at least three b -jets in the $e\mu$ channel compared with various MC generators. The $t\bar{t}H$ and $t\bar{t}V$ contributions are subtracted from data. Four ratio panels are shown, the first three of which show the ratios of various predictions to data. The last panel shows the ratio of predictions of normalised differential cross-sections from **MADGRAPH5_aMC@NLO+PYTHIA 8** including (numerator) and not including (denominator) the contributions from $t\bar{t}V$ and $t\bar{t}H$ production. Uncertainty bands represent the statistical and total systematic uncertainties as described in Section 8. Events with H_T (H_T^{had}) values outside the axis range are not included in the plot.

b -jet distributions contain mainly jets from gluon splitting. The measurement uncertainties are between 10% and 25% depending on the p_T of the jet and the top-quark decay channel. Statistical uncertainties are dominant in only the highest p_T bins. The uncertainties are dominated by systematic uncertainties in the jet-energy scale and the b -tagging algorithm.

Figures 14 and 15 show the distribution of the mass, the angular distance ΔR and p_T of the $b_1 b_2$ system built from the two highest- p_T b -jets. The p_T of the $b_1 b_2$ system is measured with a precision of 10%–15% over the full range in the $e\mu$ channel and with an uncertainty of 20%–25% in the lepton + jets channel. It is well described by the different MC predictions, which vary significantly less than the experimental uncertainty. The distributions of the ΔR between the two b -jets and the invariant mass of the $b_1 b_2$ pair are measured with slightly higher uncertainties and also show little variation between the different predictions. Good agreement between the data and the models is confirmed by the p -values listed in Table 10.

Figures 16 and 17 show the same observables but reconstructed from the pair of two closest b -jets in the event, i.e. those with the smallest ΔR , denoted by $m_{bb}^{\Delta\text{min}}$, $p_{T,bb}^{\Delta\text{min}}$, and $\Delta R^{\Delta\text{min}}(b, b)$. The experimental uncertainties are similar to those using the b -jet pair with the highest p_T . However, the model variations are larger and PowHeL+PYTHIA 8 $t\bar{t}b\bar{b}$ (5FS) does not describe the data with ≥ 3 b -jets in the $e\mu$ channel

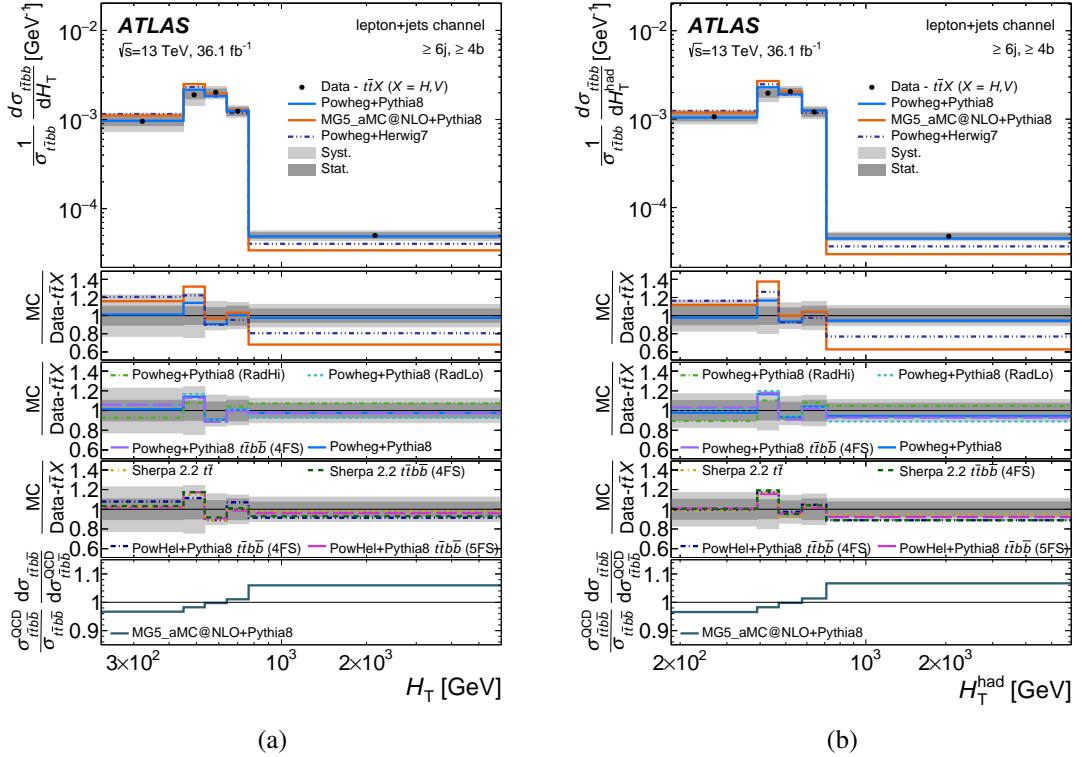


Figure 10: Relative differential cross-sections as a function of (a) H_T , (b) H_T^{had} in events with at least four b -jets in the lepton + jets channel compared with various MC generators. The $t\bar{t}H$ and $t\bar{t}V$ contributions are subtracted from data. Four ratio panels are shown, the first three of which show the ratios of various predictions to data. The last panel shows the ratio of predictions of normalised differential cross-sections from **MADGRAPH5_aMC@NLO+PYTHIA 8** including (numerator) and not including (denominator) the contributions from $t\bar{t}V$ and $t\bar{t}H$ production. Uncertainty bands represent the statistical and total systematic uncertainties as described in Section 8. Events with H_T (H_T^{had}) values outside the axis range are not included in the plot.

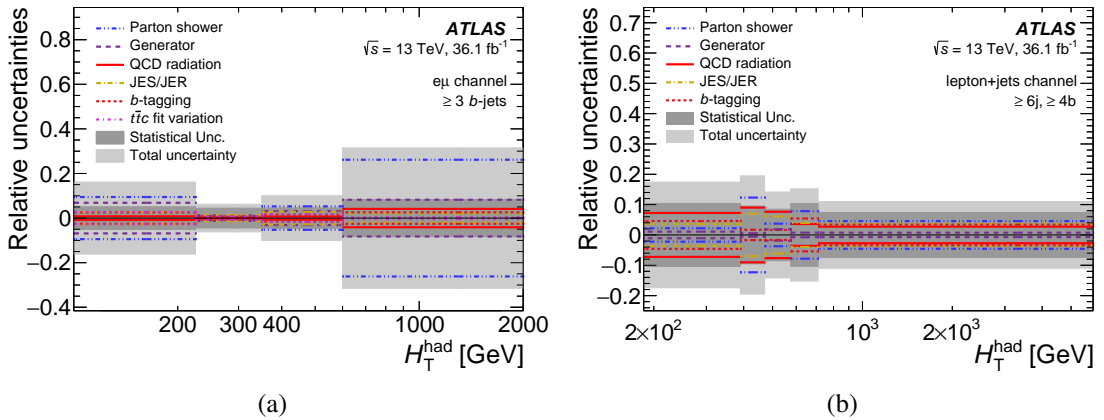


Figure 11: Relative systematic uncertainties from various theoretical and experimental sources for H_T^{had} variable measured in the (a) $e\mu$ and (b) lepton + jets channels.

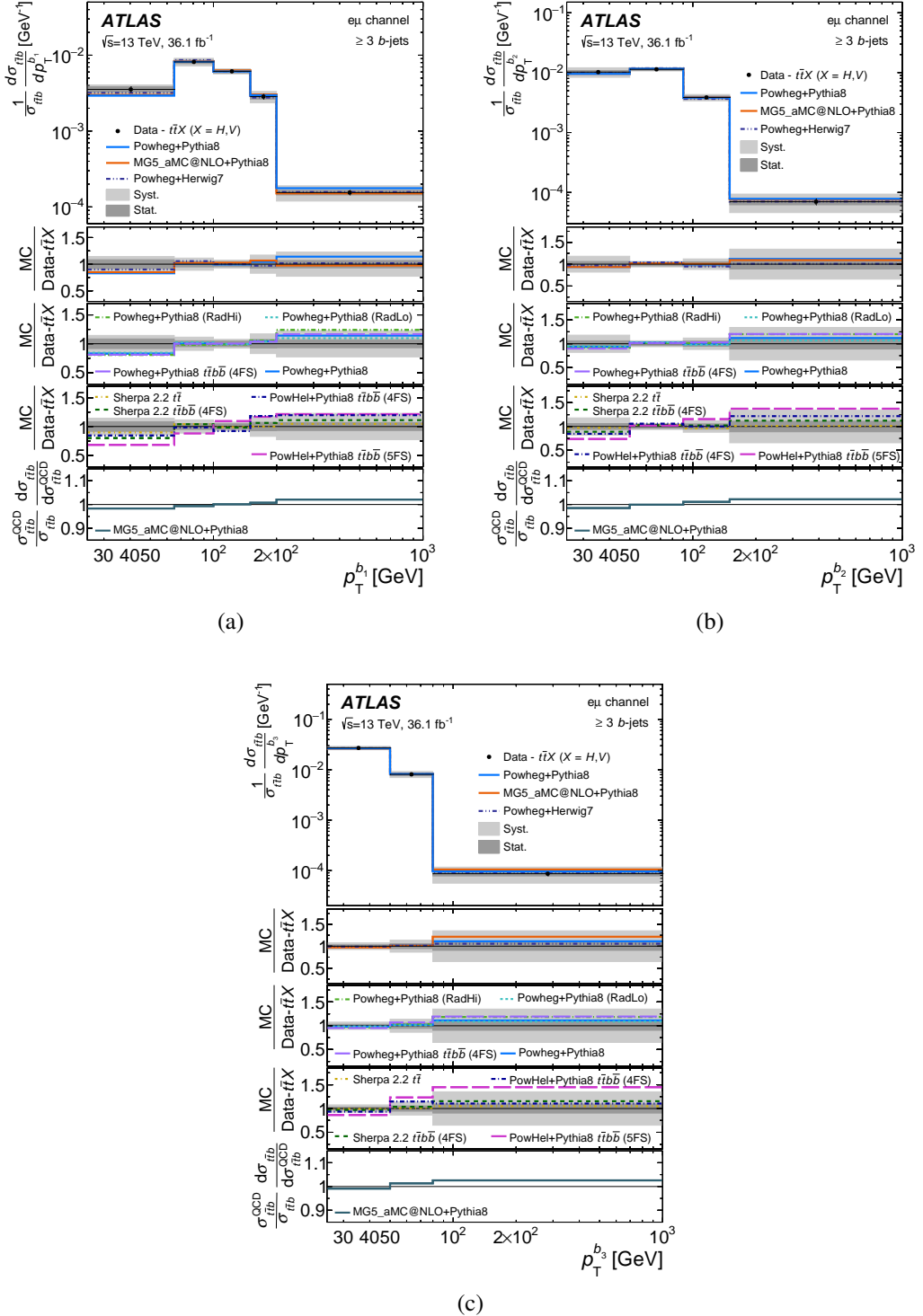


Figure 12: Relative differential cross-sections as a function of b -jets p_T for p_T -ordered b -jets in events with at least three b -jets in the $e\mu$ channel compared with various MC generators. The $t\bar{t}H$ and $t\bar{t}V$ contributions are subtracted from data. (a) leading b -jet p_T , (b) sub-leading b -jet p_T , (c) third-leading b -jet p_T . Four ratio panels are shown, the first three of which show the ratios of various predictions to data. The last panel shows the ratio of predictions of normalised differential cross-sections from `MADGRAPH5_aMC@NLO+PYTHIA 8` including (numerator) and not including (denominator) the contributions from $t\bar{t}V$ and $t\bar{t}H$ production. Uncertainty bands represent the statistical and total systematic uncertainties as described in Section 8. Events with b -jets p_T values outside the axis range are not included in the plot.

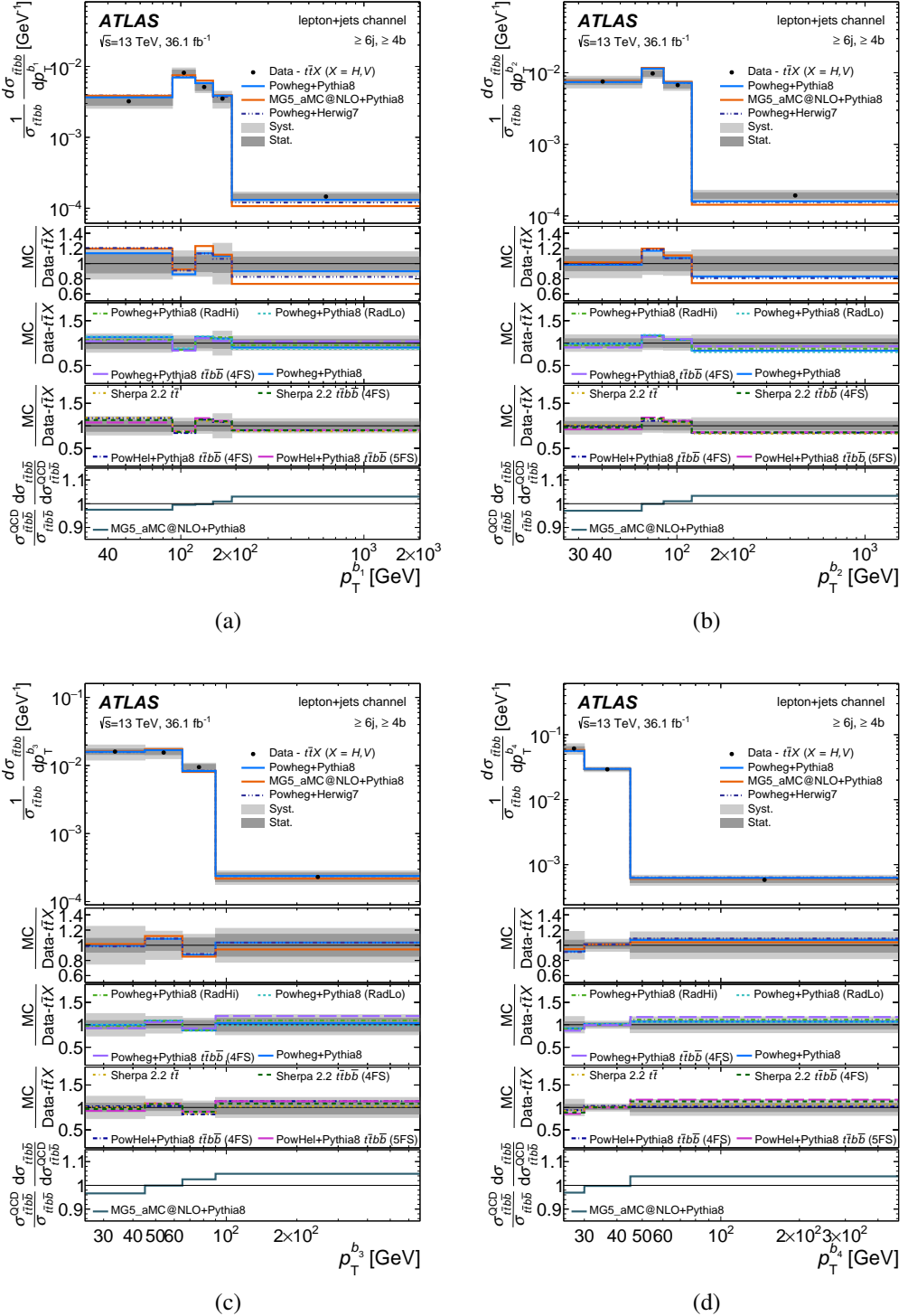


Figure 13: Relative differential cross-sections as a function of b -jets p_T for p_T -ordered b -jets in events with at least four b -jets in the lepton + jets channel compared with various MC generators. The $t\bar{t}H$ and $t\bar{t}V$ contributions are subtracted from data. (a) leading b -jet p_T , (b) sub-leading b -jet p_T , (c) third-leading b -jet p_T , (d) fourth-leading b -jet p_T . Four ratio panels are shown, the first three of which show the ratios of various predictions to data. The last panel shows the ratio of predictions of normalised differential cross-sections from `MADGRAPH5_aMC@NLO+PYTHIA 8` including (numerator) and not including (denominator) the contributions from $t\bar{t}V$ and $t\bar{t}H$ production. Uncertainty bands represent the statistical and total systematic uncertainties as described in Section 8. Events with b -jets p_T values outside the axis range are not included in the plot.

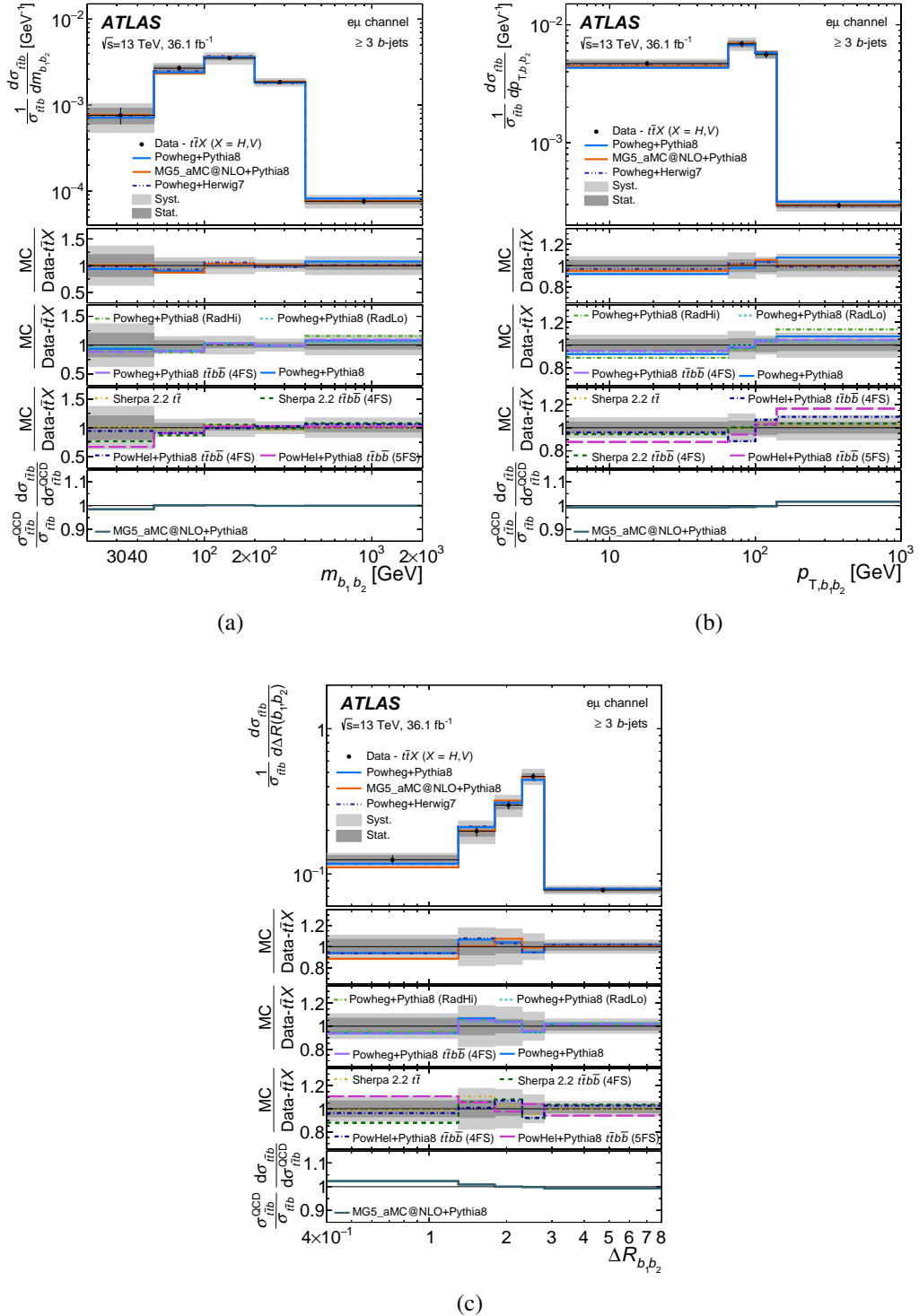


Figure 14: Relative differential cross-sections as a function of (a) $m_{b_1 b_2}$, (b) $p_{T,b_1 b_2}$, and (c) $\Delta R_{b_1, b_2}$ of two highest- p_T b -jets in events with at least three b -jets in the $e\mu$ channel compared with various MC generators. The $t\bar{t}H$ and $t\bar{t}V$ contributions are subtracted from data. Four ratio panels are shown, the first three of which show the ratios of various predictions to data. The last panel shows the ratio of predictions of normalised differential cross-sections from MADGRAPH5_aMC@NLO+PYTHIA 8 including (numerator) and not including (denominator) the contributions from $t\bar{t}V$ and $t\bar{t}H$ production. Uncertainty bands represent the statistical and total systematic uncertainties as described in Section 8. Events with observable values outside the axis range are not included in the plot.

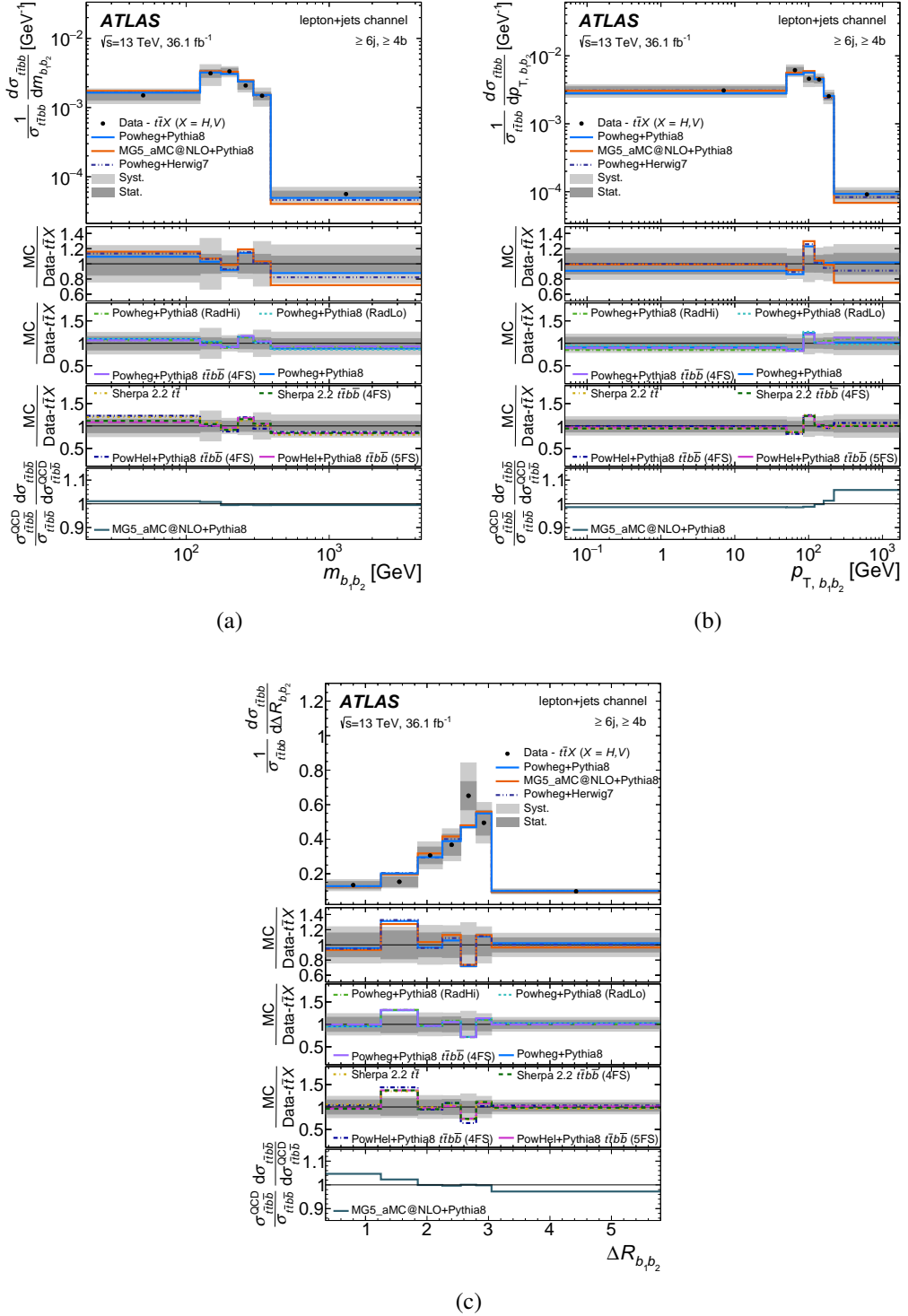


Figure 15: Relative differential cross-sections as a function of (a) $m_{b_1 b_2}$, (b) $p_{T,b_1 b_2}$, and (c) $\Delta R_{b_1 b_2}$ of the two highest- p_T b -jets in events with at least four b -jets in the lepton + jets channel compared with various MC generators. The $t\bar{t}H$ and $t\bar{t}V$ contributions are subtracted from data. Four ratio panels are shown, the first three of which show the ratios of various predictions to data. The last panel shows the ratio of predictions of normalised differential cross-sections from MADGRAPH5_aMC@NLO+PYTHIA 8 including (numerator) and not including (denominator) the contributions from $t\bar{t}V$ and $t\bar{t}H$ production. Uncertainty bands represent the statistical and total systematic uncertainties as described in Section 8. Events with observable values outside the axis range are not included in the plot.

Table 8: Values of χ^2 per degree of freedom and p -values between the unfolded normalised cross-sections and the various predictions for the H_T and H_T^{had} measurements in the $e\mu$ and lepton + jets channels. The number of degrees of freedom is equal to the number of bins in the measured distribution minus one.

Generator	H_T χ^2 / NDF	p -value	H_T^{had} χ^2 / NDF	p -value
$e\mu$ channel, $\geq 3 b$-jets				
POWHEG+PYTHIA 8	0.95 / 4	0.92	2.68 / 3	0.44
MADGRAPH5_aMC@NLO+PYTHIA 8	3.71 / 4	0.45	3.72 / 3	0.29
SHERPA 2.2 $t\bar{t}$	0.58 / 4	0.97	2.26 / 3	0.52
SHERPA 2.2 $t\bar{t}b\bar{b}$ (4FS)	0.35 / 4	0.99	0.40 / 3	0.94
PowHEL+PYTHIA 8 $t\bar{t}b\bar{b}$ (5FS)	4.88 / 4	0.30	1.85 / 3	0.60
PowHEL+PYTHIA 8 $t\bar{t}b\bar{b}$ (4FS)	1.39 / 4	0.85	3.33 / 3	0.32
POWHEG+HERWIG 7	0.26 / 4	0.99	2.28 / 3	0.52
POWHEG+PYTHIA 8 $t\bar{t}b\bar{b}$ (4FS)	0.63 / 4	0.96	3.93 / 3	0.27
POWHEG+PYTHIA 8 (RadHi)	4.09 / 4	0.39	6.43 / 3	0.09
POWHEG+PYTHIA 8 (RadLo)	0.14 / 4	1.0	1.06 / 3	0.79
lepton+jets channel, ≥ 6 jets, $\geq 4 b$-jets				
POWHEG+PYTHIA 8	0.60 / 4	0.96	1.41 / 4	0.84
MADGRAPH5_aMC@NLO+PYTHIA 8	9.88 / 4	0.04	17.6 / 4	< 0.01
SHERPA 2.2 $t\bar{t}$	0.72 / 4	0.95	1.38 / 4	0.85
SHERPA 2.2 $t\bar{t}b\bar{b}$ (4FS)	1.09 / 4	0.90	2.58 / 4	0.63
PowHEL+PYTHIA 8 $t\bar{t}b\bar{b}$ (5FS)	0.81 / 4	0.94	1.40 / 4	0.84
PowHEL+PYTHIA 8 $t\bar{t}b\bar{b}$ (4FS)	1.38 / 4	0.85	2.38 / 4	0.67
POWHEG+HERWIG 7	4.27 / 4	0.37	7.00 / 4	0.14
POWHEG+PYTHIA 8 $t\bar{t}b\bar{b}$ (4FS)	0.72 / 4	0.95	1.71 / 4	0.79
POWHEG+PYTHIA 8 (RadHi)	0.94 / 4	0.92	0.96 / 4	0.92
POWHEG+PYTHIA 8 (RadLo)	1.15 / 4	0.89	2.57 / 4	0.63

well.

10 Summary

Measurements of inclusive and normalised differential cross-sections of pairs of top-quarks in association with heavy-flavour jets in 13 TeV pp collisions are presented using a data sample of 36.1 fb^{-1} collected by the ATLAS detector at the LHC. The results are shown in both the $e\mu$ and lepton + jets channels within fiducial phase spaces. The background coming from $t\bar{t}$ production in association with additional light-flavour and charm-quark jets is evaluated using a fit to a binned b -tagging discriminant. The data after background subtraction are unfolded to particle level to correct for detector and acceptance effects. The fiducial cross-sections are measured for $\geq 3b$ and $\geq 4b$ phase spaces in the $e\mu$ channel, and for $\geq 5j$, $\geq 3b$ and $\geq 6j$, $\geq 4b$ phase spaces in the lepton + jets channel. The two cross-section measurements with the smallest uncertainties, 13% and 17%, are those for $\geq 3b$ in the $e\mu$ channel and $\geq 6j$, $\geq 4b$ in the lepton + jets channel, respectively. The measured cross-sections, after subtracting estimated contributions from $t\bar{t}H$ and $t\bar{t}V$, are compared with various $t\bar{t}b\bar{b}$ predictions and are found to be higher than predicted but compatible within the uncertainties.

Table 9: Values of χ^2 per degree of freedom and p -values between the unfolded normalised cross-sections and the various predictions for the three (four) leading b -jet p_T measurements in the $e\mu$ (lepton + jets) channel. The number of degrees of freedom is equal to the number of bins in the measured distribution minus one.

Generator	χ^2 / NDF	p -value	$p_T^{b_1}$	χ^2 / NDF	p -value	$p_T^{b_2}$	χ^2 / NDF	p -value	$p_T^{b_3}$	χ^2 / NDF	p -value	$p_T^{b_4}$	χ^2 / NDF	p -value
$e\mu$ channel, ≥ 3 b-jets														
PowHeg+Pythia 8	2.09 / 4	0.72	0.50 / 3	0.92	0.09 / 2	0.95	-	-	-	-	-	-	-	-
MADGRAPH5_aMC@NLO+Pythia 8	2.62 / 4	0.62	0.27 / 3	0.97	0.33 / 2	0.85	-	-	-	-	-	-	-	-
SHERPA 2.2 $t\bar{t}$	0.98 / 4	0.91	0.67 / 3	0.88	0.02 / 2	0.99	-	-	-	-	-	-	-	-
SHERPA 2.2 $t\bar{t}bb\bar{b}$ (4FS)	3.52 / 4	0.47	0.68 / 3	0.88	0.21 / 2	0.90	-	-	-	-	-	-	-	-
PowHel+Pythia 8 $t\bar{t}bb\bar{b}$ (5FS)	10.9 / 4	0.03	2.58 / 3	0.46	3.91 / 2	0.14	-	-	-	-	-	-	-	-
PowHel+Pythia 8 $t\bar{t}bb\bar{b}$ (4FS)	6.21 / 4	0.18	1.96 / 3	0.58	1.30 / 2	0.52	-	-	-	-	-	-	-	-
PowHel+Herwig 7	1.16 / 4	0.89	1.02 / 3	0.80	0.02 / 2	0.99	-	-	-	-	-	-	-	-
PowHeg+Pythia 8 $t\bar{t}bb\bar{b}$ (4FS)	2.62 / 4	0.62	0.53 / 3	0.91	0.46 / 2	0.80	-	-	-	-	-	-	-	-
PowHeg+Pythia 8 (RadHi)	2.71 / 4	0.61	0.56 / 3	0.91	0.26 / 2	0.88	-	-	-	-	-	-	-	-
PowHeg+Pythia 8 (RadLo)	1.93 / 4	0.75	0.64 / 3	0.89	0.05 / 2	0.97	-	-	-	-	-	-	-	-
lepton+jets channel, ≥ 6 jets, ≥ 4 b-jets														
PowHeg+Pythia 8	2.09 / 4	0.72	2.98 / 3	0.40	1.42 / 3	0.70	0.20 / 2	0.90	-	-	-	-	-	-
MADGRAPH5_aMC@NLO+Pythia 8	5.20 / 4	0.27	5.31 / 3	0.15	1.87 / 3	0.60	0.08 / 2	0.96	-	-	-	-	-	-
SHERPA 2.2 $t\bar{t}$	2.01 / 4	0.73	2.46 / 3	0.48	1.75 / 3	0.63	0.15 / 2	0.93	-	-	-	-	-	-
SHERPA 2.2 $t\bar{t}bb\bar{b}$ (4FS)	2.04 / 4	0.73	2.82 / 3	0.42	1.23 / 3	0.75	0.52 / 2	0.77	-	-	-	-	-	-
PowHel+Pythia 8 $t\bar{t}bb\bar{b}$ (5FS)	2.07 / 4	0.72	3.65 / 3	0.30	1.73 / 3	0.63	0.85 / 2	0.65	-	-	-	-	-	-
PowHel+Pythia 8 $t\bar{t}bb\bar{b}$ (4FS)	2.52 / 4	0.64	2.37 / 3	0.50	2.41 / 3	0.49	0.18 / 2	0.91	-	-	-	-	-	-
PowHeg+Herwig 7	2.58 / 4	0.63	3.50 / 3	0.32	1.30 / 3	0.73	0.26 / 2	0.88	-	-	-	-	-	-
PowHeg+Pythia 8 $t\bar{t}bb\bar{b}$ (4FS)	1.76 / 4	0.78	2.02 / 3	0.57	1.83 / 3	0.61	0.84 / 2	0.66	-	-	-	-	-	-
PowHeg+Pythia 8 (RadHi)	1.50 / 4	0.83	2.39 / 3	0.50	1.74 / 3	0.63	0.37 / 2	0.83	-	-	-	-	-	-
PowHeg+Pythia 8 (RadLo)	2.17 / 4	0.70	3.75 / 3	0.29	1.42 / 3	0.70	0.17 / 2	0.92	-	-	-	-	-	-

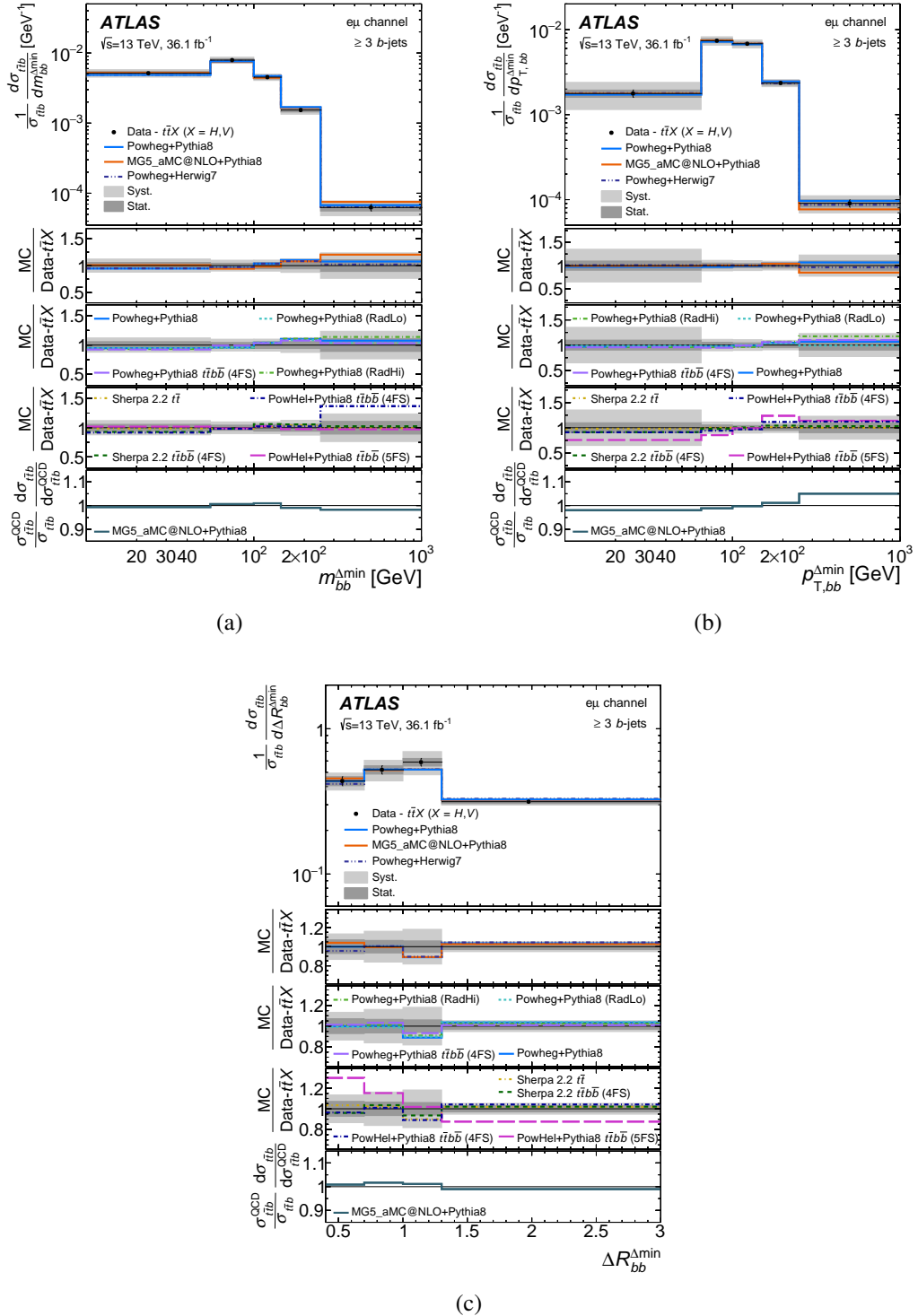


Figure 16: Relative differential cross-sections as a function of (a) $m_{bb}^{\Delta\text{min}}$, (b) $p_{T,bb}^{\Delta\text{min}}$ and (c) $\Delta R_{bb}^{\Delta\text{min}}$ of two closest b -jets in ΔR in events with at least three b -jets in the $e\mu$ channel compared with various MC generators. The $t\bar{t}H$ and $t\bar{t}V$ contributions are subtracted from data. Four ratio panels are shown, the first three of which show the ratios of various predictions to data. The last panel shows the ratio of predictions of normalised differential cross-sections from MADGRAPH5_aMC@NLO+PYTHIA 8 including (numerator) and not including (denominator) the contributions from $t\bar{t}V$ and $t\bar{t}H$ production. Uncertainty bands represent the statistical and total systematic uncertainties as described in Section 8. Events with observable values outside the axis range are not included in the plot.

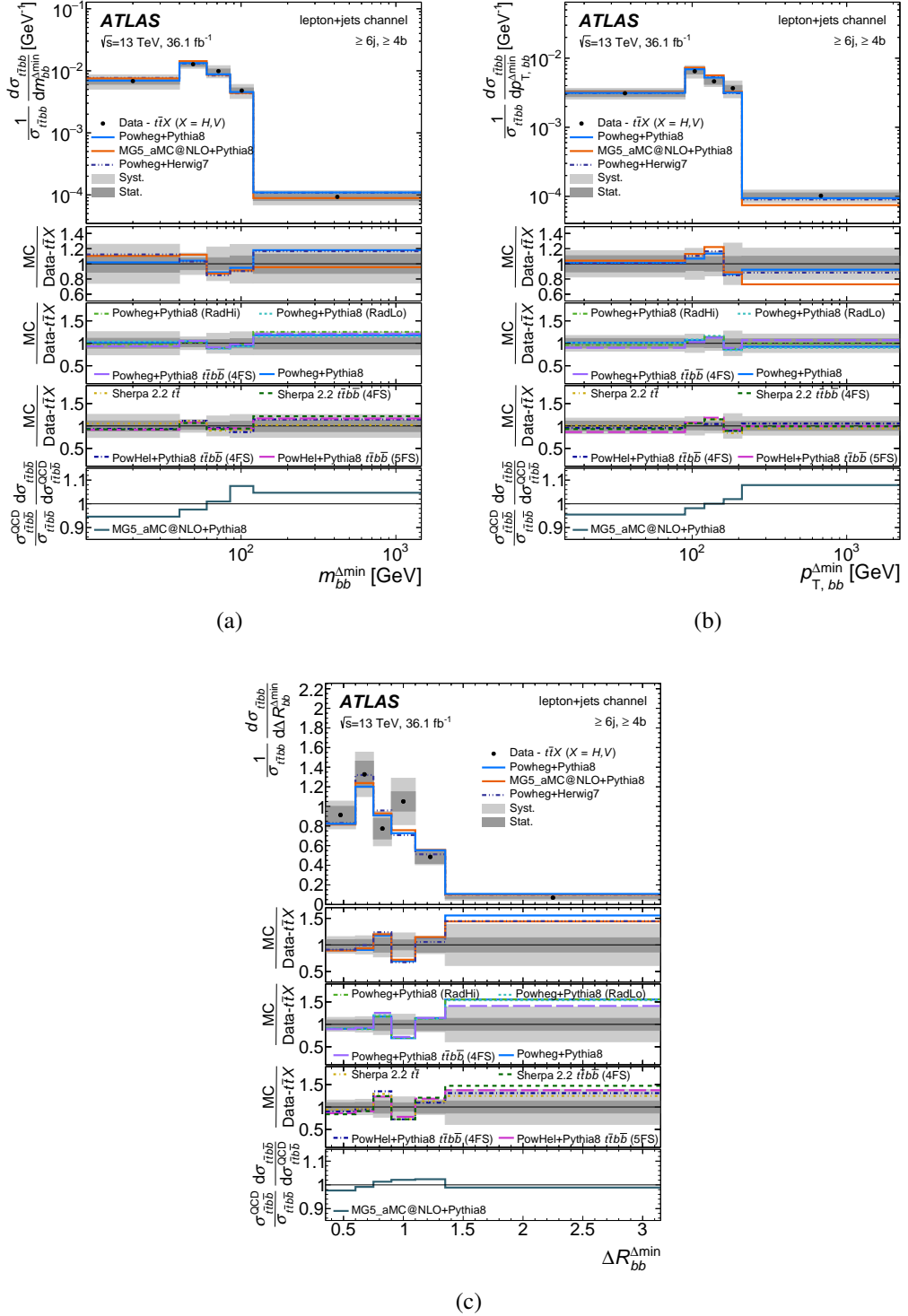


Figure 17: Relative differential cross-sections as a function of (a) $m_{bb}^{\Delta\text{min}}$, (b) $p_{T,bb}^{\Delta\text{min}}$ and (c) $\Delta R_{bb}^{\Delta\text{min}}$ of two closest b -jets in ΔR in events with at least four b -jets in the lepton + jets channel compared with various MC generators. The $t\bar{t}H$ and $t\bar{t}V$ contributions are subtracted from data. Four ratio panels are shown: the first three show the ratios of various predictions to data. The last panel shows the ratio of predictions of normalised differential cross-sections from **MADGRAPH5_aMC@NLO+PYTHIA 8** including (numerator) and not including (denominator) the contributions from $t\bar{t}V$ and $t\bar{t}H$ production. Uncertainty bands represent the statistical and total systematic uncertainties as described in Section 8. Events with observable values outside the axis range are not included in the plot.

Table 10: Values of χ^2 per degree of freedom and p -values between the unfolded normalised cross-sections and the various predictions for the mass, p_T and ΔR of the leading two b -jets in the $e\mu$ and lepton + jets channels. The number of degrees of freedom is equal to the number of bins in the measured distribution minus one.

Generator	$m_{b_1 b_2}$		$p_{T,b_1 b_2}$		$\Delta R_{b_1 b_2}$	
	χ^2 / NDF	$p\text{-value}$	χ^2 / NDF	$p\text{-value}$	χ^2 / NDF	$p\text{-value}$
$e\mu$ channel, ≥ 3 b-jets						
PowHeg+Pythia 8	1.55 / 4	0.82	1.74 / 3	0.63	0.70 / 4	0.95
MADGRAPH5_aMC@NLO+Pythia 8	1.73 / 4	0.79	1.08 / 3	0.78	3.73 / 4	0.44
SHERPA 2.2 $t\bar{t}$	0.25 / 4	0.99	0.64 / 3	0.89	0.99 / 4	0.91
SHERPA 2.2 $t\bar{t}b\bar{b}$ (4FS)	2.88 / 4	0.58	0.76 / 3	0.86	2.88 / 4	0.58
PowHel+Pythia 8 $t\bar{t}b\bar{b}$ (5FS)	3.74 / 4	0.44	4.75 / 3	0.19	4.70 / 4	0.32
PowHel+Pythia 8 $t\bar{t}b\bar{b}$ (4FS)	1.35 / 4	0.85	2.90 / 3	0.41	0.86 / 4	0.93
PowHeg+Herwig 7	0.48 / 4	0.98	0.42 / 3	0.94	0.97 / 4	0.91
PowHeg+Pythia 8 $t\bar{t}b\bar{b}$ (4FS)	1.89 / 4	0.76	0.79 / 3	0.85	0.68 / 4	0.95
PowHeg+Pythia 8 (RadHi)	3.77 / 4	0.44	3.49 / 3	0.32	0.50 / 4	0.97
PowHeg+Pythia 8 (RadLo)	1.04 / 4	0.90	0.95 / 3	0.81	1.01 / 4	0.91
lepton+jets channel, ≥ 6 jets, ≥ 4 b-jets						
PowHeg+Pythia 8	1.82 / 5	0.87	1.66 / 5	0.89	2.48 / 6	0.87
MADGRAPH5_aMC@NLO+Pythia 8	4.11 / 5	0.53	4.63 / 5	0.46	2.90 / 6	0.82
SHERPA 2.2 $t\bar{t}$	2.84 / 5	0.72	1.79 / 5	0.88	3.40 / 6	0.76
SHERPA 2.2 $t\bar{t}b\bar{b}$ (4FS)	2.40 / 5	0.79	1.76 / 5	0.88	3.37 / 6	0.76
PowHel+Pythia 8 $t\bar{t}b\bar{b}$ (5FS)	2.39 / 5	0.79	1.85 / 5	0.87	2.94 / 6	0.82
PowHel+Pythia 8 $t\bar{t}b\bar{b}$ (4FS)	3.71 / 5	0.59	2.49 / 5	0.78	4.79 / 6	0.57
PowHeg+Herwig 7	2.46 / 5	0.78	2.60 / 5	0.76	2.80 / 6	0.83
PowHeg+Pythia 8 $t\bar{t}b\bar{b}$ (4FS)	1.88 / 5	0.87	1.51 / 5	0.91	2.79 / 6	0.83
PowHeg+Pythia 8 (RadHi)	1.68 / 5	0.89	1.67 / 5	0.89	2.72 / 6	0.84
PowHeg+Pythia 8 (RadLo)	1.89 / 5	0.86	2.35 / 5	0.80	2.63 / 6	0.85

The normalised fiducial differential cross-sections are presented as a function of several relevant kinematic variables and global event properties. In general, the different observables are measured with a precision of 10% in most of the phase space, rising to 30% at the edge of the phase space for some of the observables. The observables are well described by most MC predictions in both channels. However, it is worth noting that in all the predictions where additional b -jets are dominantly produced by the parton shower, they predict too few events with more b -jets than those produced in top decays. Only SHERPA 2.2 $t\bar{t}$ describes the full b -jet multiplicity spectrum, and in events with ≥ 3 b -jets it yields the best agreement with data in most of the observables. PowHel+Pythia 8 $t\bar{t}b\bar{b}$ (5FS) shows poor agreement in some of the observables in events with ≥ 3 b -jets in the $e\mu$ channel. The differential kinematic distributions are equally well described by predictions that have additional b -jet production that is generated by the parton shower calculation and by predictions with additional b -quarks in the matrix element.

Acknowledgements

We thank CERN for the very successful operation of the LHC, as well as the support staff from our institutions without whom ATLAS could not be operated efficiently.

Table 11: Values of χ^2 per degree of freedom and p -values between the unfolded normalised cross-sections and the various predictions for the mass, p_T and ΔR of the closest two b -jets in the $e\mu$ and lepton + jets channels. The number of degrees of freedom is equal to the number of bins in the measured distribution minus one.

Generator	$m_{bb}^{\Delta\min}$		$p_{T,bb}^{\Delta\min}$		$\Delta R_{bb}^{\Delta\min}$	
	χ^2 / NDF	$p\text{-value}$	χ^2 / NDF	$p\text{-value}$	χ^2 / NDF	$p\text{-value}$
$e\mu$ channel, ≥ 3 b-jets						
POWHEG+PYTHIA 8	1.37 / 4	0.85	0.42 / 4	0.98	0.78 / 3	0.86
MADGRAPH5_aMC@NLO+PYTHIA 8	3.67 / 4	0.45	2.50 / 4	0.65	1.22 / 3	0.75
SHERPA 2.2 $t\bar{t}$	0.17 / 4	1.0	0.06 / 4	1.0	0.99 / 3	0.80
SHERPA 2.2 $t\bar{t}b\bar{b}$ (4FS)	1.36 / 4	0.85	0.52 / 4	0.97	0.21 / 3	0.98
PowHEL+PYTHIA 8 $t\bar{t}b\bar{b}$ (5FS)	0.18 / 4	1.0	12.7 / 4	0.01	27.9 / 3	< 0.01
PowHEL+PYTHIA 8 $t\bar{t}b\bar{b}$ (4FS)	4.29 / 4	0.37	2.36 / 4	0.67	0.81 / 3	0.85
POWHEG+HERWIG 7	0.87 / 4	0.93	0.06 / 4	1.0	0.95 / 3	0.81
POWHEG+PYTHIA 8 $t\bar{t}b\bar{b}$ (4FS)	1.12 / 4	0.89	1.00 / 4	0.91	0.30 / 3	0.96
POWHEG+PYTHIA 8 (RadHi)	1.94 / 4	0.75	1.31 / 4	0.86	0.51 / 3	0.92
POWHEG+PYTHIA 8 (RadLo)	0.99 / 4	0.91	0.28 / 4	0.99	0.86 / 3	0.84
lepton+jets channel, ≥ 6 jets, ≥ 4 b-jets						
POWHEG+PYTHIA 8	0.86 / 4	0.93	0.99 / 4	0.91	3.22 / 5	0.67
MADGRAPH5_aMC@NLO+PYTHIA 8	1.01 / 4	0.91	4.33 / 4	0.36	3.19 / 5	0.67
SHERPA 2.2 $t\bar{t}$	0.66 / 4	0.96	1.21 / 4	0.88	4.98 / 5	0.42
SHERPA 2.2 $t\bar{t}b\bar{b}$ (4FS)	1.44 / 4	0.84	0.89 / 4	0.93	4.07 / 5	0.54
PowHEL+PYTHIA 8 $t\bar{t}b\bar{b}$ (5FS)	1.08 / 4	0.90	1.61 / 4	0.81	3.14 / 5	0.68
PowHEL+PYTHIA 8 $t\bar{t}b\bar{b}$ (4FS)	1.93 / 4	0.75	0.30 / 4	1.0	5.43 / 5	0.37
POWHEG+HERWIG 7	1.32 / 4	0.86	1.47 / 4	0.83	4.53 / 5	0.48
POWHEG+PYTHIA 8 $t\bar{t}b\bar{b}$ (4FS)	1.05 / 4	0.90	0.82 / 4	0.94	3.87 / 5	0.57
POWHEG+PYTHIA 8 (RadHi)	1.51 / 4	0.83	0.95 / 4	0.92	2.98 / 5	0.70
POWHEG+PYTHIA 8 (RadLo)	0.77 / 4	0.94	1.51 / 4	0.83	3.25 / 5	0.66

We acknowledge the support of ANPCyT, Argentina; YerPhI, Armenia; ARC, Australia; BMWFW and FWF, Austria; ANAS, Azerbaijan; SSTC, Belarus; CNPq and FAPESP, Brazil; NSERC, NRC and CFI, Canada; CERN; CONICYT, Chile; CAS, MOST and NSFC, China; COLCIENCIAS, Colombia; MSMT CR, MPO CR and VSC CR, Czech Republic; DNRF and DNSRC, Denmark; IN2P3-CNRS, CEA-DRF/IRFU, France; SRNSFG, Georgia; BMBF, HGF, and MPG, Germany; GSRT, Greece; RGC, Hong Kong SAR, China; ISF and Benoziyo Center, Israel; INFN, Italy; MEXT and JSPS, Japan; CNRST, Morocco; NWO, Netherlands; RCN, Norway; MNiSW and NCN, Poland; FCT, Portugal; MNE/IFA, Romania; MES of Russia and NRC KI, Russian Federation; JINR; MESTD, Serbia; MSSR, Slovakia; ARRS and MIZŠ, Slovenia; DST/NRF, South Africa; MINECO, Spain; SRC and Wallenberg Foundation, Sweden; SERI, SNSF and Cantons of Bern and Geneva, Switzerland; MOST, Taiwan; TAEK, Turkey; STFC, United Kingdom; DOE and NSF, United States of America. In addition, individual groups and members have received support from BCKDF, CANARIE, CRC and Compute Canada, Canada; COST, ERC, ERDF, Horizon 2020, and Marie Skłodowska-Curie Actions, European Union; Investissements d’Avenir Labex and Idex, ANR, France; DFG and AvH Foundation, Germany; Herakleitos, Thales and Aristeia programmes co-financed by EU-ESF and the Greek NSRF, Greece; BSF-NSF and GIF, Israel; CERCA Programme Generalitat de Catalunya, Spain; The Royal Society and Leverhulme Trust, United Kingdom.

The crucial computing support from all WLCG partners is acknowledged gratefully, in particular from CERN, the ATLAS Tier-1 facilities at TRIUMF (Canada), NDGF (Denmark, Norway, Sweden), CC-IN2P3 (France), KIT/GridKA (Germany), INFN-CNAF (Italy), NL-T1 (Netherlands), PIC (Spain), ASGC (Taiwan), RAL (UK) and BNL (USA), the Tier-2 facilities worldwide and large non-WLCG resource providers. Major contributors of computing resources are listed in Ref. [85].

References

- [1] S. Hoeche et al., *Next-to-leading order QCD predictions for top-quark pair production with up to two jets merged with a parton shower*, *Phys. Lett. B* **748** (2015) 74, arXiv: [1402.6293 \[hep-ph\]](#).
- [2] F. Cascioli, P. Maierhöfer, N. Moretti, S. Pozzorini and F. Siegert, *NLO matching for $t\bar{t}bb$ production with massive b-quarks*, *Phys. Lett. B* **734** (2014) 210, arXiv: [1309.5912 \[hep-ph\]](#).
- [3] M. V. Garzelli, A. Kardos and Z. Trócsányi, *Hadroproduction of $t\bar{t}bb$ final states at LHC: predictions at NLO accuracy matched with Parton Shower*, *JHEP* **03** (2015) 083, arXiv: [1408.0266 \[hep-ph\]](#).
- [4] G. Bevilacqua, M. V. Garzelli and A. Kardos, *$t\bar{t}bb$ hadroproduction with massive bottom quarks with PowHel*, (2017), arXiv: [1709.06915 \[hep-ph\]](#).
- [5] T. Ježo, J. M. Lindert, N. Moretti and S. Pozzorini, *New NLOPS predictions for $t\bar{t} + b$ -jet production at the LHC*, *Eur. Phys. J. C* **78** (2018) 502, arXiv: [1802.00426 \[hep-ph\]](#).
- [6] ATLAS Collaboration, *Observation of a new particle in the search for the Standard Model Higgs boson with the ATLAS detector at the LHC*, *Phys. Lett. B* **716** (2012) 1, arXiv: [1207.7214 \[hep-ex\]](#).
- [7] CMS Collaboration, *Observation of a new boson at a mass of 125 GeV with the CMS experiment at the LHC*, *Phys. Lett. B* **716** (2012) 30, arXiv: [1207.7235 \[hep-ex\]](#).
- [8] ATLAS Collaboration, *Observation of Higgs boson production in association with a top quark pair at the LHC with the ATLAS detector*, *Phys. Lett. B* **784** (2018) 173, arXiv: [1806.00425 \[hep-ex\]](#).
- [9] CMS Collaboration, *Observation of $t\bar{t}H$ Production*, *Phys. Rev. Lett.* **120** (2018) 231801, arXiv: [1804.02610 \[hep-ex\]](#).
- [10] CMS Collaboration, *Observation of Higgs boson decay to bottom quarks*, *Phys. Rev. Lett.* **121** (2018) 121801, arXiv: [1808.08242 \[hep-ex\]](#).
- [11] ATLAS Collaboration, *Observation of $H \rightarrow b\bar{b}$ decays and VH production with the ATLAS detector*, *Phys. Lett. B* **786** (2018) 59, arXiv: [1808.08238 \[hep-ex\]](#).
- [12] ATLAS Collaboration, *Search for the Standard Model Higgs boson produced in association with top quarks and decaying into a $b\bar{b}$ pair in pp collisions at $\sqrt{s} = 13$ TeV with the ATLAS detector*, *Phys. Rev. D* **97** (2018) 072016, arXiv: [1712.08895 \[hep-ex\]](#).
- [13] CMS Collaboration, *Search for $t\bar{t}H$ production in the $H \rightarrow b\bar{b}$ decay channel with leptonic $t\bar{t}$ decays in proton–proton collisions at $\sqrt{s} = 13$ TeV*, (2018), arXiv: [1804.03682 \[hep-ex\]](#).

- [14] ATLAS Collaboration, *Study of heavy flavor quarks produced in association with top quark pairs at $\sqrt{s} = 7$ TeV using the ATLAS detector*, *Phys. Rev. D* **89** (2014) 072012, arXiv: [1304.6386 \[hep-ex\]](#).
- [15] ATLAS Collaboration, *Measurements of fiducial cross-sections for $t\bar{t}$ production with one or two additional b -jets in pp collisions at $\sqrt{s} = 8$ TeV using the ATLAS detector*, *Eur. Phys. J. C* **76** (2016) 11, arXiv: [1508.06868 \[hep-ex\]](#).
- [16] CMS Collaboration, *Measurement of $t\bar{t}$ production with additional jet activity, including b quark jets, in the dilepton decay channel using pp collisions at $\sqrt{s} = 8$ TeV*, *Eur. Phys. J. C* **76** (2016) 379, arXiv: [1510.03072 \[hep-ex\]](#).
- [17] CMS Collaboration, *Measurement of the cross section ratio $\sigma_{t\bar{t}bb}/\sigma_{t\bar{t}jj}$ in pp collisions at $\sqrt{s} = 8$ TeV*, *Phys. Lett. B* **746** (2015) 132, arXiv: [1411.5621 \[hep-ex\]](#).
- [18] CMS Collaboration, *Measurements of $t\bar{t}$ cross sections in association with b jets and inclusive jets and their ratio using dilepton final states in pp collisions at $\sqrt{s} = 13$ TeV*, *Phys. Lett. B* **776** (2018) 355, arXiv: [1705.10141 \[hep-ex\]](#).
- [19] ATLAS Collaboration, *Measurements of b -jet tagging efficiency with the ATLAS detector using $t\bar{t}$ events at $\sqrt{s} = 13$ TeV*, *JHEP* **08** (2018) 089, arXiv: [1805.01845 \[hep-ex\]](#).
- [20] ATLAS Collaboration, *The ATLAS Experiment at the CERN Large Hadron Collider*, *JINST* **3** (2008) S08003.
- [21] ATLAS Collaboration, *ATLAS Insertable B-Layer Technical Design Report*, (2010), *ATLAS Insertable B-Layer Technical Design Report Addendum*, ATLAS-TDR-19-ADD-1, 2012, URL: <https://cds.cern.ch/record/1451888>.
- [22] B. Abbott et al., *Production and Integration of the ATLAS Insertable B-Layer*, *JINST* **13** (2018) T05008, arXiv: [1803.00844 \[physics.ins-det\]](#).
- [23] ATLAS Collaboration, *Performance of the ATLAS Trigger System in 2010*, *Eur. Phys. J. C* **72** (2012) 1849, arXiv: [1110.1530 \[hep-ex\]](#).
- [24] ATLAS Collaboration, *Performance of the ATLAS trigger system in 2015*, *Eur. Phys. J. C* **77** (2017) 317, arXiv: [1611.09661 \[hep-ex\]](#).
- [25] P. Nason, *A new method for combining NLO QCD with shower Monte Carlo algorithms*, *JHEP* **11** (2004) 040, arXiv: [hep-ph/0409146 \[hep-ph\]](#).
- [26] S. Frixione, P. Nason and C. Oleari, *Matching NLO QCD computations with parton shower simulations: the POWHEG method*, *JHEP* **11** (2007) 070, arXiv: [0709.2092 \[hep-ph\]](#).
- [27] S. Alioli, P. Nason, C. Oleari and E. Re, *A general framework for implementing NLO calculations in shower Monte Carlo programs: the POWHEG BOX*, *JHEP* **06** (2010) 043, arXiv: [1002.2581 \[hep-ph\]](#).
- [28] S. Frixione, P. Nason and G. Ridolfi, *A positive-weight next-to-leading-order Monte Carlo for heavy flavour hadroproduction*, *JHEP* **09** (2007) 126, arXiv: [0707.3088 \[hep-ph\]](#).
- [29] T. Sjöstrand, S. Mrenna and P. Z. Skands, *An Introduction to PYTHIA 8.2*, *Comput. Phys. Commun.* **191** (2015) 159, arXiv: [1410.3012 \[hep-ph\]](#).

- [30] D. B. Richard et al., *Parton distributions with LHC data*, *Nucl. Phys. B* **867** (2013) 244, arXiv: [1207.1303 \[hep-ph\]](#).
- [31] The NNPDF Collaboration, *Parton distributions for the LHC Run II*, *JHEP* **04** (2015) 40, arXiv: [1410.8849 \[hep-ph\]](#).
- [32] ATLAS Collaboration, *ATLAS Pythia 8 tunes to 7 TeV data*, ATL-PHYS-PUB-2014-021, 2014, URL: <https://cds.cern.ch/record/1966419>.
- [33] ATLAS Collaboration, *Studies on top-quark Monte Carlo modelling for Top2016*, ATL-PHYS-PUB-2016-020, 2016, URL: <https://cds.cern.ch/record/2216168>.
- [34] J. Alwall et al., *The automated computation of tree-level and next-to-leading order differential cross sections, and their matching to parton shower simulations*, *JHEP* **07** (2014) 079, arXiv: [1405.0301 \[hep-ph\]](#).
- [35] ATLAS Collaboration, *Modelling of the $t\bar{t}H$ and $t\bar{t}V(V = W, Z)$ processes for $\sqrt{s} = 13$ TeV ATLAS analyses*, ATL-PHYS-PUB-2016-005, 2016, URL: <https://cds.cern.ch/record/2120826>.
- [36] LHC Higgs cross section working group, *Handbook of LHC Higgs cross sections*, (2017), arXiv: [1610.07922 \[hep-ph\]](#).
- [37] A. Djouadi, J. Kalinowski and M. Spira, *HDECAY: A program for Higgs boson decays in the standard model and its supersymmetric extension*, *Comput. Phys. Commun.* **108** (1998) 56, arXiv: [hep-ph/9704448 \[hep-ph\]](#).
- [38] M. Bahr et al., *Herwig++ Physics and Manual*, *Eur. Phys. J. C* **58** (2008) 639, arXiv: [0803.0883 \[hep-ph\]](#).
- [39] B. Johannes et al., *Herwig 7.0/Herwig++ 3.0 release note*, *Eur. Phys. J. C* **76** (2016) 196, arXiv: [1512.01178 \[hep-ph\]](#).
- [40] T. Gleisberg, S. Höche, F. Krauss, M. Schönherr, S. Schumann et al., *Event generation with SHERPA 1.1*, *JHEP* **02** (2009) 007, arXiv: [0811.4622 \[hep-ph\]](#).
- [41] S. Höche, F. Krauss, M. Schönherr and F. Siegert, *QCD matrix elements + parton showers: The NLO case*, *JHEP* **04** (2013) 027, arXiv: [1207.5030 \[hep-ph\]](#).
- [42] M. Czakon and A. Mitov, *Top++: A program for the calculation of the top-pair cross-section at hadron colliders*, *Comput. Phys. Commun.* **185** (2014) 2930, arXiv: [1112.5675 \[hep-ph\]](#).
- [43] M. Botje et al., *The PDF4LHC Working Group Interim Recommendations*, (2011), arXiv: [1101.0538 \[hep-ph\]](#).
- [44] A. D. Martin, W. J. Stirling, R. S. Thorne and G. Watt, *Uncertainties on alpha(S) in global PDF analyses and implications for predicted hadronic cross sections*, *Eur. Phys. J. C* **64** (2009) 653, arXiv: [0905.3531 \[hep-ph\]](#).
- [45] J. Gao et al., *CT10 next-to-next-to-leading order global analysis of QCD*, *Phys. Rev. D* **89** (2014) 033009, arXiv: [1302.6246 \[hep-ph\]](#).
- [46] R. D. Ball et al., *Parton distributions with LHC data*, *Nucl. Phys. B* **867** (2013) 244, arXiv: [1207.1303 \[hep-ph\]](#).
- [47] T. Gleisberg and S. Höche, *Comix, a new matrix element generator*, *JHEP* **12** (2008) 039, arXiv: [0808.3674 \[hep-ph\]](#).

- [48] F. Cascioli, P. Maierhofer and S. Pozzorini, *Scattering Amplitudes with Open Loops*, *Phys. Rev. Lett.* **108** (2012) 111601, arXiv: [1111.5206 \[hep-ph\]](#).
- [49] S. Schumann and F. Krauss, *A Parton shower algorithm based on Catani-Seymour dipole factorisation*, *JHEP* **03** (2008) 038, arXiv: [0709.1027 \[hep-ph\]](#).
- [50] D. J. Lange, *The EvtGen particle decay simulation package*, *Nucl. Instrum. Meth. A* **462** (2001) 152.
- [51] S. Frixione, E. Laenen, P. Motylinski and B. R. Webber, *Angular correlations of lepton pairs from vector boson and top quark decays in Monte Carlo simulations*, *JHEP* **04** (2007) 081, arXiv: [hep-ph/0702198 \[HEP-PH\]](#).
- [52] P. Artoisenet, R. Frederix, O. Mattelaer and R. Rietkerk, *Automatic spin-entangled decays of heavy resonances in Monte Carlo simulations*, *JHEP* **03** (2013) 015, arXiv: [1212.3460 \[hep-ph\]](#).
- [53] S. Frixione, E. Laenen, P. Motylinski, B. R. Webber and C. D. White, *Single-top hadroproduction in association with a W boson*, *JHEP* **07** (2008) 029, arXiv: [0805.3067 \[hep-ph\]](#).
- [54] T. Sjöstrand, S. Mrenna and P. Z. Skands, *PYTHIA 6.4 Physics and Manual*, *JHEP* **05** (2006) 026, arXiv: [hep-ph/0603175](#).
- [55] J. Pumplin et al., *New generation of parton distributions with uncertainties from global QCD analysis*, *JHEP* **07** (2002) 012, arXiv: [hep-ph/0201195 \[hep-ph\]](#).
- [56] P. Z. Skands, *Tuning Monte Carlo Generators: The Perugia Tunes*, *Phys. Rev. D* **82** (2010) 074018, arXiv: [1005.3457 \[hep-ph\]](#).
- [57] M. Aliev et al., *HATHOR: HAdronic Top and Heavy quarks crOss section calculatoR*, *Comput. Phys. Commun.* **182** (2011) 1034, arXiv: [1007.1327 \[hep-ph\]](#).
- [58] P. Kant et al., *HatHor for single top-quark production: Updated predictions and uncertainty estimates for single top-quark production in hadronic collisions*, *Comput. Phys. Commun.* **191** (2015) 74, arXiv: [1406.4403 \[hep-ph\]](#).
- [59] N. Kidonakis, *Two-loop soft anomalous dimensions for single top quark associated production with a W- or H-*, *Phys. Rev. D* **82** (2010) 054018, arXiv: [1005.4451 \[hep-ph\]](#).
- [60] C. Anastasiou, L. J. Dixon, K. Melnikov and F. Petriello, *High precision QCD at hadron colliders: Electroweak gauge boson rapidity distributions at NNLO*, *Phys. Rev. D* **69** (2004) 094008, arXiv: [hep-ph/0312266 \[hep-ph\]](#).
- [61] ATLAS Collaboration, *Summary of ATLAS Pythia 8 tunes*, ATL-PHYS-PUB-2012-003, 2012, URL: <https://cds.cern.ch/record/1474107>.
- [62] A. Martin, W. Stirling, R. Thorne and G. Watt, *Parton distributions for the LHC*, *Eur. Phys. J. C* **63** (2009) 189, arXiv: [0901.0002 \[hep-ph\]](#).
- [63] ATLAS Collaboration, *Electron efficiency measurements with the ATLAS detector using the 2015 LHC proton-proton collision data*, ATLAS-CONF-2016-024, 2016, URL: <https://cds.cern.ch/record/2157687>.

- [64] ATLAS Collaboration, *Muon reconstruction performance of the ATLAS detector in proton–proton collision data at $\sqrt{s} = 13$ TeV*, *Eur. Phys. J. C* **76** (2016) 292, arXiv: [1603.05598 \[hep-ex\]](#).
- [65] M. Cacciari, G. P. Salam and G. Soyez, *The anti- k_t jet clustering algorithm*, *JHEP* **04** (2008) 063, arXiv: [0802.1189 \[hep-ph\]](#).
- [66] ATLAS Collaboration, *Topological cell clustering in the ATLAS calorimeters and its performance in LHC Run 1*, *Eur. Phys. J. C* **77** (2017) 490, arXiv: [1603.02934 \[hep-ex\]](#).
- [67] ATLAS Collaboration, *Jet energy scale measurements and their systematic uncertainties in proton–proton collisions at $\sqrt{s} = 13$ TeV with the ATLAS detector*, *Phys. Rev. D* **96** (2017) 072002, arXiv: [1703.09665 \[hep-ex\]](#).
- [68] ATLAS Collaboration, *Tagging and suppression of pileup jets with the ATLAS detector*, ATLAS-CONF-2014-018, 2014, URL: <https://cds.cern.ch/record/1700870>.
- [69] ATLAS Collaboration, *Optimisation of the ATLAS b-tagging performance for the 2016 LHC Run*, ATL-PHYS-PUB-2016-012, 2016, URL: <https://cds.cern.ch/record/2160731>.
- [70] M. Cacciari, G. P. Salam and G. Soyez, *The catchment area of jets*, *JHEP* **04** (2008) 005, arXiv: [0802.1188 \[hep-ph\]](#).
- [71] ATLAS Collaboration, *Measurement of the $t\bar{t}$ production cross-section using $e\mu$ events with b-tagged jets in pp collisions at $\sqrt{s} = 13$ TeV with the ATLAS detector*, *Phys. Lett. B* **761** (2016) 136, arXiv: [1606.02699 \[hep-ex\]](#).
- [72] ATLAS Collaboration, *Estimation of non-prompt and fake lepton backgrounds in final states with top quarks produced in proton–proton collisions at $\sqrt{s} = 8$ TeV with the ATLAS Detector*, ATLAS-CONF-2014-058, 2014, URL: <https://cds.cern.ch/record/1951336>.
- [73] ATLAS Collaboration, *Measurement of jet activity produced in top-quark events with an electron, a muon and two b-tagged jets in the final state in pp collisions at $\sqrt{s} = 13$ TeV with the ATLAS detector*, *Eur. Phys. J. C* **77** (2017) 220, arXiv: [1610.09978 \[hep-ex\]](#).
- [74] G. D’Agostini, *A Multidimensional unfolding method based on Bayes’ theorem*, *Nucl. Instrum. Meth. A* **362** (1995) 487.
- [75] T. Adye, *Unfolding algorithms and tests using RooUnfold*, (2011), arXiv: [1105.1160 \[physics.data-an\]](#).
- [76] ATLAS Collaboration, *Luminosity determination in pp collisions at $\sqrt{s} = 8$ TeV using the ATLAS detector at the LHC*, *Eur. Phys. J. C* **76** (2016) 653, arXiv: [1608.03953 \[hep-ex\]](#).
- [77] G. Avoni et al., *The new LUCID-2 detector for luminosity measurement and monitoring in ATLAS*, *JINST* **13** (2018) P07017.
- [78] ATLAS Collaboration, *Electron and photon energy calibration with the ATLAS detector using data collected in 2015 at $\sqrt{s} = 13$ TeV*, ATL-PHYS-PUB-2016-015, 2016, URL: <https://cds.cern.ch/record/2203514>.
- [79] ATLAS Collaboration, *Performance of pile-up mitigation techniques for jets in pp collisions at $\sqrt{s} = 8$ TeV using the ATLAS detector*, *Eur. Phys. J. C* **76** (2016) 581, arXiv: [1510.03823 \[hep-ex\]](#).

- [80] ATLAS Collaboration, *Jet energy resolution in proton–proton collisions at $\sqrt{s} = 7$ TeV recorded in 2010 with the ATLAS detector*, *Eur. Phys. J. C* **73** (2013) 2306, arXiv: [1210.6210 \[hep-ex\]](https://arxiv.org/abs/1210.6210).
- [81] ATLAS Collaboration, *Calibration of light-flavour b-jet mistagging rates using ATLAS proton–proton collision data at $\sqrt{s} = 13$ TeV*, ATLAS-CONF-2018-006, 2018,
URL: <http://cdsweb.cern.ch/record/2314418>.
- [82] ATLAS Collaboration, *Measurement of b-tagging efficiency of c-jets in $t\bar{t}$ events using a likelihood approach with the ATLAS detector*, ATLAS-CONF-2018-001, 2018,
URL: <https://cds.cern.ch/record/2306649>.
- [83] J. Butterworth et al., *PDF4LHC recommendations for LHC Run II*, *J. Phys. G* **43** (2016) 023001, arXiv: [1510.03865 \[hep-ph\]](https://arxiv.org/abs/1510.03865).
- [84] ATLAS Collaboration, *Measurement of the $t\bar{t}Z$ and $t\bar{t}W$ production cross sections in multilepton final states using 3.2 fb^{-1} of pp collisions at $\sqrt{s} = 13$ TeV with the ATLAS detector*, *Eur. Phys. J. C* **77** (2017) 40, arXiv: [1609.01599 \[hep-ex\]](https://arxiv.org/abs/1609.01599).
- [85] ATLAS Collaboration, *ATLAS Computing Acknowledgements*, ATL-GEN-PUB-2016-002,
URL: <https://cds.cern.ch/record/2202407>.

The ATLAS Collaboration

M. Aaboud^{34d}, G. Aad⁹⁹, B. Abbott¹²⁵, O. Abdinov^{13,*}, B. Abeloos¹²⁹, D.K. Abhayasinghe⁹¹, S.H. Abidi¹⁶⁴, O.S. AbouZeid³⁹, N.L. Abraham¹⁵³, H. Abramowicz¹⁵⁸, H. Abreu¹⁵⁷, Y. Abulaiti⁶, B.S. Acharya^{64a,64b,p}, S. Adachi¹⁶⁰, L. Adam⁹⁷, L. Adamczyk^{81a}, J. Adelman¹¹⁹, M. Adersberger¹¹², A. Adiguzel^{12c,aj}, T. Adye¹⁴¹, A.A. Affolder¹⁴³, Y. Afik¹⁵⁷, C. Agheorghiesei^{27c}, J.A. Aguilar-Saavedra^{137f,137a,ai}, F. Ahmadov^{77,ag}, G. Aielli^{71a,71b}, S. Akatsuka⁸³, T.P.A. Åkesson⁹⁴, E. Akilli⁵², A.V. Akimov¹⁰⁸, G.L. Alberghi^{23b,23a}, J. Albert¹⁷³, P. Albicocco⁴⁹, M.J. Alconada Verzini⁸⁶, S. Alderweireldt¹¹⁷, M. Aleksa³⁵, I.N. Aleksandrov⁷⁷, C. Alexa^{27b}, T. Alexopoulos¹⁰, M. Alhoob¹²⁵, B. Ali¹³⁹, G. Alimonti^{66a}, J. Alison³⁶, S.P. Alkire¹⁴⁵, C. Allaire¹²⁹, B.M.M. Allbrooke¹⁵³, B.W. Allen¹²⁸, P.P. Allport²¹, A. Aloisio^{67a,67b}, A. Alonso³⁹, F. Alonso⁸⁶, C. Alpigiani¹⁴⁵, A.A. Alshehri⁵⁵, M.I. Alstaty⁹⁹, B. Alvarez Gonzalez³⁵, D. Álvarez Piqueras¹⁷¹, M.G. Alviggi^{67a,67b}, B.T. Amadio¹⁸, Y. Amaral Coutinho^{78b}, A. Ambler¹⁰¹, L. Ambroz¹³², C. Amelung²⁶, D. Amidei¹⁰³, S.P. Amor Dos Santos^{137a,137c}, S. Amoroso⁴⁴, C.S. Amrouche⁵², C. Anastopoulos¹⁴⁶, L.S. Ancu⁵², N. Andari¹⁴², T. Andeen¹¹, C.F. Anders^{59b}, J.K. Anders²⁰, K.J. Anderson³⁶, A. Andreazza^{66a,66b}, V. Andrei^{59a}, C.R. Anelli¹⁷³, S. Angelidakis³⁷, I. Angelozzi¹¹⁸, A. Angerami³⁸, A.V. Anisenkov^{120b,120a}, A. Annovi^{69a}, C. Antel^{59a}, M.T. Anthony¹⁴⁶, M. Antonelli⁴⁹, D.J.A. Antrim¹⁶⁸, F. Anulli^{70a}, M. Aoki⁷⁹, J.A. Aparisi Pozo¹⁷¹, L. Aperio Bella³⁵, G. Arabidze¹⁰⁴, J.P. Araque^{137a}, V. Araujo Ferraz^{78b}, R. Araujo Pereira^{78b}, A.T.H. Arce⁴⁷, R.E. Ardell⁹¹, F.A. Arduh⁸⁶, J-F. Arguin¹⁰⁷, S. Argyropoulos⁷⁵, A.J. Armbruster³⁵, L.J. Armitage⁹⁰, A. Armstrong¹⁶⁸, O. Arnaez¹⁶⁴, H. Arnold¹¹⁸, M. Arratia³¹, O. Arslan²⁴, A. Artamonov^{109,*}, G. Artoni¹³², S. Artz⁹⁷, S. Asai¹⁶⁰, N. Asbah⁵⁷, E.M. Asimakopoulou¹⁶⁹, L. Asquith¹⁵³, K. Assamagan²⁹, R. Astalos^{28a}, R.J. Atkin^{32a}, M. Atkinson¹⁷⁰, N.B. Atlay¹⁴⁸, K. Augsten¹³⁹, G. Avolio³⁵, R. Avramidou^{58a}, M.K. Ayoub^{15a}, A.M. Azoulay^{165b}, G. Azuelos^{107,av}, A.E. Baas^{59a}, M.J. Baca²¹, H. Bachacou¹⁴², K. Bachas^{65a,65b}, M. Backes¹³², P. Bagnaia^{70a,70b}, M. Bahmani⁸², H. Bahrasemani¹⁴⁹, A.J. Bailey¹⁷¹, J.T. Baines¹⁴¹, M. Bajic³⁹, C. Bakalis¹⁰, O.K. Baker¹⁸⁰, P.J. Bakker¹¹⁸, D. Bakshi Gupta⁸, S. Balaji¹⁵⁴, E.M. Baldin^{120b,120a}, P. Balek¹⁷⁷, F. Balli¹⁴², W.K. Balunas¹³⁴, J. Balz⁹⁷, E. Banas⁸², A. Bandyopadhyay²⁴, S. Banerjee^{178,1}, A.A.E. Bannoura¹⁷⁹, L. Barak¹⁵⁸, W.M. Barbe³⁷, E.L. Barberio¹⁰², D. Barberis^{53b,53a}, M. Barbero⁹⁹, T. Barillari¹¹³, M-S. Barisits³⁵, J. Barkeloo¹²⁸, T. Barklow¹⁵⁰, R. Barnea¹⁵⁷, S.L. Barnes^{58c}, B.M. Barnett¹⁴¹, R.M. Barnett¹⁸, Z. Barnovska-Blenessy^{58a}, A. Baroncelli^{72a}, G. Barone²⁹, A.J. Barr¹³², L. Barranco Navarro¹⁷¹, F. Barreiro⁹⁶, J. Barreiro Guimarães da Costa^{15a}, R. Bartoldus¹⁵⁰, A.E. Barton⁸⁷, P. Bartos^{28a}, A. Basalaev¹³⁵, A. Bassalat¹²⁹, R.L. Bates⁵⁵, S.J. Batista¹⁶⁴, S. Batlamous^{34e}, J.R. Batley³¹, M. Battaglia¹⁴³, M. Bauce^{70a,70b}, F. Bauer¹⁴², K.T. Bauer¹⁶⁸, H.S. Bawa^{150,n}, J.B. Beacham¹²³, T. Beau¹³³, P.H. Beauchemin¹⁶⁷, P. Bechtle²⁴, H.C. Beck⁵¹, H.P. Beck^{20,s}, K. Becker⁵⁰, M. Becker⁹⁷, C. Becot⁴⁴, A. Beddall^{12d}, A.J. Beddall^{12a}, V.A. Bednyakov⁷⁷, M. Bedognetti¹¹⁸, C.P. Bee¹⁵², T.A. Beermann⁷⁴, M. Begalli^{78b}, M. Begel²⁹, A. Behera¹⁵², J.K. Behr⁴⁴, A.S. Bell⁹², G. Bella¹⁵⁸, L. Bellagamba^{23b}, A. Bellerive³³, M. Bellomo¹⁵⁷, P. Bellos⁹, K. Belotskiy¹¹⁰, N.L. Belyaev¹¹⁰, O. Benary^{158,*}, D. Benchekroun^{34a}, M. Bender¹¹², N. Benekos¹⁰, Y. Benhammou¹⁵⁸, E. Benhar Noccioli¹⁸⁰, J. Benitez⁷⁵, D.P. Benjamin⁴⁷, M. Benoit⁵², J.R. Bensinger²⁶, S. Bentvelsen¹¹⁸, L. Beresford¹³², M. Beretta⁴⁹, D. Berge⁴⁴, E. Bergeaas Kuutmann¹⁶⁹, N. Berger⁵, B. Bergmann¹³⁹, L.J. Bergsten²⁶, J. Beringer¹⁸, S. Berlendis⁷, N.R. Bernard¹⁰⁰, G. Bernardi¹³³, C. Bernius¹⁵⁰, F.U. Bernlochner²⁴, T. Berry⁹¹, P. Berta⁹⁷, C. Bertella^{15a}, G. Bertoli^{43a,43b}, I.A. Bertram⁸⁷, G.J. Besjes³⁹, O. Bessidskaia Bylund¹⁷⁹, M. Bessner⁴⁴, N. Besson¹⁴², A. Bethani⁹⁸, S. Bethke¹¹³, A. Betti²⁴, A.J. Bevan⁹⁰, J. Beyer¹¹³, R. Bi¹³⁶, R.M. Bianchi¹³⁶, O. Biebel¹¹², D. Biedermann¹⁹, R. Bielski³⁵, K. Bierwagen⁹⁷, N.V. Biesuz^{69a,69b}, M. Biglietti^{72a}, T.R.V. Billoud¹⁰⁷, M. Bindi⁵¹, A. Bingul^{12d}, C. Bini^{70a,70b}, S. Biondi^{23b,23a}, M. Birman¹⁷⁷, T. Bisanz⁵¹, J.P. Biswal¹⁵⁸, C. Bittrich⁴⁶, D.M. Bjergaard⁴⁷, J.E. Black¹⁵⁰, K.M. Black²⁵, T. Blazek^{28a}, I. Bloch⁴⁴,

C. Blocker²⁶, A. Blue⁵⁵, U. Blumenschein⁹⁰, Dr. Blunier^{144a}, G.J. Bobbink¹¹⁸, V.S. Bobrovnikov^{120b,120a}, S.S. Bocchetta⁹⁴, A. Bocci⁴⁷, D. Boerner¹⁷⁹, D. Bogavac¹¹², A.G. Bogdanchikov^{120b,120a}, C. Bohm^{43a}, V. Boisvert⁹¹, P. Bokan¹⁶⁹, T. Bold^{81a}, A.S. Boldyrev¹¹¹, A.E. Bolz^{59b}, M. Bomben¹³³, M. Bona⁹⁰, J.S. Bonilla¹²⁸, M. Boonekamp¹⁴², A. Borisov¹²¹, G. Borissov⁸⁷, J. Bortfeldt³⁵, D. Bortolotto¹³², V. Bortolotto^{71a,71b}, D. Boscherini^{23b}, M. Bosman¹⁴, J.D. Bossio Sola³⁰, K. Bouaouda^{34a}, J. Boudreau¹³⁶, E.V. Bouhova-Thacker⁸⁷, D. Boumediene³⁷, C. Bourdarios¹²⁹, S.K. Boutle⁵⁵, A. Boveia¹²³, J. Boyd³⁵, D. Boye^{32b}, I.R. Boyko⁷⁷, A.J. Bozson⁹¹, J. Bracinik²¹, N. Brahimi⁹⁹, A. Brandt⁸, G. Brandt¹⁷⁹, O. Brandt^{59a}, F. Braren⁴⁴, U. Bratzler¹⁶¹, B. Brau¹⁰⁰, J.E. Brau¹²⁸, W.D. Breaden Madden⁵⁵, K. Brendlinger⁴⁴, L. Brenner⁴⁴, R. Brenner¹⁶⁹, S. Bressler¹⁷⁷, B. Brickwedde⁹⁷, D.L. Briglin²¹, D. Britton⁵⁵, D. Britzger¹¹³, I. Brock²⁴, R. Brock¹⁰⁴, G. Brooijmans³⁸, T. Brooks⁹¹, W.K. Brooks^{144b}, E. Brost¹¹⁹, J.H. Broughton²¹, P.A. Bruckman de Renstrom⁸², D. Bruncko^{28b}, A. Bruni^{23b}, G. Bruni^{23b}, L.S. Bruni¹¹⁸, S. Bruno^{71a,71b}, B.H. Brunt³¹, M. Bruschi^{23b}, N. Bruscino¹³⁶, P. Bryant³⁶, L. Bryngemark⁴⁴, T. Buanes¹⁷, Q. Buat³⁵, P. Buchholz¹⁴⁸, A.G. Buckley⁵⁵, I.A. Budagov⁷⁷, M.K. Bugge¹³¹, F. Bührer⁵⁰, O. Bulekov¹¹⁰, D. Bullock⁸, T.J. Burch¹¹⁹, S. Burdin⁸⁸, C.D. Burgard¹¹⁸, A.M. Burger⁵, B. Burghgrave¹¹⁹, K. Burka⁸², S. Burke¹⁴¹, I. Burmeister⁴⁵, J.T.P. Burr¹³², V. Büscher⁹⁷, E. Buschmann⁵¹, P. Bussey⁵⁵, J.M. Butler²⁵, C.M. Buttar⁵⁵, J.M. Butterworth⁹², P. Butti³⁵, W. Buttinger³⁵, A. Buzatu¹⁵⁵, A.R. Buzykaev^{120b,120a}, G. Cabras^{23b,23a}, S. Cabrera Urbán¹⁷¹, D. Caforio¹³⁹, H. Cai¹⁷⁰, V.M.M. Cairo², O. Cakir^{4a}, N. Calace⁵², P. Calafiura¹⁸, A. Calandri⁹⁹, G. Calderini¹³³, P. Calfayan⁶³, G. Callea^{40b,40a}, L.P. Caloba^{78b}, S. Calvente Lopez⁹⁶, D. Calvet³⁷, S. Calvet³⁷, T.P. Calvet¹⁵², M. Calvetti^{69a,69b}, R. Camacho Toro¹³³, S. Camarda³⁵, D. Camarero Munoz⁹⁶, P. Camarri^{71a,71b}, D. Cameron¹³¹, R. Caminal Armadans¹⁰⁰, C. Camincher³⁵, S. Campana³⁵, M. Campanelli⁹², A. Camplani³⁹, A. Campoverde¹⁴⁸, V. Canale^{67a,67b}, M. Cano Bret^{58c}, J. Cantero¹²⁶, T. Cao¹⁵⁸, Y. Cao¹⁷⁰, M.D.M. Capeans Garrido³⁵, I. Caprini^{27b}, M. Caprini^{27b}, M. Capua^{40b,40a}, R.M. Carbone³⁸, R. Cardarelli^{71a}, F.C. Cardillo¹⁴⁶, I. Carli¹⁴⁰, T. Carli³⁵, G. Carlino^{67a}, B.T. Carlson¹³⁶, L. Carminati^{66a,66b}, R.M.D. Carney^{43a,43b}, S. Caron¹¹⁷, E. Carquin^{144b}, S. Carrá^{66a,66b}, G.D. Carrillo-Montoya³⁵, D. Casadei^{32b}, M.P. Casado^{14,g}, A.F. Casha¹⁶⁴, D.W. Casper¹⁶⁸, R. Castelijn¹¹⁸, F.L. Castillo¹⁷¹, V. Castillo Gimenez¹⁷¹, N.F. Castro^{137a,137e}, A. Catinaccio³⁵, J.R. Catmore¹³¹, A. Cattai³⁵, J. Caudron²⁴, V. Cavaliere²⁹, E. Cavallaro¹⁴, D. Cavalli^{66a}, M. Cavalli-Sforza¹⁴, V. Cavasinni^{69a,69b}, E. Celebi^{12b}, F. Ceradini^{72a,72b}, L. Cerdà Alberich¹⁷¹, A.S. Cerqueira^{78a}, A. Cerri¹⁵³, L. Cerrito^{71a,71b}, F. Cerutti¹⁸, A. Cervelli^{23b,23a}, S.A. Cetin^{12b}, A. Chafaq^{34a}, D. Chakraborty¹¹⁹, S.K. Chan⁵⁷, W.S. Chan¹¹⁸, Y.L. Chan^{61a}, J.D. Chapman³¹, B. Chargeishvili^{156b}, D.G. Charlton²¹, C.C. Chau³³, C.A. Chavez Barajas¹⁵³, S. Che¹²³, A. Chegwidden¹⁰⁴, S. Chekanov⁶, S.V. Chekulaev^{165a}, G.A. Chelkov^{77,au}, M.A. Chelstowska³⁵, C. Chen^{58a}, C.H. Chen⁷⁶, H. Chen²⁹, J. Chen^{58a}, J. Chen³⁸, S. Chen¹³⁴, S.J. Chen^{15c}, X. Chen^{15b,at}, Y. Chen⁸⁰, Y-H. Chen⁴⁴, H.C. Cheng¹⁰³, H.J. Cheng^{15d}, A. Cheplakov⁷⁷, E. Cheremushkina¹²¹, R. Cherkaoui El Moursli^{34e}, E. Cheu⁷, K. Cheung⁶², L. Chevalier¹⁴², V. Chiarella⁴⁹, G. Chiarelli^{69a}, G. Chiodini^{65a}, A.S. Chisholm^{35,21}, A. Chitan^{27b}, I. Chiu¹⁶⁰, Y.H. Chiu¹⁷³, M.V. Chizhov⁷⁷, K. Choi⁶³, A.R. Chomont¹²⁹, S. Chouridou¹⁵⁹, Y.S. Chow¹¹⁸, V. Christodoulou⁹², M.C. Chu^{61a}, J. Chudoba¹³⁸, A.J. Chuinard¹⁰¹, J.J. Chwastowski⁸², L. Chytka¹²⁷, D. Cinca⁴⁵, V. Cindro⁸⁹, I.A. Cioară²⁴, A. Ciocio¹⁸, F. Cirotto^{67a,67b}, Z.H. Citron¹⁷⁷, M. Citterio^{66a}, A. Clark⁵², M.R. Clark³⁸, P.J. Clark⁴⁸, C. Clement^{43a,43b}, Y. Coadou⁹⁹, M. Cobal^{64a,64c}, A. Coccaro^{53b,53a}, J. Cochran⁷⁶, H. Cohen¹⁵⁸, A.E.C. Coimbra¹⁷⁷, L. Colasurdo¹¹⁷, B. Cole³⁸, A.P. Colijn¹¹⁸, J. Collot⁵⁶, P. Conde Muñoz^{137a,i}, E. Coniavitis⁵⁰, S.H. Connell^{32b}, I.A. Connelly⁹⁸, S. Constantinescu^{27b}, F. Conventi^{67a,aw}, A.M. Cooper-Sarkar¹³², F. Cormier¹⁷², K.J.R. Cormier¹⁶⁴, L.D. Corpe⁹², M. Corradi^{70a,70b}, E.E. Corrigan⁹⁴, F. Corriveau^{101,ae}, A. Cortes-Gonzalez³⁵, M.J. Costa¹⁷¹, F. Costanza⁵, D. Costanzo¹⁴⁶, G. Cottin³¹, G. Cowan⁹¹, B.E. Cox⁹⁸, J. Crane⁹⁸, K. Cranmer¹²², S.J. Crawley⁵⁵, R.A. Creager¹³⁴, G. Cree³³, S. Crépé-Renaudin⁵⁶, F. Crescioli¹³³, M. Cristinziani²⁴, V. Croft¹²², G. Crosetti^{40b,40a}, A. Cueto⁹⁶, T. Cuhadar Donszelmann¹⁴⁶, A.R. Cukierman¹⁵⁰, S. Czekierda⁸²,

P. Czodrowski³⁵, M.J. Da Cunha Sargedas De Sousa^{58b}, C. Da Via⁹⁸, W. Dabrowski^{81a}, T. Dado^{28a,z},
 S. Dahbi^{34e}, T. Dai¹⁰³, F. Dallaire¹⁰⁷, C. Dallapiccola¹⁰⁰, M. Dam³⁹, G. D'amen^{23b,23a}, J. Damp⁹⁷,
 J.R. Dandoy¹³⁴, M.F. Daneri³⁰, N.P. Dang^{178,l}, N.D Dann⁹⁸, M. Danninger¹⁷², V. Dao³⁵, G. Darbo^{53b},
 S. Darmora⁸, O. Dartsi⁵, A. Dattagupta¹²⁸, T. Daubney⁴⁴, S. D'Auria^{66a,66b}, W. Davey²⁴, C. David⁴⁴,
 T. Davidek¹⁴⁰, D.R. Davis⁴⁷, E. Dawe¹⁰², I. Dawson¹⁴⁶, K. De⁸, R. De Asmundis^{67a}, A. De Benedetti¹²⁵,
 M. De Beurs¹¹⁸, S. De Castro^{23b,23a}, S. De Cecco^{70a,70b}, N. De Groot¹¹⁷, P. de Jong¹¹⁸, H. De la Torre¹⁰⁴,
 F. De Lorenzi⁷⁶, A. De Maria^{51,u}, D. De Pedis^{70a}, A. De Salvo^{70a}, U. De Sanctis^{71a,71b}, M. De Santis^{71a,71b},
 A. De Santo¹⁵³, K. De Vasconcelos Corga⁹⁹, J.B. De Vivie De Regie¹²⁹, C. Debenedetti¹⁴³,
 D.V. Dedovich⁷⁷, N. Dehghanian³, M. Del Gaudio^{40b,40a}, J. Del Peso⁹⁶, Y. Delabat Diaz⁴⁴, D. Delgove¹²⁹,
 F. Deliot¹⁴², C.M. Delitzsch⁷, M. Della Pietra^{67a,67b}, D. Della Volpe⁵², A. Dell'Acqua³⁵, L. Dell'Asta²⁵,
 M. Delmastro⁵, C. Delporte¹²⁹, P.A. Delsart⁵⁶, D.A. DeMarco¹⁶⁴, S. Demers¹⁸⁰, M. Demichev⁷⁷,
 S.P. Denisov¹²¹, D. Denysiuk¹¹⁸, L. D'Eramo¹³³, D. Derendarz⁸², J.E. Derkaoui^{34d}, F. Derue¹³³,
 P. Dervan⁸⁸, K. Desch²⁴, C. Deterre⁴⁴, K. Dette¹⁶⁴, M.R. Devesa³⁰, P.O. Deviveiros³⁵, A. Dewhurst¹⁴¹,
 S. Dhaliwal²⁶, F.A. Di Bello⁵², A. Di Ciaccio^{71a,71b}, L. Di Ciaccio⁵, W.K. Di Clemente¹³⁴,
 C. Di Donato^{67a,67b}, A. Di Girolamo³⁵, G. Di Gregorio^{69a,69b}, B. Di Micco^{72a,72b}, R. Di Nardo¹⁰⁰,
 K.F. Di Petrillo⁵⁷, R. Di Sipio¹⁶⁴, D. Di Valentino³³, C. Diaconu⁹⁹, M. Diamond¹⁶⁴, F.A. Dias³⁹,
 T. Dias Do Vale^{137a}, M.A. Diaz^{144a}, J. Dickinson¹⁸, E.B. Diehl¹⁰³, J. Dietrich¹⁹, S. Díez Cornell⁴⁴,
 A. Dimitrievska¹⁸, J. Dingfelder²⁴, F. Dittus³⁵, F. Djama⁹⁹, T. Djobava^{156b}, J.I. Djuvsland^{59a},
 M.A.B. Do Vale^{78c}, M. Dobre^{27b}, D. Dodsworth²⁶, C. Doglioni⁹⁴, J. Dolejsi¹⁴⁰, Z. Dolezal¹⁴⁰,
 M. Donadelli^{78d}, J. Donini³⁷, A. D'onofrio⁹⁰, M. D'Onofrio⁸⁸, J. Dopke¹⁴¹, A. Doria^{67a}, M.T. Dova⁸⁶,
 A.T. Doyle⁵⁵, E. Drechsler⁵¹, E. Dreyer¹⁴⁹, T. Dreyer⁵¹, Y. Du^{58b}, F. Dubinin¹⁰⁸, M. Dubovsky^{28a},
 A. Dubreuil⁵², E. Duchovni¹⁷⁷, G. Duckeck¹¹², A. Ducourthial¹³³, O.A. Ducu^{107,y}, D. Duda¹¹³,
 A. Dudarev³⁵, A.C. Dudder⁹⁷, E.M. Duffield¹⁸, L. Duflot¹²⁹, M. Dührssen³⁵, C. Dülsen¹⁷⁹,
 M. Dumancic¹⁷⁷, A.E. Dumitriu^{27b,e}, A.K. Duncan⁵⁵, M. Dunford^{59a}, A. Duperrin⁹⁹, H. Duran Yildiz^{4a},
 M. Düren⁵⁴, A. Durglishvili^{156b}, D. Duschinger⁴⁶, B. Dutta⁴⁴, D. Duvnjak¹, M. Dyndal⁴⁴, S. Dysch⁹⁸,
 B.S. Dziedzic⁸², C. Eckardt⁴⁴, K.M. Ecker¹¹³, R.C. Edgar¹⁰³, T. Eifert³⁵, G. Eigen¹⁷, K. Einsweiler¹⁸,
 T. Ekelof¹⁶⁹, M. El Kacimi^{34c}, R. El Kosseifi⁹⁹, V. Ellajosyula⁹⁹, M. Ellert¹⁶⁹, F. Ellinghaus¹⁷⁹,
 A.A. Elliot⁹⁰, N. Ellis³⁵, J. Elmsheuser²⁹, M. Elsing³⁵, D. Emeliyanov¹⁴¹, A. Emerman³⁸, Y. Enari¹⁶⁰,
 J.S. Ennis¹⁷⁵, M.B. Epland⁴⁷, J. Erdmann⁴⁵, A. Ereditato²⁰, S. Errede¹⁷⁰, M. Escalier¹²⁹, C. Escobar¹⁷¹,
 O. Estrada Pastor¹⁷¹, A.I. Etievre¹⁴², E. Etzion¹⁵⁸, H. Evans⁶³, A. Ezhilov¹³⁵, M. Ezzi^{34e}, F. Fabbri⁵⁵,
 L. Fabbri^{23b,23a}, V. Fabiani¹¹⁷, G. Facini⁹², R.M. Faisca Rodrigues Pereira^{137a}, R.M. Fakhrutdinov¹²¹,
 S. Falciano^{70a}, P.J. Falke⁵, S. Falke⁵, J. Faltova¹⁴⁰, Y. Fang^{15a}, M. Fanti^{66a,66b}, A. Farbin⁸, A. Farilla^{72a},
 E.M. Farina^{68a,68b}, T. Farooque¹⁰⁴, S. Farrell¹⁸, S.M. Farrington¹⁷⁵, P. Farthouat³⁵, F. Fassi^{34e},
 P. Fassnacht³⁵, D. Fassouliotis⁹, M. Fucci Giannelli⁴⁸, A. Favareto^{53b,53a}, W.J. Fawcett³¹, L. Fayard¹²⁹,
 O.L. Fedin^{135,q}, W. Fedorko¹⁷², M. Feickert⁴¹, S. Feigl¹³¹, L. Feligioni⁹⁹, C. Feng^{58b}, E.J. Feng³⁵,
 M. Feng⁴⁷, M.J. Fenton⁵⁵, A.B. Fenyuk¹²¹, L. Feremenga⁸, J. Ferrando⁴⁴, A. Ferrari¹⁶⁹, P. Ferrari¹¹⁸,
 R. Ferrari^{68a}, D.E. Ferreira de Lima^{59b}, A. Ferrer¹⁷¹, D. Ferrere⁵², C. Ferretti¹⁰³, F. Fiedler⁹⁷, A. Filipčič⁸⁹,
 F. Filthaut¹¹⁷, K.D. Finelli²⁵, M.C.N. Fiolhais^{137a,137c,a}, L. Fiorini¹⁷¹, C. Fischer¹⁴, W.C. Fisher¹⁰⁴,
 N. Flaschel⁴⁴, I. Fleck¹⁴⁸, P. Fleischmann¹⁰³, R.R.M. Fletcher¹³⁴, T. Flick¹⁷⁹, B.M. Flierl¹¹²,
 L.M. Flores¹³⁴, L.R. Flores Castillo^{61a}, F.M. Follega^{73a,73b}, N. Fomin¹⁷, G.T. Forcolin^{73a,73b},
 A. Formica¹⁴², F.A. Förster¹⁴, A.C. Forti⁹⁸, A.G. Foster²¹, D. Fournier¹²⁹, H. Fox⁸⁷, S. Fracchia¹⁴⁶,
 P. Francavilla^{69a,69b}, M. Franchini^{23b,23a}, S. Franchino^{59a}, D. Francis³⁵, L. Franconi¹⁴³, M. Franklin⁵⁷,
 M. Frate¹⁶⁸, M. Fraternali^{68a,68b}, A.N. Fray⁹⁰, D. Freeborn⁹², S.M. Fressard-Batraneanu³⁵, B. Freund¹⁰⁷,
 W.S. Freund^{78b}, E.M. Freundlich⁴⁵, D.C. Frizzell¹²⁵, D. Froidevaux³⁵, J.A. Frost¹³², C. Fukunaga¹⁶¹,
 E. Fullana Torregrosa¹⁷¹, T. Fusayasu¹¹⁴, J. Fuster¹⁷¹, O. Gabizon¹⁵⁷, A. Gabrielli^{23b,23a}, A. Gabrielli¹⁸,
 G.P. Gach^{81a}, S. Gadatsch⁵², P. Gadow¹¹³, G. Gagliardi^{53b,53a}, L.G. Gagnon¹⁰⁷, C. Galea^{27b},
 B. Galhardo^{137a,137c}, E.J. Gallas¹³², B.J. Gallop¹⁴¹, P. Gallus¹³⁹, G. Galster³⁹, R. Gamboa Goni⁹⁰,

K.K. Gan¹²³, S. Ganguly¹⁷⁷, J. Gao^{58a}, Y. Gao⁸⁸, Y.S. Gao^{150,n}, C. García¹⁷¹, J.E. García Navarro¹⁷¹,
 J.A. García Pascual^{15a}, M. Garcia-Sciveres¹⁸, R.W. Gardner³⁶, N. Garelli¹⁵⁰, V. Garonne¹³¹,
 K. Gasnikova⁴⁴, A. Gaudiello^{53b,53a}, G. Gaudio^{68a}, I.L. Gavrilenko¹⁰⁸, A. Gavriluk¹⁰⁹, C. Gay¹⁷²,
 G. Gaycken²⁴, E.N. Gazis¹⁰, C.N.P. Gee¹⁴¹, J. Geisen⁵¹, M. Geisen⁹⁷, M.P. Geisler^{59a},
 K. Gellerstedt^{43a,43b}, C. Gemme^{53b}, M.H. Genest⁵⁶, C. Geng¹⁰³, S. Gentile^{70a,70b}, S. George⁹¹,
 D. Gerbaudo¹⁴, G. Gessner⁴⁵, S. Ghasemi¹⁴⁸, M. Ghasemi Bostanabad¹⁷³, M. Ghneimat²⁴,
 B. Giacobbe^{23b}, S. Giagu^{70a,70b}, N. Giangiacomi^{23b,23a}, P. Giannetti^{69a}, A. Giannini^{67a,67b}, S.M. Gibson⁹¹,
 M. Gignac¹⁴³, D. Gillberg³³, G. Gilles¹⁷⁹, D.M. Gingrich^{3,av}, M.P. Giordani^{64a,64c}, F.M. Giorgi^{23b},
 P.F. Giraud¹⁴², P. Giromini⁵⁷, G. Giugliarelli^{64a,64c}, D. Giugni^{66a}, F. Giuli¹³², M. Giulini^{59b},
 S. Gkaitatzis¹⁵⁹, I. Gkialas^{9,k}, E.L. Gkougkousis¹⁴, P. Gkountoumis¹⁰, L.K. Gladilin¹¹¹, C. Glasman⁹⁶,
 J. Glatzer¹⁴, P.C.F. Glaysher⁴⁴, A. Glazov⁴⁴, M. Goblirsch-Kolb²⁶, J. Godlewski⁸², S. Goldfarb¹⁰²,
 T. Golling⁵², D. Golubkov¹²¹, A. Gomes^{137a,137b}, R. Goncalves Gama^{78a}, R. Gonçalo^{137a}, G. Gonella⁵⁰,
 L. Gonella²¹, A. Gongadze⁷⁷, F. Gonnella²¹, J.L. Gonski⁵⁷, S. González de la Hoz¹⁷¹,
 S. Gonzalez-Sevilla⁵², L. Goossens³⁵, P.A. Gorbounov¹⁰⁹, H.A. Gordon²⁹, B. Gorini³⁵, E. Gorini^{65a,65b},
 A. Gorišek⁸⁹, A.T. Goshaw⁴⁷, C. Gössling⁴⁵, M.I. Gostkin⁷⁷, C.A. Gottardo²⁴, C.R. Goudet¹²⁹,
 D. Goujdami^{34c}, A.G. Goussiou¹⁴⁵, N. Govender^{32b,c}, C. Goy⁵, E. Gozani¹⁵⁷, I. Grabowska-Bold^{81a},
 P.O.J. Gradin¹⁶⁹, E.C. Graham⁸⁸, J. Gramling¹⁶⁸, E. Gramstad¹³¹, S. Grancagnolo¹⁹, V. Gratchev¹³⁵,
 P.M. Gravila^{27f}, F.G. Gravili^{65a,65b}, C. Gray⁵⁵, H.M. Gray¹⁸, Z.D. Greenwood^{93,al}, C. Grefe²⁴,
 K. Gregersen⁹⁴, I.M. Gregor⁴⁴, P. Grenier¹⁵⁰, K. Grevtsov⁴⁴, N.A. Grieser¹²⁵, J. Griffiths⁸, A.A. Grillo¹⁴³,
 K. Grimm^{150,b}, S. Grinstein^{14,aa}, Ph. Gris³⁷, J.-F. Grivaz¹²⁹, S. Groh⁹⁷, E. Gross¹⁷⁷, J. Grosse-Knetter⁵¹,
 G.C. Grossi⁹³, Z.J. Grout⁹², C. Grud¹⁰³, A. Grummer¹¹⁶, L. Guan¹⁰³, W. Guan¹⁷⁸, J. Guenther³⁵,
 A. Guerguichon¹²⁹, F. Guescini^{165a}, D. Guest¹⁶⁸, R. Gugel⁵⁰, B. Gui¹²³, T. Guillemin⁵, S. Guindon³⁵,
 U. Gul⁵⁵, C. Gumpert³⁵, J. Guo^{58c}, W. Guo¹⁰³, Y. Guo^{58a,t}, Z. Guo⁹⁹, R. Gupta⁴⁴, S. Gurbuz^{12c},
 G. Gustavino¹²⁵, B.J. Gutelman¹⁵⁷, P. Gutierrez¹²⁵, C. Gutschow⁹², C. Guyot¹⁴², M.P. Guzik^{81a},
 C. Gwenlan¹³², C.B. Gwilliam⁸⁸, A. Haas¹²², C. Haber¹⁸, H.K. Hadavand⁸, N. Haddad^{34e}, A. Hadef^{58a},
 S. Hageböck²⁴, M. Hagihara¹⁶⁶, H. Hakobyan^{181,*}, M. Haleem¹⁷⁴, J. Haley¹²⁶, G. Halladjian¹⁰⁴,
 G.D. Hallewell⁹⁹, K. Hamacher¹⁷⁹, P. Hamal¹²⁷, K. Hamano¹⁷³, A. Hamilton^{32a}, G.N. Hamity¹⁴⁶,
 K. Han^{58a,ak}, L. Han^{58a}, S. Han^{15d}, K. Hanagaki^{79,w}, M. Hance¹⁴³, D.M. Handl¹¹², B. Haney¹³⁴,
 R. Hankache¹³³, P. Hanke^{59a}, E. Hansen⁹⁴, J.B. Hansen³⁹, J.D. Hansen³⁹, M.C. Hansen²⁴, P.H. Hansen³⁹,
 K. Hara¹⁶⁶, A.S. Hard¹⁷⁸, T. Harenberg¹⁷⁹, S. Harkusha¹⁰⁵, P.F. Harrison¹⁷⁵, N.M. Hartmann¹¹²,
 Y. Hasegawa¹⁴⁷, A. Hasib⁴⁸, S. Hassani¹⁴², S. Haug²⁰, R. Hauser¹⁰⁴, L. Hauswald⁴⁶, L.B. Havener³⁸,
 M. Havranek¹³⁹, C.M. Hawkes²¹, R.J. Hawkings³⁵, D. Hayden¹⁰⁴, C. Hayes¹⁵², C.P. Hays¹³², J.M. Hays⁹⁰,
 H.S. Hayward⁸⁸, S.J. Haywood¹⁴¹, M.P. Heath⁴⁸, V. Hedberg⁹⁴, L. Heelan⁸, S. Heer²⁴, K.K. Heidegger⁵⁰,
 J. Heilman³³, S. Heim⁴⁴, T. Heim¹⁸, B. Heinemann^{44,aq}, J.J. Heinrich¹¹², L. Heinrich¹²², C. Heinz⁵⁴,
 J. Hejbal¹³⁸, L. Helary³⁵, A. Held¹⁷², S. Hellesund¹³¹, S. Hellman^{43a,43b}, C. Helsens³⁵,
 R.C.W. Henderson⁸⁷, Y. Heng¹⁷⁸, S. Henkelmann¹⁷², A.M. Henriques Correia³⁵, G.H. Herbert¹⁹,
 H. Herde²⁶, V. Herget¹⁷⁴, Y. Hernández Jiménez^{32c}, H. Herr⁹⁷, M.G. Herrmann¹¹², T. Herrmann⁴⁶,
 G. Herten⁵⁰, R. Hertenberger¹¹², L. Hervas³⁵, T.C. Herwig¹³⁴, G.G. Hesketh⁹², N.P. Hessey^{165a},
 S. Higashino⁷⁹, E. Higón-Rodríguez¹⁷¹, K. Hildebrand³⁶, E. Hill¹⁷³, J.C. Hill³¹, K.K. Hill²⁹, K.H. Hiller⁴⁴,
 S.J. Hillier²¹, M. Hils⁴⁶, I. Hinchliffe¹⁸, M. Hirose¹³⁰, D. Hirschbuehl¹⁷⁹, B. Hiti⁸⁹, O. Hladík¹³⁸,
 D.R. Hlaluku^{32c}, X. Hoad⁴⁸, J. Hobbs¹⁵², N. Hod^{165a}, M.C. Hodgkinson¹⁴⁶, A. Hoecker³⁵,
 M.R. Hoeferkamp¹¹⁶, F. Hoenig¹¹², D. Hohn²⁴, D. Hohov¹²⁹, T.R. Holmes³⁶, M. Holzbock¹¹²,
 M. Homann⁴⁵, S. Honda¹⁶⁶, T. Honda⁷⁹, T.M. Hong¹³⁶, A. Hönl¹¹³, B.H. Hooberman¹⁷⁰,
 W.H. Hopkins¹²⁸, Y. Horii¹¹⁵, P. Horn⁴⁶, A.J. Horton¹⁴⁹, L.A. Horyn³⁶, J-Y. Hostachy⁵⁶, A. Hostiuc¹⁴⁵,
 S. Hou¹⁵⁵, A. Hoummada^{34a}, J. Howarth⁹⁸, J. Hoya⁸⁶, M. Hrabovsky¹²⁷, I. Hristova¹⁹, J. Hrvnac¹²⁹,
 A. Hrynevich¹⁰⁶, T. Hryń'ova⁵, P.J. Hsu⁶², S.-C. Hsu¹⁴⁵, Q. Hu²⁹, S. Hu^{58c}, Y. Huang^{15a}, Z. Hubacek¹³⁹,
 F. Hubaut⁹⁹, M. Huebner²⁴, F. Huegging²⁴, T.B. Huffman¹³², M. Huhtinen³⁵, R.F.H. Hunter³³, P. Huo¹⁵²,

A.M. Hupe³³, N. Huseynov^{77,ag}, J. Huston¹⁰⁴, J. Huth⁵⁷, R. Hyneman¹⁰³, G. Iacobucci⁵², G. Iakovidis²⁹, I. Ibragimov¹⁴⁸, L. Iconomidou-Fayard¹²⁹, Z. Idrissi^{34e}, P. Iengo³⁵, R. Ignazzi³⁹, O. Igonkina^{118,ac}, R. Iguchi¹⁶⁰, T. Iizawa⁵², Y. Ikegami⁷⁹, M. Ikeno⁷⁹, D. Iliadis¹⁵⁹, N. Illic¹¹⁷, F. Iltzsche⁴⁶, G. Introzzi^{68a,68b}, M. Iodice^{72a}, K. Iordanidou³⁸, V. Ippolito^{70a,70b}, M.F. Isacson¹⁶⁹, N. Ishijima¹³⁰, M. Ishino¹⁶⁰, M. Ishitsuka¹⁶², W. Islam¹²⁶, C. Issever¹³², S. Istin¹⁵⁷, F. Ito¹⁶⁶, J.M. Iturbe Ponce^{61a}, R. Iuppa^{73a,73b}, A. Ivina¹⁷⁷, H. Iwasaki⁷⁹, J.M. Izen⁴², V. Izzo^{67a}, P. Jacka¹³⁸, P. Jackson¹, R.M. Jacobs²⁴, V. Jain², G. Jäkel¹⁷⁹, K.B. Jakobi⁹⁷, K. Jakobs⁵⁰, S. Jakobsen⁷⁴, T. Jakoubek¹³⁸, D.O. Jamin¹²⁶, R. Jansky⁵², J. Janssen²⁴, M. Janus⁵¹, P.A. Janus^{81a}, G. Jarlskog⁹⁴, N. Javadov^{77,ag}, T. Javůrek³⁵, M. Javurkova⁵⁰, F. Jeanneau¹⁴², L. Jeanty¹⁸, J. Jejelava^{156a,ah}, A. Jelinskas¹⁷⁵, P. Jenni^{50,d}, J. Jeong⁴⁴, N. Jeong⁴⁴, S. Jézéquel⁵, H. Ji¹⁷⁸, J. Jia¹⁵², H. Jiang⁷⁶, Y. Jiang^{58a}, Z. Jiang^{150,r}, S. Jiggins⁵⁰, F.A. Jimenez Morales³⁷, J. Jimenez Pena¹⁷¹, S. Jin^{15c}, A. Jinaru^{27b}, O. Jinnouchi¹⁶², H. Jivan^{32c}, P. Johansson¹⁴⁶, K.A. Johns⁷, C.A. Johnson⁶³, W.J. Johnson¹⁴⁵, K. Jon-And^{43a,43b}, R.W.L. Jones⁸⁷, S.D. Jones¹⁵³, S. Jones⁷, T.J. Jones⁸⁸, J. Jongmanns^{59a}, P.M. Jorge^{137a,137b}, J. Jovicevic^{165a}, X. Ju¹⁸, J.J. Junggeburth¹¹³, A. Juste Rozas^{14,aa}, A. Kaczmarska⁸², M. Kado¹²⁹, H. Kagan¹²³, M. Kagan¹⁵⁰, T. Kaji¹⁷⁶, E. Kajomovitz¹⁵⁷, C.W. Kalderon⁹⁴, A. Kaluza⁹⁷, S. Kama⁴¹, A. Kamenshchikov¹²¹, L. Kanjir⁸⁹, Y. Kano¹⁶⁰, V.A. Kantserov¹¹⁰, J. Kanzaki⁷⁹, B. Kaplan¹²², L.S. Kaplan¹⁷⁸, D. Kar^{32c}, M.J. Kareem^{165b}, E. Karentzos¹⁰, S.N. Karpov⁷⁷, Z.M. Karpova⁷⁷, V. Kartvelishvili⁸⁷, A.N. Karyukhin¹²¹, L. Kashif¹⁷⁸, R.D. Kass¹²³, A. Kastanas^{43a,43b}, Y. Kataoka¹⁶⁰, C. Kato^{58d,58c}, J. Katzy⁴⁴, K. Kawade⁸⁰, K. Kawagoe⁸⁵, T. Kawamoto¹⁶⁰, G. Kawamura⁵¹, E.F. Kay⁸⁸, V.F. Kazanin^{120b,120a}, R. Keeler¹⁷³, R. Kehoe⁴¹, J.S. Keller³³, E. Kellermann⁹⁴, J.J. Kempster²¹, J. Kendrick²¹, O. Kepka¹³⁸, S. Kersten¹⁷⁹, B.P. Kerševan⁸⁹, S. Ketabchi Haghighat¹⁶⁴, R.A. Keyes¹⁰¹, M. Khader¹⁷⁰, F. Khalil-Zada¹³, A. Khanov¹²⁶, A.G. Kharlamov^{120b,120a}, T. Kharlamova^{120b,120a}, E.E. Khoda¹⁷², A. Khodinov¹⁶³, T.J. Khoo⁵², E. Khramov⁷⁷, J. Khubua^{156b}, S. Kido⁸⁰, M. Kiehn⁵², C.R. Kilby⁹¹, Y.K. Kim³⁶, N. Kimura^{64a,64c}, O.M. Kind¹⁹, B.T. King⁸⁸, D. Kirchmeier⁴⁶, J. Kirk¹⁴¹, A.E. Kiryunin¹¹³, T. Kishimoto¹⁶⁰, D. Kisielewska^{81a}, V. Kitali⁴⁴, O. Kivernyk⁵, E. Kladiva^{28b,*}, T. Klapdor-Kleingrothaus⁵⁰, M.H. Klein¹⁰³, M. Klein⁸⁸, U. Klein⁸⁸, K. Kleinknecht⁹⁷, P. Klimek¹¹⁹, A. Klimentov²⁹, T. Klingl²⁴, T. Klioutchnikova³⁵, F.F. Klitzner¹¹², P. Kluit¹¹⁸, S. Kluth¹¹³, E. Kneringer⁷⁴, E.B.F.G. Knoops⁹⁹, A. Knue⁵⁰, A. Kobayashi¹⁶⁰, D. Kobayashi⁸⁵, T. Kobayashi¹⁶⁰, M. Kobel⁴⁶, M. Kocian¹⁵⁰, P. Kodys¹⁴⁰, P.T. Koenig²⁴, T. Koffas³³, E. Koffeman¹¹⁸, N.M. Köhler¹¹³, T. Koi¹⁵⁰, M. Kolb^{59b}, I. Koletsou⁵, T. Kondo⁷⁹, N. Kondrashova^{58c}, K. Köneke⁵⁰, A.C. König¹¹⁷, T. Kono⁷⁹, R. Konoplich^{122,an}, V. Konstantinides⁹², N. Konstantinidis⁹², B. Konya⁹⁴, R. Kopeliansky⁶³, S. Koperny^{81a}, K. Korcyl⁸², K. Kordas¹⁵⁹, G. Koren¹⁵⁸, A. Korn⁹², I. Korolkov¹⁴, E.V. Korolkova¹⁴⁶, N. Korotkova¹¹¹, O. Kortner¹¹³, S. Kortner¹¹³, T. Kosek¹⁴⁰, V.V. Kostyukhin²⁴, A. Kotwal⁴⁷, A. Koulouris¹⁰, A. Kourkoumeli-Charalampidi^{68a,68b}, C. Kourkoumelis⁹, E. Kourlitis¹⁴⁶, V. Kouskoura²⁹, A.B. Kowalewska⁸², R. Kowalewski¹⁷³, T.Z. Kowalski^{81a}, C. Kozakai¹⁶⁰, W. Kozanecki¹⁴², A.S. Kozhin¹²¹, V.A. Kramarenko¹¹¹, G. Kramberger⁸⁹, D. Krasnopevtsev^{58a}, M.W. Krasny¹³³, A. Krasznahorkay³⁵, D. Krauss¹¹³, J.A. Kremer^{81a}, J. Kretzschmar⁸⁸, P. Krieger¹⁶⁴, K. Krizka¹⁸, K. Kroeninger⁴⁵, H. Kroha¹¹³, J. Kroll¹³⁸, J. Kroll¹³⁴, J. Krstic¹⁶, U. Kruchonak⁷⁷, H. Krüger²⁴, N. Krumnack⁷⁶, M.C. Kruse⁴⁷, T. Kubota¹⁰², S. Kuday^{4b}, J.T. Kuechler¹⁷⁹, S. Kuehn³⁵, A. Kugel^{59a}, F. Kuger¹⁷⁴, T. Kuhl⁴⁴, V. Kukhtin⁷⁷, R. Kukla⁹⁹, Y. Kulchitsky¹⁰⁵, S. Kuleshov^{144b}, Y.P. Kulinich¹⁷⁰, M. Kuna⁵⁶, T. Kunigo⁸³, A. Kupco¹³⁸, T. Kupfer⁴⁵, O. Kuprash¹⁵⁸, H. Kurashige⁸⁰, L.I. Kurchaninov^{165a}, Y.A. Kurochkin¹⁰⁵, A. Kurova¹¹⁰, M.G. Kurth^{15d}, E.S. Kuwertz³⁵, M. Kuze¹⁶², J. Kvita¹²⁷, T. Kwan¹⁰¹, A. La Rosa¹¹³, J.L. La Rosa Navarro^{78d}, L. La Rotonda^{40b,40a}, F. La Ruffa^{40b,40a}, C. Lacasta¹⁷¹, F. Lacava^{70a,70b}, J. Lacey⁴⁴, D.P.J. Lack⁹⁸, H. Lacker¹⁹, D. Lacour¹³³, E. Ladygin⁷⁷, R. Lafaye⁵, B. Laforge¹³³, T. Lagouri^{32c}, S. Lai⁵¹, S. Lammers⁶³, W. Lampl⁷, E. Lançon²⁹, U. Landgraf⁵⁰, M.P.J. Landon⁹⁰, M.C. Lanfermann⁵², V.S. Lang⁴⁴, J.C. Lange⁵¹, R.J. Langenberg³⁵, A.J. Lankford¹⁶⁸, F. Lanni²⁹, K. Lantzsch²⁴, A. Lanza^{68a}, A. Lapertosa^{53b,53a}, S. Laplace¹³³, J.F. Laporte¹⁴², T. Lari^{66a}, F. Lasagni Manghi^{23b,23a}, M. Lassnig³⁵, T.S. Lau^{61a}, A. Laudrain¹²⁹, M. Lavorgna^{67a,67b}, A.T. Law¹⁴³,

M. Lazzaroni^{66a,66b}, B. Le¹⁰², O. Le Dortz¹³³, E. Le Guirriec⁹⁹, E.P. Le Quilleuc¹⁴², M. LeBlanc⁷, T. LeCompte⁶, F. Ledroit-Guillon⁵⁶, C.A. Lee²⁹, G.R. Lee^{144a}, L. Lee⁵⁷, S.C. Lee¹⁵⁵, B. Lefebvre¹⁰¹, M. Lefebvre¹⁷³, F. Legger¹¹², C. Leggett¹⁸, K. Lehmann¹⁴⁹, N. Lehmann¹⁷⁹, G. Lehmann Miotto³⁵, W.A. Leight⁴⁴, A. Leisos^{159,x}, M.A.L. Leite^{78d}, R. Leitner¹⁴⁰, D. Lellouch¹⁷⁷, K.J.C. Leney⁹², T. Lenz²⁴, B. Lenzi³⁵, R. Leone⁷, S. Leone^{69a}, C. Leonidopoulos⁴⁸, G. Lerner¹⁵³, C. Leroy¹⁰⁷, R. Les¹⁶⁴, A.A.J. Lesage¹⁴², C.G. Lester³¹, M. Levchenko¹³⁵, J. Levêque⁵, D. Levin¹⁰³, L.J. Levinson¹⁷⁷, D. Lewis⁹⁰, B. Li¹⁰³, C.-Q. Li^{58a,am}, H. Li^{58b}, L. Li^{58c}, M. Li^{15a}, Q. Li^{15d}, Q.Y. Li^{58a}, S. Li^{58d,58c}, X. Li^{58c}, Y. Li¹⁴⁸, Z. Liang^{15a}, B. Liberti^{71a}, A. Liblong¹⁶⁴, K. Lie^{61c}, S. Liem¹¹⁸, A. Limosani¹⁵⁴, C.Y. Lin³¹, K. Lin¹⁰⁴, T.H. Lin⁹⁷, R.A. Linck⁶³, J.H. Lindon²¹, B.E. Lindquist¹⁵², A.L. Lioni⁵², E. Lipeles¹³⁴, A. Lipniacka¹⁷, M. Lisovyi^{59b}, T.M. Liss^{170,as}, A. Lister¹⁷², A.M. Litke¹⁴³, J.D. Little⁸, B. Liu⁷⁶, B.L. Liu⁶, H.B. Liu²⁹, H. Liu¹⁰³, J.B. Liu^{58a}, J.K.K. Liu¹³², K. Liu¹³³, M. Liu^{58a}, P. Liu¹⁸, Y. Liu^{15a}, Y.L. Liu^{58a}, Y.W. Liu^{58a}, M. Livan^{68a,68b}, A. Lleres⁵⁶, J. Llorente Merino^{15a}, S.L. Lloyd⁹⁰, C.Y. Lo^{61b}, F. Lo Sterzo⁴¹, E.M. Lobodzinska⁴⁴, P. Loch⁷, T. Lohse¹⁹, K. Lohwasser¹⁴⁶, M. Lokajicek¹³⁸, J.D. Long¹⁷⁰, R.E. Long⁸⁷, L. Longo^{65a,65b}, K.A.Looper¹²³, J.A. Lopez^{144b}, I. Lopez Paz⁹⁸, A. Lopez Solis¹⁴⁶, J. Lorenz¹¹², N. Lorenzo Martinez⁵, M. Losada²², P.J. Lösel¹¹², A. Lösle⁵⁰, X. Lou⁴⁴, X. Lou^{15a}, A. Lounis¹²⁹, J. Love⁶, P.A. Love⁸⁷, J.J. Lozano Bahilo¹⁷¹, H. Lu^{61a}, M. Lu^{58a}, N. Lu¹⁰³, Y.J. Lu⁶², H.J. Lubatti¹⁴⁵, C. Luci^{70a,70b}, A. Lucotte⁵⁶, C. Luedtke⁵⁰, F. Luehring⁶³, I. Luise¹³³, L. Luminari^{70a}, B. Lund-Jensen¹⁵¹, M.S. Lutz¹⁰⁰, P.M. Luzi¹³³, D. Lynn²⁹, R. Lysak¹³⁸, E. Lytken⁹⁴, F. Lyu^{15a}, V. Lyubushkin⁷⁷, T. Lyubushkina⁷⁷, H. Ma²⁹, L.L. Ma^{58b}, Y. Ma^{58b}, G. Maccarrone⁴⁹, A. Macchiolo¹¹³, C.M. Macdonald¹⁴⁶, J. Machado Miguens^{134,137b}, D. Madaffari¹⁷¹, R. Madar³⁷, W.F. Mader⁴⁶, A. Madsen⁴⁴, N. Madysa⁴⁶, J. Maeda⁸⁰, K. Maekawa¹⁶⁰, S. Maeland¹⁷, T. Maeno²⁹, M. Maerker⁴⁶, A.S. Maevskiy¹¹¹, V. Magerl⁵⁰, D.J. Mahon³⁸, C. Maidantchik^{78b}, T. Maier¹¹², A. Maio^{137a,137b,137d}, O. Majersky^{28a}, S. Majewski¹²⁸, Y. Makida⁷⁹, N. Makovec¹²⁹, B. Malaescu¹³³, Pa. Malecki⁸², V.P. Maleev¹³⁵, F. Malek⁵⁶, U. Mallik⁷⁵, D. Malon⁶, C. Malone³¹, S. Maltezos¹⁰, S. Malyukov³⁵, J. Mamuzic¹⁷¹, G. Mancini⁴⁹, I. Mandic⁸⁹, J. Maneira^{137a}, L. Manhaes de Andrade Filho^{78a}, J. Manjarres Ramos⁴⁶, K.H. Mankinen⁹⁴, A. Mann¹¹², A. Manousos⁷⁴, B. Mansoulie¹⁴², J.D. Mansour^{15a}, M. Mantoani⁵¹, S. Manzoni^{66a,66b}, A. Marantis¹⁵⁹, G. Marceca³⁰, L. March⁵², L. Marchese¹³², G. Marchiori¹³³, M. Marcisovsky¹³⁸, C.A. Marin Tobon³⁵, M. Marjanovic³⁷, D.E. Marley¹⁰³, F. Marroquim^{78b}, Z. Marshall¹⁸, M.U.F Martensson¹⁶⁹, S. Marti-Garcia¹⁷¹, C.B. Martin¹²³, T.A. Martin¹⁷⁵, V.J. Martin⁴⁸, B. Martin dit Latour¹⁷, M. Martinez^{14,aa}, V.I. Martinez Outschoorn¹⁰⁰, S. Martin-Haugh¹⁴¹, V.S. Martoiu^{27b}, A.C. Martyniuk⁹², A. Marzin³⁵, L. Masetti⁹⁷, T. Mashimo¹⁶⁰, R. Mashinistov¹⁰⁸, J. Masik⁹⁸, A.L. Maslennikov^{120b,120a}, L.H. Mason¹⁰², L. Massa^{71a,71b}, P. Massarotti^{67a,67b}, P. Mastrandrea⁵, A. Mastroberardino^{40b,40a}, T. Masubuchi¹⁶⁰, P. Mättig¹⁷⁹, J. Maurer^{27b}, B. Maček⁸⁹, S.J. Maxfield⁸⁸, D.A. Maximov^{120b,120a}, R. Mazini¹⁵⁵, I. Maznas¹⁵⁹, S.M. Mazza¹⁴³, G. Mc Goldrick¹⁶⁴, S.P. Mc Kee¹⁰³, A. McCarn¹⁰³, T.G. McCarthy¹¹³, L.I. McClymont⁹², E.F. McDonald¹⁰², J.A. Mcfayden³⁵, G. Mchedlidze⁵¹, M.A. McKay⁴¹, K.D. McLean¹⁷³, S.J. McMahon¹⁴¹, P.C. McNamara¹⁰², C.J. McNicol¹⁷⁵, R.A. McPherson^{173,ae}, J.E. Mdhluli^{32c}, Z.A. Meadows¹⁰⁰, S. Meehan¹⁴⁵, T.M. Megy⁵⁰, S. Mehlhase¹¹², A. Mehta⁸⁸, T. Meideck⁵⁶, B. Meirose⁴², D. Melini^{171,h}, B.R. Mellado Garcia^{32c}, J.D. Mellenthin⁵¹, M. Melo^{28a}, F. Meloni⁴⁴, A. Melzer²⁴, S.B. Menary⁹⁸, E.D. Mendes Gouveia^{137a}, L. Meng⁸⁸, X.T. Meng¹⁰³, A. Mengarelli^{23b,23a}, S. Menke¹¹³, E. Meoni^{40b,40a}, S. Mergelmeyer¹⁹, S.A.M. Merkt¹³⁶, C. Merlassino²⁰, P. Mermod⁵², L. Merola^{67a,67b}, C. Meroni^{66a}, F.S. Merritt³⁶, A. Messina^{70a,70b}, J. Metcalfe⁶, A.S. Mete¹⁶⁸, C. Meyer¹³⁴, J. Meyer¹⁵⁷, J-P. Meyer¹⁴², H. Meyer Zu Theenhausen^{59a}, F. Miano¹⁵³, R.P. Middleton¹⁴¹, L. Mijović⁴⁸, G. Mikenberg¹⁷⁷, M. Mikestikova¹³⁸, M. Mikuž⁸⁹, M. Milesi¹⁰², A. Milic¹⁶⁴, D.A. Millar⁹⁰, D.W. Miller³⁶, A. Milov¹⁷⁷, D.A. Milstead^{43a,43b}, A.A. Minaenko¹²¹, M. Miñano Moya¹⁷¹, I.A. Minashvili^{156b}, A.I. Mincer¹²², B. Mindur^{81a}, M. Mineev⁷⁷, Y. Minegishi¹⁶⁰, Y. Ming¹⁷⁸, L.M. Mir¹⁴, A. Mirto^{65a,65b}, K.P. Mistry¹³⁴, T. Mitani¹⁷⁶, J. Mitrevski¹¹², V.A. Mitsou¹⁷¹, A. Miucci²⁰, P.S. Miyagawa¹⁴⁶, A. Mizukami⁷⁹, J.U. Mjörnmark⁹⁴, T. Mkrtchyan¹⁸¹, M. Mlynarikova¹⁴⁰, T. Moa^{43a,43b}, K. Mochizuki¹⁰⁷,

P. Mogg⁵⁰, S. Mohapatra³⁸, S. Molander^{43a,43b}, R. Moles-Valls²⁴, M.C. Mondragon¹⁰⁴, K. Mönig⁴⁴, J. Monk³⁹, E. Monnier⁹⁹, A. Montalbano¹⁴⁹, J. Montejo Berlingen³⁵, F. Monticelli⁸⁶, S. Monzani^{66a}, N. Morange¹²⁹, D. Moreno²², M. Moreno Llácer³⁵, P. Morettini^{53b}, M. Morgenstern¹¹⁸, S. Morgenstern⁴⁶, D. Mori¹⁴⁹, M. Mori⁵⁷, M. Morinaga¹⁷⁶, V. Morisbak¹³¹, A.K. Morley³⁵, G. Mornacchi³⁵, A.P. Morris⁹², J.D. Morris⁹⁰, L. Morvaj¹⁵², P. Moschovakos¹⁰, M. Mosidze^{156b}, H.J. Moss¹⁴⁶, J. Moss^{150,o}, K. Motohashi¹⁶², R. Mount¹⁵⁰, E. Mountricha³⁵, E.J.W. Moyse¹⁰⁰, S. Muanza⁹⁹, F. Mueller¹¹³, J. Mueller¹³⁶, R.S.P. Mueller¹¹², D. Muenstermann⁸⁷, G.A. Mullier⁹⁴, F.J. Munoz Sanchez⁹⁸, P. Murin^{28b}, W.J. Murray^{175,141}, A. Murrone^{66a,66b}, M. Muškinja⁸⁹, C. Mwewa^{32a}, A.G. Myagkov^{121,ao}, J. Myers¹²⁸, M. Myska¹³⁹, B.P. Nachman¹⁸, O. Nackenhorst⁴⁵, K. Nagai¹³², K. Nagano⁷⁹, Y. Nagasaka⁶⁰, M. Nagel⁵⁰, E. Nagy⁹⁹, A.M. Nairz³⁵, Y. Nakahama¹¹⁵, K. Nakamura⁷⁹, T. Nakamura¹⁶⁰, I. Nakano¹²⁴, H. Nanjo¹³⁰, F. Napolitano^{59a}, R.F. Naranjo Garcia⁴⁴, R. Narayan¹¹, D.I. Narrias Villar^{59a}, I. Naryshkin¹³⁵, T. Naumann⁴⁴, G. Navarro²², R. Nayyar⁷, H.A. Neal^{103,*}, P.Y. Nechaeva¹⁰⁸, T.J. Neep¹⁴², A. Negri^{68a,68b}, M. Negrini^{23b}, S. Nektarijevic¹¹⁷, C. Nellist⁵¹, M.E. Nelson¹³², S. Nemecek¹³⁸, P. Nemethy¹²², M. Nessi^{35,f}, M.S. Neubauer¹⁷⁰, M. Neumann¹⁷⁹, P.R. Newman²¹, T.Y. Ng^{61c}, Y.S. Ng¹⁹, H.D.N. Nguyen⁹⁹, T. Nguyen Manh¹⁰⁷, E. Nibigira³⁷, R.B. Nickerson¹³², R. Nicolaïdou¹⁴², D.S. Nielsen³⁹, J. Nielsen¹⁴³, N. Nikiforou¹¹, V. Nikolaenko^{121,ao}, I. Nikolic-Audit¹³³, K. Nikolopoulos²¹, P. Nilsson²⁹, Y. Ninomiya⁷⁹, A. Nisati^{70a}, N. Nishu^{58c}, R. Nisius¹¹³, I. Nitsche⁴⁵, T. Nitta¹⁷⁶, T. Nobe¹⁶⁰, Y. Noguchi⁸³, M. Nomachi¹³⁰, I. Nomidis¹³³, M.A. Nomura²⁹, T. Nooney⁹⁰, M. Nordberg³⁵, N. Norjoharuddeen¹³², T. Novak⁸⁹, O. Novgorodova⁴⁶, R. Novotny¹³⁹, L. Nozka¹²⁷, K. Ntekas¹⁶⁸, E. Nurse⁹², F. Nuti¹⁰², F.G. Oakham^{33,av}, H. Oberlack¹¹³, J. Ocariz¹³³, A. Ochi⁸⁰, I. Ochoa³⁸, J.P. Ochoa-Ricoux^{144a}, K. O'Connor²⁶, S. Oda⁸⁵, S. Odaka⁷⁹, S. Oerdeke⁵¹, A. Oh⁹⁸, S.H. Oh⁴⁷, C.C. Ohm¹⁵¹, H. Oide^{53b,53a}, M.L. Ojeda¹⁶⁴, H. Okawa¹⁶⁶, Y. Okazaki⁸³, Y. Okumura¹⁶⁰, T. Okuyama⁷⁹, A. Olariu^{27b}, L.F. Oleiro Seabra^{137a}, S.A. Olivares Pino^{144a}, D. Oliveira Damazio²⁹, J.L. Oliver¹, M.J.R. Olsson³⁶, A. Olszewski⁸², J. Olszowska⁸², D.C. O'Neil¹⁴⁹, A. Onofre^{137a,137e}, K. Onogi¹¹⁵, P.U.E. Onyisi¹¹, H. Oppen¹³¹, M.J. Oreglia³⁶, G.E. Orellana⁸⁶, Y. Oren¹⁵⁸, D. Orestano^{72a,72b}, E.C. Orgill⁹⁸, N. Orlando^{61b}, A.A. O'Rourke⁴⁴, R.S. Orr¹⁶⁴, B. Osculati^{53b,53a,*}, V. O'Shea⁵⁵, R. Ospanov^{58a}, G. Otero y Garzon³⁰, H. Otono⁸⁵, M. Ouchrif^{34d}, F. Ould-Saada¹³¹, A. Ouraou¹⁴², Q. Ouyang^{15a}, M. Owen⁵⁵, R.E. Owen²¹, V.E. Ozcan^{12c}, N. Ozturk⁸, J. Pacalt¹²⁷, H.A. Pacey³¹, K. Pachal¹⁴⁹, A. Pacheco Pages¹⁴, L. Pacheco Rodriguez¹⁴², C. Padilla Aranda¹⁴, S. Pagan Griso¹⁸, M. Paganini¹⁸⁰, G. Palacino⁶³, S. Palazzo^{40b,40a}, S. Palestini³⁵, M. Palka^{81b}, D. Pallin³⁷, I. Panagoulias¹⁰, C.E. Pandini³⁵, J.G. Panduro Vazquez⁹¹, P. Pani³⁵, G. Panizzo^{64a,64c}, L. Paolozzi⁵², T.D. Papadopoulou¹⁰, K. Papageorgiou^{9,k}, A. Paramonov⁶, D. Paredes Hernandez^{61b}, S.R. Paredes Saenz¹³², B. Parida¹⁶³, T.H. Park³³, A.J. Parker⁸⁷, K.A. Parker⁴⁴, M.A. Parker³¹, F. Parodi^{53b,53a}, J.A. Parsons³⁸, U. Parzefall⁵⁰, V.R. Pascuzzi¹⁶⁴, J.M.P. Pasner¹⁴³, E. Pasqualucci^{70a}, S. Passaggio^{53b}, F. Pastore⁹¹, P. Pasuwant^{43a,43b}, S. Pataraia⁹⁷, J.R. Pater⁹⁸, A. Pathak^{178,1}, T. Pauly³⁵, B. Pearson¹¹³, M. Pedersen¹³¹, L. Pedraza Diaz¹¹⁷, R. Pedro^{137a,137b}, S.V. Peleganchuk^{120b,120a}, O. Penc¹³⁸, C. Peng^{15d}, H. Peng^{58a}, B.S. Peralva^{78a}, M.M. Perego¹²⁹, A.P. Pereira Peixoto^{137a}, D.V. Perepelitsa²⁹, F. Peri¹⁹, L. Perini^{66a,66b}, H. Pernegger³⁵, S. Perrella^{67a,67b}, V.D. Peshekhanov^{77,*}, K. Peters⁴⁴, R.F.Y. Peters⁹⁸, B.A. Petersen³⁵, T.C. Petersen³⁹, E. Petit⁵⁶, A. Petridis¹, C. Petridou¹⁵⁹, P. Petroff¹²⁹, M. Petrov¹³², F. Petrucci^{72a,72b}, M. Pettee¹⁸⁰, N.E. Pettersson¹⁰⁰, A. Peyaud¹⁴², R. Pezoa^{144b}, T. Pham¹⁰², F.H. Phillips¹⁰⁴, P.W. Phillips¹⁴¹, M.W. Phipps¹⁷⁰, G. Piacquadio¹⁵², E. Pianori¹⁸, A. Picazio¹⁰⁰, M.A. Pickering¹³², R.H. Pickles⁹⁸, R. Piegaia³⁰, J.E. Pilcher³⁶, A.D. Pilkington⁹⁸, M. Pinamonti^{71a,71b}, J.L. Pinfold³, M. Pitt¹⁷⁷, L. Pizzimenti^{71a,71b}, M.-A. Pleier²⁹, V. Pleskot¹⁴⁰, E. Plotnikova⁷⁷, D. Pluth⁷⁶, P. Podberezk^{120b,120a}, R. Poettgen⁹⁴, R. Poggi⁵², L. Poggioli¹²⁹, I. Pogrebnyak¹⁰⁴, D. Pohl²⁴, I. Pokharel⁵¹, G. Polesello^{68a}, A. Poley¹⁸, A. Policicchio^{70a,70b}, R. Polifka³⁵, A. Polini^{23b}, C.S. Pollard⁴⁴, V. Polychronakos²⁹, D. Ponomarenko¹¹⁰, L. Pontecorvo³⁵, G.A. Popenciu^{27d}, D.M. Portillo Quintero¹³³, S. Pospisil¹³⁹, K. Potamianos⁴⁴, I.N. Potrap⁷⁷, C.J. Potter³¹, H. Potti¹¹, T. Poulsen⁹⁴, J. Poveda³⁵, T.D. Powell¹⁴⁶,

M.E. Pozo Astigarraga³⁵, P. Pralavorio⁹⁹, S. Prell⁷⁶, D. Price⁹⁸, M. Primavera^{65a}, S. Prince¹⁰¹,
 N. Proklova¹¹⁰, K. Prokofiev^{61c}, F. Prokoshin^{144b}, S. Protopopescu²⁹, J. Proudfoot⁶, M. Przybycien^{81a},
 A. Puri¹⁷⁰, P. Puzo¹²⁹, J. Qian¹⁰³, Y. Qin⁹⁸, A. Quadt⁵¹, M. Queitsch-Maitland⁴⁴, A. Qureshi¹, P. Rados¹⁰²,
 F. Ragusa^{66a,66b}, G. Rahal⁹⁵, J.A. Raine⁵², S. Rajagopalan²⁹, A. Ramirez Morales⁹⁰, T. Rashid¹²⁹,
 S. Raspopov⁵, M.G. Ratti^{66a,66b}, D.M. Rauch⁴⁴, F. Rauscher¹¹², S. Rave⁹⁷, B. Ravina¹⁴⁶, I. Ravinovich¹⁷⁷,
 J.H. Rawling⁹⁸, M. Raymond³⁵, A.L. Read¹³¹, N.P. Readioff⁵⁶, M. Reale^{65a,65b}, D.M. Rebuzzi^{68a,68b},
 A. Redelbach¹⁷⁴, G. Redlinger²⁹, R. Reece¹⁴³, R.G. Reed^{32c}, K. Reeves⁴², L. Rehnisch¹⁹, J. Reichert¹³⁴,
 D. Reikher¹⁵⁸, A. Reiss⁹⁷, C. Rembser³⁵, H. Ren^{15d}, M. Rescigno^{70a}, S. Resconi^{66a}, E.D. Ressegue¹³⁴,
 S. Rettie¹⁷², E. Reynolds²¹, O.L. Rezanova^{120b,120a}, P. Reznicek¹⁴⁰, E. Ricci^{73a,73b}, R. Richter¹¹³,
 S. Richter⁴⁴, E. Richter-Was^{81b}, O. Ricken²⁴, M. Ridel¹³³, P. Rieck¹¹³, C.J. Riegel¹⁷⁹, O. Rifki⁴⁴,
 M. Rijssenbeek¹⁵², A. Rimoldi^{68a,68b}, M. Rimoldi²⁰, L. Rinaldi^{23b}, G. Ripellino¹⁵¹, B. Ristic⁸⁷,
 E. Ritsch³⁵, I. Riu¹⁴, J.C. Rivera Vergara^{144a}, F. Rizatdinova¹²⁶, E. Rizvi⁹⁰, C. Rizzi¹⁴, R.T. Roberts⁹⁸,
 S.H. Robertson^{101,ae}, M. Robin⁴⁴, D. Robinson³¹, J.E.M. Robinson⁴⁴, A. Robson⁵⁵, E. Rocco⁹⁷,
 C. Roda^{69a,69b}, Y. Rodina⁹⁹, S. Rodriguez Bosca¹⁷¹, A. Rodriguez Perez¹⁴, D. Rodriguez Rodriguez¹⁷¹,
 A.M. Rodríguez Vera^{165b}, S. Roe³⁵, C.S. Rogan⁵⁷, O. Røhne¹³¹, R. Röhrlig¹¹³, C.P.A. Roland⁶³, J. Roloff⁵⁷,
 A. Romaniouk¹¹⁰, M. Romano^{23b,23a}, N. Rompotis⁸⁸, M. Ronzani¹²², L. Roos¹³³, S. Rosati^{70a},
 K. Rosbach⁵⁰, N-A. Rosien⁵¹, B.J. Rosser¹³⁴, E. Rossi⁴⁴, E. Rossi^{72a,72b}, E. Rossi^{67a,67b}, L.P. Rossi^{53b},
 L. Rossini^{66a,66b}, J.H.N. Rosten³¹, R. Rosten¹⁴, M. Rotaru^{27b}, J. Rothberg¹⁴⁵, D. Rousseau¹²⁹, D. Roy^{32c},
 A. Rozanov⁹⁹, Y. Rozen¹⁵⁷, X. Ruan^{32c}, F. Rubbo¹⁵⁰, F. Rühr⁵⁰, A. Ruiz-Martinez¹⁷¹, Z. Rurikova⁵⁰,
 N.A. Rusakovich⁷⁷, H.L. Russell¹⁰¹, J.P. Rutherford⁷, E.M. Rüttinger^{44,m}, Y.F. Ryabov¹³⁵, M. Rybar¹⁷⁰,
 G. Rybkin¹²⁹, S. Ryu⁶, A. Ryzhov¹²¹, G.F. Rzehorž⁵¹, P. Sabatini⁵¹, G. Sabato¹¹⁸, S. Sacerdoti¹²⁹,
 H.F-W. Sadrozinski¹⁴³, R. Sadykov⁷⁷, F. Safai Tehrani^{70a}, P. Saha¹¹⁹, M. Sahinsoy^{59a}, A. Sahu¹⁷⁹,
 M. Saimpert⁴⁴, M. Saito¹⁶⁰, T. Saito¹⁶⁰, H. Sakamoto¹⁶⁰, A. Sakharov^{122,an}, D. Salamani⁵²,
 G. Salamanna^{72a,72b}, J.E. Salazar Loyola^{144b}, P.H. Sales De Bruin¹⁶⁹, D. Salihagic¹¹³, A. Salnikov¹⁵⁰,
 J. Salt¹⁷¹, D. Salvatore^{40b,40a}, F. Salvatore¹⁵³, A. Salvucci^{61a,61b,61c}, A. Salzburger³⁵, J. Samarati³⁵,
 D. Sammel⁵⁰, D. Sampsonidis¹⁵⁹, D. Sampsonidou¹⁵⁹, J. Sánchez¹⁷¹, A. Sanchez Pineda^{64a,64c},
 H. Sandaker¹³¹, C.O. Sander⁴⁴, M. Sandhoff¹⁷⁹, C. Sandoval²², D.P.C. Sankey¹⁴¹, M. Sannino^{53b,53a},
 Y. Sano¹¹⁵, A. Sansoni⁴⁹, C. Santoni³⁷, H. Santos^{137a}, I. Santoyo Castillo¹⁵³, A. Santra¹⁷¹, A. Sapronov⁷⁷,
 J.G. Saraiva^{137a,137d}, O. Sasaki⁷⁹, K. Sato¹⁶⁶, E. Sauvan⁵, P. Savard^{164,av}, N. Savic¹¹³, R. Sawada¹⁶⁰,
 C. Sawyer¹⁴¹, L. Sawyer^{93,al}, C. Sbarra^{23b}, A. Sbrizzi^{23a}, T. Scanlon⁹², J. Schaarschmidt¹⁴⁵, P. Schacht¹¹³,
 B.M. Schachtner¹¹², D. Schaefer³⁶, L. Schaefer¹³⁴, J. Schaeffer⁹⁷, S. Schaepe³⁵, U. Schäfer⁹⁷,
 A.C. Schaffer¹²⁹, D. Schaille¹¹², R.D. Schamberger¹⁵², N. Scharmburg⁹⁸, V.A. Schegelsky¹³⁵,
 D. Scheirich¹⁴⁰, F. Schenck¹⁹, M. Schernau¹⁶⁸, C. Schiavi^{53b,53a}, S. Schier¹⁴³, L.K. Schildgen²⁴,
 Z.M. Schillaci²⁶, E.J. Schioppa³⁵, M. Schioppa^{40b,40a}, K.E. Schleicher⁵⁰, S. Schlenker³⁵,
 K.R. Schmidt-Sommerfeld¹¹³, K. Schmieden³⁵, C. Schmitt⁹⁷, S. Schmitt⁴⁴, S. Schmitz⁹⁷,
 J.C. Schmoeckel⁴⁴, U. Schnoor⁵⁰, L. Schoeffel¹⁴², A. Schoening^{59b}, E. Schopf¹³², M. Schott⁹⁷,
 J.F.P. Schouwenberg¹¹⁷, J. Schovancova³⁵, S. Schramm⁵², A. Schulte⁹⁷, H-C. Schultz-Coulon^{59a},
 M. Schumacher⁵⁰, B.A. Schumm¹⁴³, Ph. Schune¹⁴², A. Schwartzman¹⁵⁰, T.A. Schwarz¹⁰³,
 Ph. Schwemling¹⁴², R. Schwienhorst¹⁰⁴, A. Sciandra²⁴, G. Sciolla²⁶, M. Scornajenghi^{40b,40a}, F. Scuri^{69a},
 F. Scutti¹⁰², L.M. Scyboz¹¹³, C.D. Sebastiani^{70a,70b}, P. Seema¹⁹, S.C. Seidel¹¹⁶, A. Seiden¹⁴³, T. Seiss³⁶,
 J.M. Seixas^{78b}, G. Sekhniaidze^{67a}, K. Sekhon¹⁰³, S.J. Sekula⁴¹, N. Semprini-Cesari^{23b,23a}, S. Sen⁴⁷,
 S. Senkin³⁷, C. Serfon¹³¹, L. Serin¹²⁹, L. Serkin^{64a,64b}, M. Sessa^{58a}, H. Severini¹²⁵, F. Sforza¹⁶⁷,
 A. Sfyrla⁵², E. Shabalina⁵¹, J.D. Shahinian¹⁴³, N.W. Shaikh^{43a,43b}, L.Y. Shan^{15a}, R. Shang¹⁷⁰, J.T. Shank²⁵,
 M. Shapiro¹⁸, A.S. Sharma¹, A. Sharma¹³², P.B. Shatalov¹⁰⁹, K. Shaw¹⁵³, S.M. Shaw⁹⁸,
 A. Shcherbakova¹³⁵, Y. Shen¹²⁵, N. Sherafati³³, A.D. Sherman²⁵, P. Sherwood⁹², L. Shi^{155,ar}, S. Shimizu⁷⁹,
 C.O. Shimmin¹⁸⁰, Y. Shimogama¹⁷⁶, M. Shimojima¹¹⁴, I.P.J. Shipsey¹³², S. Shirabe⁸⁵, M. Shiyakova⁷⁷,
 J. Shlomi¹⁷⁷, A. Shmeleva¹⁰⁸, D. Shoaleh Saadi¹⁰⁷, M.J. Shochet³⁶, S. Shoaiii¹⁰², D.R. Shope¹²⁵,

S. Shrestha¹²³, E. Shulga¹¹⁰, P. Sicho¹³⁸, A.M. Sickles¹⁷⁰, P.E. Sidebo¹⁵¹, E. Sideras Haddad^{32c}, O. Sidiropoulou³⁵, A. Sidoti^{23b,23a}, F. Siegert⁴⁶, Dj. Sijacki¹⁶, J. Silva^{137a}, M. Silva Jr.¹⁷⁸, M.V. Silva Oliveira^{78a}, S.B. Silverstein^{43a}, S. Simion¹²⁹, E. Simioni⁹⁷, M. Simon⁹⁷, R. Simonello⁹⁷, P. Sinervo¹⁶⁴, N.B. Sinev¹²⁸, M. Sioli^{23b,23a}, G. Siragusa¹⁷⁴, I. Siral¹⁰³, S.Yu. Sivoklokov¹¹¹, J. Sjölin^{43a,43b}, P. Skubic¹²⁵, M. Slater²¹, T. Slavicek¹³⁹, M. Slawinska⁸², K. Sliwa¹⁶⁷, R. Slovak¹⁴⁰, V. Smakhtin¹⁷⁷, B.H. Smart⁵, J. Smiesko^{28a}, N. Smirnov¹¹⁰, S.Yu. Smirnov¹¹⁰, Y. Smirnov¹¹⁰, L.N. Smirnova¹¹¹, O. Smirnova⁹⁴, J.W. Smith⁵¹, M. Smizanska⁸⁷, K. Smolek¹³⁹, A. Smykiewicz⁸², A.A. Snesarev¹⁰⁸, I.M. Snyder¹²⁸, S. Snyder²⁹, R. Sobie^{173,ae}, A.M. Soffa¹⁶⁸, A. Soffer¹⁵⁸, A. Søgaard⁴⁸, D.A. Soh¹⁵⁵, G. Sokhrannyi⁸⁹, C.A. Solans Sanchez³⁵, M. Solar¹³⁹, E.Yu. Soldatov¹¹⁰, U. Soldevila¹⁷¹, A.A. Solodkov¹²¹, A. Soloshenko⁷⁷, O.V. Solovyev¹²¹, V. Solovyev¹³⁵, P. Sommer¹⁴⁶, H. Son¹⁶⁷, W. Song¹⁴¹, W.Y. Song^{165b}, A. Sopczak¹³⁹, F. Sopkova^{28b}, C.L. Sotiropoulou^{69a,69b}, S. Sottocornola^{68a,68b}, R. Soualah^{64a,64c,j}, A.M. Soukharev^{120b,120a}, D. South⁴⁴, B.C. Sowden⁹¹, S. Spagnolo^{65a,65b}, M. Spalla¹¹³, M. Spangenberg¹⁷⁵, F. Spanò⁹¹, D. Sperlich¹⁹, T.M. Spieker^{59a}, R. Spighi^{23b}, G. Spigo³⁵, L.A. Spiller¹⁰², D.P. Spiteri⁵⁵, M. Spousta¹⁴⁰, A. Stabile^{66a,66b}, R. Stamen^{59a}, S. Stamm¹⁹, E. Stanecka⁸², R.W. Stanek⁶, C. Stanescu^{72a}, B. Stanislaus¹³², M.M. Stanitzki⁴⁴, B. Stapf¹¹⁸, S. Stapnes¹³¹, E.A. Starchenko¹²¹, G.H. Stark³⁶, J. Stark⁵⁶, S.H Stark³⁹, P. Staroba¹³⁸, P. Starovoitov^{59a}, S. Stärz³⁵, R. Staszewski⁸², M. Stegler⁴⁴, P. Steinberg²⁹, B. Stelzer¹⁴⁹, H.J. Stelzer³⁵, O. Stelzer-Chilton^{165a}, H. Stenzel⁵⁴, T.J. Stevenson⁹⁰, G.A. Stewart³⁵, M.C. Stockton³⁵, G. Stoicea^{27b}, P. Stolte⁵¹, S. Stonjek¹¹³, A. Straessner⁴⁶, J. Strandberg¹⁵¹, S. Strandberg^{43a,43b}, M. Strauss¹²⁵, P. Strizenec^{28b}, R. Ströhmer¹⁷⁴, D.M. Strom¹²⁸, R. Stroynowski⁴¹, A. Strubig⁴⁸, S.A. Stucci²⁹, B. Stugu¹⁷, J. Stupak¹²⁵, N.A. Styles⁴⁴, D. Su¹⁵⁰, J. Su¹³⁶, S. Suchek^{59a}, Y. Sugaya¹³⁰, M. Suk¹³⁹, V.V. Sulin¹⁰⁸, M.J. Sullivan⁸⁸, D.M.S. Sultan⁵², S. Sultansoy^{4c}, T. Sumida⁸³, S. Sun¹⁰³, X. Sun³, K. Suruliz¹⁵³, C.J.E. Suster¹⁵⁴, M.R. Sutton¹⁵³, S. Suzuki⁷⁹, M. Svatos¹³⁸, M. Swiatlowski³⁶, S.P. Swift², A. Sydorenko⁹⁷, I. Sykora^{28a}, T. Sykora¹⁴⁰, D. Ta⁹⁷, K. Tackmann^{44,ab}, J. Taenzer¹⁵⁸, A. Taffard¹⁶⁸, R. Tafirout^{165a}, E. Tahirovic⁹⁰, N. Taiblum¹⁵⁸, H. Takai²⁹, R. Takashima⁸⁴, E.H. Takasugi¹¹³, K. Takeda⁸⁰, T. Takeshita¹⁴⁷, Y. Takubo⁷⁹, M. Talby⁹⁹, A.A. Talyshев^{120b,120a}, J. Tanaka¹⁶⁰, M. Tanaka¹⁶², R. Tanaka¹²⁹, B.B. Tannenwald¹²³, S. Tapia Araya^{144b}, S. Tapprogge⁹⁷, A. Tarek Abouelfadl Mohamed¹³³, S. Tarem¹⁵⁷, G. Tarna^{27b,e}, G.F. Tartarelli^{66a}, P. Tas¹⁴⁰, M. Tasevsky¹³⁸, T. Tashiro⁸³, E. Tassi^{40b,40a}, A. Tavares Delgado^{137a,137b}, Y. Tayalati^{34e}, A.C. Taylor¹¹⁶, A.J. Taylor⁴⁸, G.N. Taylor¹⁰², P.T.E. Taylor¹⁰², W. Taylor^{165b}, A.S. Tee⁸⁷, P. Teixeira-Dias⁹¹, H. Ten Kate³⁵, J.J. Teoh¹¹⁸, S. Terada⁷⁹, K. Terashi¹⁶⁰, J. Terron⁹⁶, S. Terzo¹⁴, M. Testa⁴⁹, R.J. Teuscher^{164,ae}, S.J. Thais¹⁸⁰, T. Theveneaux-Pelzer⁴⁴, F. Thiele³⁹, D.W. Thomas⁹¹, J.P. Thomas²¹, A.S. Thompson⁵⁵, P.D. Thompson²¹, L.A. Thomsen¹⁸⁰, E. Thomson¹³⁴, Y. Tian³⁸, R.E. Ticse Torres⁵¹, V.O. Tikhomirov^{108,ap}, Yu.A. Tikhonov^{120b,120a}, S. Timoshenko¹¹⁰, P. Tipton¹⁸⁰, S. Tisserant⁹⁹, K. Todome¹⁶², S. Todorova-Nova⁵, S. Todt⁴⁶, J. Tojo⁸⁵, S. Tokár^{28a}, K. Tokushuku⁷⁹, E. Tolley¹²³, K.G. Tomiwa^{32c}, M. Tomoto¹¹⁵, L. Tompkins^{150,r}, K. Toms¹¹⁶, B. Tong⁵⁷, P. Tornambe⁵⁰, E. Torrence¹²⁸, H. Torres⁴⁶, E. Torró Pastor¹⁴⁵, C. Toscirci¹³², J. Toth^{99,ad}, F. Touchard⁹⁹, D.R. Tovey¹⁴⁶, C.J. Treado¹²², T. Trefzger¹⁷⁴, F. Tresoldi¹⁵³, A. Tricoli²⁹, I.M. Trigger^{165a}, S. Trincaz-Duvoid¹³³, M.F. Tripiana¹⁴, W. Trischuk¹⁶⁴, B. Trocmé⁵⁶, A. Trofymov¹²⁹, C. Troncon^{66a}, M. Trovatelli¹⁷³, F. Trovato¹⁵³, L. Truong^{32b}, M. Trzebinski⁸², A. Trzupek⁸², F. Tsai⁴⁴, J.C.-L. Tseng¹³², P.V. Tsiareshka¹⁰⁵, A. Tsirigotis¹⁵⁹, N. Tsirintanis⁹, V. Tsiskaridze¹⁵², E.G. Tskhadadze^{156a}, I.I. Tsukerman¹⁰⁹, V. Tsulaia¹⁸, S. Tsuno⁷⁹, D. Tsybychev^{152,163}, Y. Tu^{61b}, A. Tudorache^{27b}, V. Tudorache^{27b}, T.T. Tulbure^{27a}, A.N. Tuna⁵⁷, S. Turchikhin⁷⁷, D. Turgeman¹⁷⁷, I. Turk Cakir^{4b,v}, R. Turra^{66a}, P.M. Tuts³⁸, E. Tzovara⁹⁷, G. Ucchielli^{23b,23a}, I. Ueda⁷⁹, M. Ughetto^{43a,43b}, F. Ukegawa¹⁶⁶, G. Unal³⁵, A. Undrus²⁹, G. Unel¹⁶⁸, F.C. Ungaro¹⁰², Y. Unno⁷⁹, K. Uno¹⁶⁰, J. Urban^{28b}, P. Urquijo¹⁰², P. Urrejola⁹⁷, G. Usai⁸, J. Usui⁷⁹, L. Vacavant⁹⁹, V. Vacek¹³⁹, B. Vachon¹⁰¹, K.O.H. Vadla¹³¹, A. Vaidya⁹², C. Valderanis¹¹², E. Valdes Santurio^{43a,43b}, M. Valente⁵², S. Valentini^{23b,23a}, A. Valero¹⁷¹, L. Valéry⁴⁴, R.A. Vallance²¹, A. Vallier⁵, J.A. Valls Ferrer¹⁷¹, T.R. Van Daalen¹⁴, H. Van der Graaf¹¹⁸, P. Van Gemmeren⁶,

J. Van Nieuwkoop¹⁴⁹, I. Van Vulpen¹¹⁸, M. Vanadja^{71a,71b}, W. Vandelli³⁵, A. Vaniachine¹⁶³, P. Vankov¹¹⁸, R. Vari^{70a}, E.W. Varnes⁷, C. Varni^{53b,53a}, T. Varol⁴¹, D. Varouchas¹²⁹, K.E. Varvell¹⁵⁴, G.A. Vasquez^{144b}, J.G. Vasquez¹⁸⁰, F. Vazeille³⁷, D. Vazquez Furelos¹⁴, T. Vazquez Schroeder³⁵, J. Veatch⁵¹, V. Vecchio^{72a,72b}, L.M. Veloce¹⁶⁴, F. Veloso^{137a,137c}, S. Veneziano^{70a}, A. Ventura^{65a,65b}, M. Venturi¹⁷³, N. Venturi³⁵, V. Vercesi^{68a}, M. Verducci^{72a,72b}, C.M. Vergel Infante⁷⁶, C. Vergis²⁴, W. Verkerke¹¹⁸, A.T. Vermeulen¹¹⁸, J.C. Vermeulen¹¹⁸, M.C. Vetterli^{149,av}, N. Viaux Maira^{144b}, M. Vicente Barreto Pinto⁵², I. Vichou^{170,*}, T. Vickey¹⁴⁶, O.E. Vickey Boeriu¹⁴⁶, G.H.A. Viehhauser¹³², S. Viel¹⁸, L. Vigani¹³², M. Villa^{23b,23a}, M. Villapiana Perez^{66a,66b}, E. Vilucchi⁴⁹, M.G. Vinchter³³, V.B. Vinogradov⁷⁷, A. Vishwakarma⁴⁴, C. Vittori^{23b,23a}, I. Vivarelli¹⁵³, S. Vlachos¹⁰, M. Vogel¹⁷⁹, P. Vokac¹³⁹, G. Volpi¹⁴, S.E. von Buddenbrock^{32c}, E. Von Toerne²⁴, V. Vorobel¹⁴⁰, K. Vorobev¹¹⁰, M. Vos¹⁷¹, J.H. Vossebeld⁸⁸, N. Vranjes¹⁶, M. Vranjes Milosavljevic¹⁶, V. Vrba¹³⁹, M. Vreeswijk¹¹⁸, T. Šfiligoj⁸⁹, R. Vuillermet³⁵, I. Vukotic³⁶, T. Ženiš^{28a}, L. Živković¹⁶, P. Wagner²⁴, W. Wagner¹⁷⁹, J. Wagner-Kuhr¹¹², H. Wahlberg⁸⁶, S. Wahrmund⁴⁶, K. Wakamiya⁸⁰, V.M. Walbrecht¹¹³, J. Walder⁸⁷, R. Walker¹¹², S.D. Walker⁹¹, W. Walkowiak¹⁴⁸, V. Wallangen^{43a,43b}, A.M. Wang⁵⁷, C. Wang^{58b,e}, F. Wang¹⁷⁸, H. Wang¹⁸, H. Wang³, J. Wang¹⁵⁴, J. Wang^{59b}, P. Wang⁴¹, Q. Wang¹²⁵, R.-J. Wang¹³³, R. Wang^{58a}, R. Wang⁶, S.M. Wang¹⁵⁵, W.T. Wang^{58a}, W. Wang^{15c,af}, W.X. Wang^{58a,af}, Y. Wang^{58a,am}, Z. Wang^{58c}, C. Wanotayaroj⁴⁴, A. Warburton¹⁰¹, C.P. Ward³¹, D.R. Wardrope⁹², A. Washbrook⁴⁸, P.M. Watkins²¹, A.T. Watson²¹, M.F. Watson²¹, G. Watts¹⁴⁵, S. Watts⁹⁸, B.M. Waugh⁹², A.F. Webb¹¹, S. Webb⁹⁷, C. Weber¹⁸⁰, M.S. Weber²⁰, S.A. Weber³³, S.M. Weber^{59a}, A.R. Weidberg¹³², B. Weinert⁶³, J. Weingarten⁴⁵, M. Weirich⁹⁷, C. Weiser⁵⁰, P.S. Wells³⁵, T. Wenaus²⁹, T. Wengler³⁵, S. Wenig³⁵, N. Wermes²⁴, M.D. Werner⁷⁶, P. Werner³⁵, M. Wessels^{59a}, T.D. Weston²⁰, K. Whalen¹²⁸, N.L. Whallon¹⁴⁵, A.M. Wharton⁸⁷, A.S. White¹⁰³, A. White⁸, M.J. White¹, R. White^{144b}, D. Whiteson¹⁶⁸, B.W. Whitmore⁸⁷, F.J. Wickens¹⁴¹, W. Wiedenmann¹⁷⁸, M. Wielers¹⁴¹, C. Wiglesworth³⁹, L.A.M. Wiik-Fuchs⁵⁰, F. Wilk⁹⁸, H.G. Wilkens³⁵, L.J. Wilkins⁹¹, H.H. Williams¹³⁴, S. Williams³¹, C. Willis¹⁰⁴, S. Willocq¹⁰⁰, J.A. Wilson²¹, I. Wingerter-Seez⁵, E. Winkels¹⁵³, F. Winklmeier¹²⁸, O.J. Winston¹⁵³, B.T. Winter⁵⁰, M. Wittgen¹⁵⁰, M. Wobisch⁹³, A. Wolf⁹⁷, T.M.H. Wolf¹¹⁸, R. Wolff⁹⁹, M.W. Wolter⁸², H. Wolters^{137a,137c}, V.W.S. Wong¹⁷², N.L. Woods¹⁴³, S.D. Worm²¹, B.K. Wosiek⁸², K.W. Woźniak⁸², K. Wraight⁵⁵, M. Wu³⁶, S.L. Wu¹⁷⁸, X. Wu⁵², Y. Wu^{58a}, T.R. Wyatt⁹⁸, B.M. Wynne⁴⁸, S. Xella³⁹, Z. Xi¹⁰³, L. Xia¹⁷⁵, D. Xu^{15a}, H. Xu^{58a,e}, L. Xu²⁹, T. Xu¹⁴², W. Xu¹⁰³, B. Yabsley¹⁵⁴, S. Yacoob^{32a}, K. Yajima¹³⁰, D.P. Yallup⁹², D. Yamaguchi¹⁶², Y. Yamaguchi¹⁶², A. Yamamoto⁷⁹, T. Yamanaka¹⁶⁰, F. Yamane⁸⁰, M. Yamatani¹⁶⁰, T. Yamazaki¹⁶⁰, Y. Yamazaki⁸⁰, Z. Yan²⁵, H.J. Yang^{58c,58d}, H.T. Yang¹⁸, S. Yang⁷⁵, Y. Yang¹⁶⁰, Z. Yang¹⁷, W-M. Yao¹⁸, Y.C. Yap⁴⁴, Y. Yasu⁷⁹, E. Yatsenko^{58c,58d}, J. Ye⁴¹, S. Ye²⁹, I. Yeletskikh⁷⁷, E. Yigitbasi²⁵, E. Yildirim⁹⁷, K. Yorita¹⁷⁶, K. Yoshihara¹³⁴, C.J.S. Young³⁵, C. Young¹⁵⁰, J. Yu⁸, J. Yu⁷⁶, X. Yue^{59a}, S.P.Y. Yuen²⁴, B. Zabinski⁸², G. Zacharis¹⁰, E. Zaffaroni⁵², R. Zaidan¹⁴, A.M. Zaitsev^{121,ao}, T. Zakareishvili^{156b}, N. Zakharchuk³³, J. Zalieckas¹⁷, S. Zambito⁵⁷, D. Zanzi³⁵, D.R. Zaripovas⁵⁵, S.V. Zeißner⁴⁵, C. Zeitnitz¹⁷⁹, G. Zemaitytė¹³², J.C. Zeng¹⁷⁰, Q. Zeng¹⁵⁰, O. Zenin¹²¹, D. Zerwas¹²⁹, M. Zgubič¹³², D.F. Zhang^{58b}, D. Zhang¹⁰³, F. Zhang¹⁷⁸, G. Zhang^{58a}, H. Zhang^{15c}, J. Zhang⁶, L. Zhang^{15c}, L. Zhang^{58a}, M. Zhang¹⁷⁰, P. Zhang^{15c}, R. Zhang^{58a}, R. Zhang²⁴, X. Zhang^{58b}, Y. Zhang^{15d}, Z. Zhang¹²⁹, P. Zhao⁴⁷, Y. Zhao^{58b,129,ak}, Z. Zhao^{58a}, A. Zhemchugov⁷⁷, Z. Zheng¹⁰³, D. Zhong¹⁷⁰, B. Zhou¹⁰³, C. Zhou¹⁷⁸, L. Zhou⁴¹, M.S. Zhou^{15d}, M. Zhou¹⁵², N. Zhou^{58c}, Y. Zhou⁷, C.G. Zhu^{58b}, H.L. Zhu^{58a}, H. Zhu^{15a}, J. Zhu¹⁰³, Y. Zhu^{58a}, X. Zhuang^{15a}, K. Zhukov¹⁰⁸, V. Zhulanov^{120b,120a}, A. Zibell¹⁷⁴, D. Ziernska⁶³, N.I. Zimine⁷⁷, S. Zimmermann⁵⁰, Z. Zinonos¹¹³, M. Zinser⁹⁷, M. Ziolkowski¹⁴⁸, G. Zobernig¹⁷⁸, A. Zoccoli^{23b,23a}, K. Zoch⁵¹, T.G. Zorbas¹⁴⁶, R. Zou³⁶, M. Zur Nedden¹⁹, L. Zwalinski³⁵.

¹Department of Physics, University of Adelaide, Adelaide; Australia.

²Physics Department, SUNY Albany, Albany NY; United States of America.

³Department of Physics, University of Alberta, Edmonton AB; Canada.

- ^{4(a)}Department of Physics, Ankara University, Ankara; ^(b)Istanbul Aydin University, Istanbul; ^(c)Division of Physics, TOBB University of Economics and Technology, Ankara; Turkey.
- ⁵LAPP, Université Grenoble Alpes, Université Savoie Mont Blanc, CNRS/IN2P3, Annecy; France.
- ⁶High Energy Physics Division, Argonne National Laboratory, Argonne IL; United States of America.
- ⁷Department of Physics, University of Arizona, Tucson AZ; United States of America.
- ⁸Department of Physics, University of Texas at Arlington, Arlington TX; United States of America.
- ⁹Physics Department, National and Kapodistrian University of Athens, Athens; Greece.
- ¹⁰Physics Department, National Technical University of Athens, Zografou; Greece.
- ¹¹Department of Physics, University of Texas at Austin, Austin TX; United States of America.
- ^{12(a)}Bahcesehir University, Faculty of Engineering and Natural Sciences, Istanbul; ^(b)Istanbul Bilgi University, Faculty of Engineering and Natural Sciences, Istanbul; ^(c)Department of Physics, Bogazici University, Istanbul; ^(d)Department of Physics Engineering, Gaziantep University, Gaziantep; Turkey.
- ¹³Institute of Physics, Azerbaijan Academy of Sciences, Baku; Azerbaijan.
- ¹⁴Institut de Física d'Altes Energies (IFAE), Barcelona Institute of Science and Technology, Barcelona; Spain.
- ^{15(a)}Institute of High Energy Physics, Chinese Academy of Sciences, Beijing; ^(b)Physics Department, Tsinghua University, Beijing; ^(c)Department of Physics, Nanjing University, Nanjing; ^(d)University of Chinese Academy of Science (UCAS), Beijing; China.
- ¹⁶Institute of Physics, University of Belgrade, Belgrade; Serbia.
- ¹⁷Department for Physics and Technology, University of Bergen, Bergen; Norway.
- ¹⁸Physics Division, Lawrence Berkeley National Laboratory and University of California, Berkeley CA; United States of America.
- ¹⁹Institut für Physik, Humboldt Universität zu Berlin, Berlin; Germany.
- ²⁰Albert Einstein Center for Fundamental Physics and Laboratory for High Energy Physics, University of Bern, Bern; Switzerland.
- ²¹School of Physics and Astronomy, University of Birmingham, Birmingham; United Kingdom.
- ²²Centro de Investigaciones, Universidad Antonio Nariño, Bogota; Colombia.
- ^{23(a)}Dipartimento di Fisica e Astronomia, Università di Bologna, Bologna; ^(b)INFN Sezione di Bologna; Italy.
- ²⁴Physikalischs Institut, Universität Bonn, Bonn; Germany.
- ²⁵Department of Physics, Boston University, Boston MA; United States of America.
- ²⁶Department of Physics, Brandeis University, Waltham MA; United States of America.
- ^{27(a)}Transilvania University of Brasov, Brasov; ^(b)Horia Hulubei National Institute of Physics and Nuclear Engineering, Bucharest; ^(c)Department of Physics, Alexandru Ioan Cuza University of Iasi, Iasi; ^(d)National Institute for Research and Development of Isotopic and Molecular Technologies, Physics Department, Cluj-Napoca; ^(e)University Politehnica Bucharest, Bucharest; ^(f)West University in Timisoara, Timisoara; Romania.
- ^{28(a)}Faculty of Mathematics, Physics and Informatics, Comenius University, Bratislava; ^(b)Department of Subnuclear Physics, Institute of Experimental Physics of the Slovak Academy of Sciences, Kosice; Slovak Republic.
- ²⁹Physics Department, Brookhaven National Laboratory, Upton NY; United States of America.
- ³⁰Departamento de Física, Universidad de Buenos Aires, Buenos Aires; Argentina.
- ³¹Cavendish Laboratory, University of Cambridge, Cambridge; United Kingdom.
- ^{32(a)}Department of Physics, University of Cape Town, Cape Town; ^(b)Department of Mechanical Engineering Science, University of Johannesburg, Johannesburg; ^(c)School of Physics, University of the Witwatersrand, Johannesburg; South Africa.
- ³³Department of Physics, Carleton University, Ottawa ON; Canada.

- ^{34(a)}Faculté des Sciences Ain Chock, Réseau Universitaire de Physique des Hautes Energies - Université Hassan II, Casablanca; ^(b)Centre National de l'Energie des Sciences Techniques Nucleaires (CNESTEN), Rabat; ^(c)Faculté des Sciences Semlalia, Université Cadi Ayyad, LPHEA-Marrakech; ^(d)Faculté des Sciences, Université Mohamed Premier and LPTPM, Oujda; ^(e)Faculté des sciences, Université Mohammed V, Rabat; Morocco.
- ³⁵CERN, Geneva; Switzerland.
- ³⁶Enrico Fermi Institute, University of Chicago, Chicago IL; United States of America.
- ³⁷LPC, Université Clermont Auvergne, CNRS/IN2P3, Clermont-Ferrand; France.
- ³⁸Nevis Laboratory, Columbia University, Irvington NY; United States of America.
- ³⁹Niels Bohr Institute, University of Copenhagen, Copenhagen; Denmark.
- ^{40(a)}Dipartimento di Fisica, Università della Calabria, Rende; ^(b)INFN Gruppo Collegato di Cosenza, Laboratori Nazionali di Frascati; Italy.
- ⁴¹Physics Department, Southern Methodist University, Dallas TX; United States of America.
- ⁴²Physics Department, University of Texas at Dallas, Richardson TX; United States of America.
- ^{43(a)}Department of Physics, Stockholm University; ^(b)Oskar Klein Centre, Stockholm; Sweden.
- ⁴⁴Deutsches Elektronen-Synchrotron DESY, Hamburg and Zeuthen; Germany.
- ⁴⁵Lehrstuhl für Experimentelle Physik IV, Technische Universität Dortmund, Dortmund; Germany.
- ⁴⁶Institut für Kern- und Teilchenphysik, Technische Universität Dresden, Dresden; Germany.
- ⁴⁷Department of Physics, Duke University, Durham NC; United States of America.
- ⁴⁸SUPA - School of Physics and Astronomy, University of Edinburgh, Edinburgh; United Kingdom.
- ⁴⁹INFN e Laboratori Nazionali di Frascati, Frascati; Italy.
- ⁵⁰Physikalisch Institut, Albert-Ludwigs-Universität Freiburg, Freiburg; Germany.
- ⁵¹II. Physikalisch Institut, Georg-August-Universität Göttingen, Göttingen; Germany.
- ⁵²Département de Physique Nucléaire et Corpusculaire, Université de Genève, Genève; Switzerland.
- ^{53(a)}Dipartimento di Fisica, Università di Genova, Genova; ^(b)INFN Sezione di Genova; Italy.
- ⁵⁴II. Physikalisch Institut, Justus-Liebig-Universität Giessen, Giessen; Germany.
- ⁵⁵SUPA - School of Physics and Astronomy, University of Glasgow, Glasgow; United Kingdom.
- ⁵⁶LPSC, Université Grenoble Alpes, CNRS/IN2P3, Grenoble INP, Grenoble; France.
- ⁵⁷Laboratory for Particle Physics and Cosmology, Harvard University, Cambridge MA; United States of America.
- ^{58(a)}Department of Modern Physics and State Key Laboratory of Particle Detection and Electronics, University of Science and Technology of China, Hefei; ^(b)Institute of Frontier and Interdisciplinary Science and Key Laboratory of Particle Physics and Particle Irradiation (MOE), Shandong University, Qingdao; ^(c)School of Physics and Astronomy, Shanghai Jiao Tong University, KLPPAC-MoE, SKLPPC, Shanghai; ^(d)Tsung-Dao Lee Institute, Shanghai; China.
- ^{59(a)}Kirchhoff-Institut für Physik, Ruprecht-Karls-Universität Heidelberg, Heidelberg; ^(b)Physikalisch Institut, Ruprecht-Karls-Universität Heidelberg, Heidelberg; Germany.
- ⁶⁰Faculty of Applied Information Science, Hiroshima Institute of Technology, Hiroshima; Japan.
- ^{61(a)}Department of Physics, Chinese University of Hong Kong, Shatin, N.T., Hong Kong; ^(b)Department of Physics, University of Hong Kong, Hong Kong; ^(c)Department of Physics and Institute for Advanced Study, Hong Kong University of Science and Technology, Clear Water Bay, Kowloon, Hong Kong; China.
- ⁶²Department of Physics, National Tsing Hua University, Hsinchu; Taiwan.
- ⁶³Department of Physics, Indiana University, Bloomington IN; United States of America.
- ^{64(a)}INFN Gruppo Collegato di Udine, Sezione di Trieste, Udine; ^(b)ICTP, Trieste; ^(c)Dipartimento di Chimica, Fisica e Ambiente, Università di Udine, Udine; Italy.
- ^{65(a)}INFN Sezione di Lecce; ^(b)Dipartimento di Matematica e Fisica, Università del Salento, Lecce; Italy.
- ^{66(a)}INFN Sezione di Milano; ^(b)Dipartimento di Fisica, Università di Milano, Milano; Italy.

- ^{67(a)}INFN Sezione di Napoli;^(b)Dipartimento di Fisica, Università di Napoli, Napoli; Italy.
^{68(a)}INFN Sezione di Pavia;^(b)Dipartimento di Fisica, Università di Pavia, Pavia; Italy.
^{69(a)}INFN Sezione di Pisa;^(b)Dipartimento di Fisica E. Fermi, Università di Pisa, Pisa; Italy.
^{70(a)}INFN Sezione di Roma;^(b)Dipartimento di Fisica, Sapienza Università di Roma, Roma; Italy.
^{71(a)}INFN Sezione di Roma Tor Vergata;^(b)Dipartimento di Fisica, Università di Roma Tor Vergata, Roma; Italy.
^{72(a)}INFN Sezione di Roma Tre;^(b)Dipartimento di Matematica e Fisica, Università Roma Tre, Roma; Italy.
^{73(a)}INFN-TIFPA;^(b)Università degli Studi di Trento, Trento; Italy.
⁷⁴Institut für Astro- und Teilchenphysik, Leopold-Franzens-Universität, Innsbruck; Austria.
⁷⁵University of Iowa, Iowa City IA; United States of America.
⁷⁶Department of Physics and Astronomy, Iowa State University, Ames IA; United States of America.
⁷⁷Joint Institute for Nuclear Research, Dubna; Russia.
^{78(a)}Departamento de Engenharia Elétrica, Universidade Federal de Juiz de Fora (UFJF), Juiz de Fora;^(b)Universidade Federal do Rio De Janeiro COPPE/EE/IF, Rio de Janeiro;^(c)Universidade Federal de São João del Rei (UFSJ), São João del Rei;^(d)Instituto de Física, Universidade de São Paulo, São Paulo; Brazil.
⁷⁹KEK, High Energy Accelerator Research Organization, Tsukuba; Japan.
⁸⁰Graduate School of Science, Kobe University, Kobe; Japan.
^{81(a)}AGH University of Science and Technology, Faculty of Physics and Applied Computer Science, Krakow;^(b)Marian Smoluchowski Institute of Physics, Jagiellonian University, Krakow; Poland.
⁸²Institute of Nuclear Physics Polish Academy of Sciences, Krakow; Poland.
⁸³Faculty of Science, Kyoto University, Kyoto; Japan.
⁸⁴Kyoto University of Education, Kyoto; Japan.
⁸⁵Research Center for Advanced Particle Physics and Department of Physics, Kyushu University, Fukuoka ; Japan.
⁸⁶Instituto de Física La Plata, Universidad Nacional de La Plata and CONICET, La Plata; Argentina.
⁸⁷Physics Department, Lancaster University, Lancaster; United Kingdom.
⁸⁸Oliver Lodge Laboratory, University of Liverpool, Liverpool; United Kingdom.
⁸⁹Department of Experimental Particle Physics, Jožef Stefan Institute and Department of Physics, University of Ljubljana, Ljubljana; Slovenia.
⁹⁰School of Physics and Astronomy, Queen Mary University of London, London; United Kingdom.
⁹¹Department of Physics, Royal Holloway University of London, Egham; United Kingdom.
⁹²Department of Physics and Astronomy, University College London, London; United Kingdom.
⁹³Louisiana Tech University, Ruston LA; United States of America.
⁹⁴Fysiska institutionen, Lunds universitet, Lund; Sweden.
⁹⁵Centre de Calcul de l’Institut National de Physique Nucléaire et de Physique des Particules (IN2P3), Villeurbanne; France.
⁹⁶Departamento de Física Teórica C-15 and CIAFF, Universidad Autónoma de Madrid, Madrid; Spain.
⁹⁷Institut für Physik, Universität Mainz, Mainz; Germany.
⁹⁸School of Physics and Astronomy, University of Manchester, Manchester; United Kingdom.
⁹⁹CPPM, Aix-Marseille Université, CNRS/IN2P3, Marseille; France.
¹⁰⁰Department of Physics, University of Massachusetts, Amherst MA; United States of America.
¹⁰¹Department of Physics, McGill University, Montreal QC; Canada.
¹⁰²School of Physics, University of Melbourne, Victoria; Australia.
¹⁰³Department of Physics, University of Michigan, Ann Arbor MI; United States of America.
¹⁰⁴Department of Physics and Astronomy, Michigan State University, East Lansing MI; United States of America.

- ¹⁰⁵B.I. Stepanov Institute of Physics, National Academy of Sciences of Belarus, Minsk; Belarus.
- ¹⁰⁶Research Institute for Nuclear Problems of Byelorussian State University, Minsk; Belarus.
- ¹⁰⁷Group of Particle Physics, University of Montreal, Montreal QC; Canada.
- ¹⁰⁸P.N. Lebedev Physical Institute of the Russian Academy of Sciences, Moscow; Russia.
- ¹⁰⁹Institute for Theoretical and Experimental Physics (ITEP), Moscow; Russia.
- ¹¹⁰National Research Nuclear University MEPhI, Moscow; Russia.
- ¹¹¹D.V. Skobeltsyn Institute of Nuclear Physics, M.V. Lomonosov Moscow State University, Moscow; Russia.
- ¹¹²Fakultät für Physik, Ludwig-Maximilians-Universität München, München; Germany.
- ¹¹³Max-Planck-Institut für Physik (Werner-Heisenberg-Institut), München; Germany.
- ¹¹⁴Nagasaki Institute of Applied Science, Nagasaki; Japan.
- ¹¹⁵Graduate School of Science and Kobayashi-Maskawa Institute, Nagoya University, Nagoya; Japan.
- ¹¹⁶Department of Physics and Astronomy, University of New Mexico, Albuquerque NM; United States of America.
- ¹¹⁷Institute for Mathematics, Astrophysics and Particle Physics, Radboud University Nijmegen/Nikhef, Nijmegen; Netherlands.
- ¹¹⁸Nikhef National Institute for Subatomic Physics and University of Amsterdam, Amsterdam; Netherlands.
- ¹¹⁹Department of Physics, Northern Illinois University, DeKalb IL; United States of America.
- ¹²⁰^(a)Budker Institute of Nuclear Physics and NSU, SB RAS, Novosibirsk;^(b)Novosibirsk State University Novosibirsk; Russia.
- ¹²¹Institute for High Energy Physics of the National Research Centre Kurchatov Institute, Protvino; Russia.
- ¹²²Department of Physics, New York University, New York NY; United States of America.
- ¹²³Ohio State University, Columbus OH; United States of America.
- ¹²⁴Faculty of Science, Okayama University, Okayama; Japan.
- ¹²⁵Homer L. Dodge Department of Physics and Astronomy, University of Oklahoma, Norman OK; United States of America.
- ¹²⁶Department of Physics, Oklahoma State University, Stillwater OK; United States of America.
- ¹²⁷Palacký University, RCPTM, Joint Laboratory of Optics, Olomouc; Czech Republic.
- ¹²⁸Center for High Energy Physics, University of Oregon, Eugene OR; United States of America.
- ¹²⁹LAL, Université Paris-Sud, CNRS/IN2P3, Université Paris-Saclay, Orsay; France.
- ¹³⁰Graduate School of Science, Osaka University, Osaka; Japan.
- ¹³¹Department of Physics, University of Oslo, Oslo; Norway.
- ¹³²Department of Physics, Oxford University, Oxford; United Kingdom.
- ¹³³LPNHE, Sorbonne Université, Paris Diderot Sorbonne Paris Cité, CNRS/IN2P3, Paris; France.
- ¹³⁴Department of Physics, University of Pennsylvania, Philadelphia PA; United States of America.
- ¹³⁵Konstantinov Nuclear Physics Institute of National Research Centre "Kurchatov Institute", PNPI, St. Petersburg; Russia.
- ¹³⁶Department of Physics and Astronomy, University of Pittsburgh, Pittsburgh PA; United States of America.
- ¹³⁷^(a)Laboratório de Instrumentação e Física Experimental de Partículas - LIP;^(b)Departamento de Física, Faculdade de Ciências, Universidade de Lisboa, Lisboa;^(c)Departamento de Física, Universidade de Coimbra, Coimbra;^(d)Centro de Física Nuclear da Universidade de Lisboa, Lisboa;^(e)Departamento de Física, Universidade do Minho, Braga;^(f)Departamento de Física Teorica y del Cosmos, Universidad de Granada, Granada (Spain);^(g)Dep Física and CEFITEC of Faculdade de Ciências e Tecnologia, Universidade Nova de Lisboa, Caparica; Portugal.
- ¹³⁸Institute of Physics, Academy of Sciences of the Czech Republic, Prague; Czech Republic.

- ¹³⁹Czech Technical University in Prague, Prague; Czech Republic.
- ¹⁴⁰Charles University, Faculty of Mathematics and Physics, Prague; Czech Republic.
- ¹⁴¹Particle Physics Department, Rutherford Appleton Laboratory, Didcot; United Kingdom.
- ¹⁴²IRFU, CEA, Université Paris-Saclay, Gif-sur-Yvette; France.
- ¹⁴³Santa Cruz Institute for Particle Physics, University of California Santa Cruz, Santa Cruz CA; United States of America.
- ¹⁴⁴(*a*)Departamento de Física, Pontificia Universidad Católica de Chile, Santiago; (*b*)Departamento de Física, Universidad Técnica Federico Santa María, Valparaíso; Chile.
- ¹⁴⁵Department of Physics, University of Washington, Seattle WA; United States of America.
- ¹⁴⁶Department of Physics and Astronomy, University of Sheffield, Sheffield; United Kingdom.
- ¹⁴⁷Department of Physics, Shinshu University, Nagano; Japan.
- ¹⁴⁸Department Physik, Universität Siegen, Siegen; Germany.
- ¹⁴⁹Department of Physics, Simon Fraser University, Burnaby BC; Canada.
- ¹⁵⁰SLAC National Accelerator Laboratory, Stanford CA; United States of America.
- ¹⁵¹Physics Department, Royal Institute of Technology, Stockholm; Sweden.
- ¹⁵²Departments of Physics and Astronomy, Stony Brook University, Stony Brook NY; United States of America.
- ¹⁵³Department of Physics and Astronomy, University of Sussex, Brighton; United Kingdom.
- ¹⁵⁴School of Physics, University of Sydney, Sydney; Australia.
- ¹⁵⁵Institute of Physics, Academia Sinica, Taipei; Taiwan.
- ¹⁵⁶(*a*)E. Andronikashvili Institute of Physics, Iv. Javakhishvili Tbilisi State University, Tbilisi; (*b*)High Energy Physics Institute, Tbilisi State University, Tbilisi; Georgia.
- ¹⁵⁷Department of Physics, Technion, Israel Institute of Technology, Haifa; Israel.
- ¹⁵⁸Raymond and Beverly Sackler School of Physics and Astronomy, Tel Aviv University, Tel Aviv; Israel.
- ¹⁵⁹Department of Physics, Aristotle University of Thessaloniki, Thessaloniki; Greece.
- ¹⁶⁰International Center for Elementary Particle Physics and Department of Physics, University of Tokyo, Tokyo; Japan.
- ¹⁶¹Graduate School of Science and Technology, Tokyo Metropolitan University, Tokyo; Japan.
- ¹⁶²Department of Physics, Tokyo Institute of Technology, Tokyo; Japan.
- ¹⁶³Tomsk State University, Tomsk; Russia.
- ¹⁶⁴Department of Physics, University of Toronto, Toronto ON; Canada.
- ¹⁶⁵(*a*)TRIUMF, Vancouver BC; (*b*)Department of Physics and Astronomy, York University, Toronto ON; Canada.
- ¹⁶⁶Division of Physics and Tomonaga Center for the History of the Universe, Faculty of Pure and Applied Sciences, University of Tsukuba, Tsukuba; Japan.
- ¹⁶⁷Department of Physics and Astronomy, Tufts University, Medford MA; United States of America.
- ¹⁶⁸Department of Physics and Astronomy, University of California Irvine, Irvine CA; United States of America.
- ¹⁶⁹Department of Physics and Astronomy, University of Uppsala, Uppsala; Sweden.
- ¹⁷⁰Department of Physics, University of Illinois, Urbana IL; United States of America.
- ¹⁷¹Instituto de Física Corpuscular (IFIC), Centro Mixto Universidad de Valencia - CSIC, Valencia; Spain.
- ¹⁷²Department of Physics, University of British Columbia, Vancouver BC; Canada.
- ¹⁷³Department of Physics and Astronomy, University of Victoria, Victoria BC; Canada.
- ¹⁷⁴Fakultät für Physik und Astronomie, Julius-Maximilians-Universität Würzburg, Würzburg; Germany.
- ¹⁷⁵Department of Physics, University of Warwick, Coventry; United Kingdom.
- ¹⁷⁶Waseda University, Tokyo; Japan.
- ¹⁷⁷Department of Particle Physics, Weizmann Institute of Science, Rehovot; Israel.

- ¹⁷⁸Department of Physics, University of Wisconsin, Madison WI; United States of America.
- ¹⁷⁹Fakultät für Mathematik und Naturwissenschaften, Fachgruppe Physik, Bergische Universität Wuppertal, Wuppertal; Germany.
- ¹⁸⁰Department of Physics, Yale University, New Haven CT; United States of America.
- ¹⁸¹Yerevan Physics Institute, Yerevan; Armenia.
- ^a Also at Borough of Manhattan Community College, City University of New York, NY; United States of America.
- ^b Also at California State University, East Bay; United States of America.
- ^c Also at Centre for High Performance Computing, CSIR Campus, Rosebank, Cape Town; South Africa.
- ^d Also at CERN, Geneva; Switzerland.
- ^e Also at CPPM, Aix-Marseille Université, CNRS/IN2P3, Marseille; France.
- ^f Also at Département de Physique Nucléaire et Corpusculaire, Université de Genève, Genève; Switzerland.
- ^g Also at Departament de Fisica de la Universitat Autonoma de Barcelona, Barcelona; Spain.
- ^h Also at Departamento de Física Teorica y del Cosmos, Universidad de Granada, Granada (Spain); Spain.
- ⁱ Also at Departamento de Física, Instituto Superior Técnico, Universidade de Lisboa, Lisboa; Portugal.
- ^j Also at Department of Applied Physics and Astronomy, University of Sharjah, Sharjah; United Arab Emirates.
- ^k Also at Department of Financial and Management Engineering, University of the Aegean, Chios; Greece.
- ^l Also at Department of Physics and Astronomy, University of Louisville, Louisville, KY; United States of America.
- ^m Also at Department of Physics and Astronomy, University of Sheffield, Sheffield; United Kingdom.
- ⁿ Also at Department of Physics, California State University, Fresno CA; United States of America.
- ^o Also at Department of Physics, California State University, Sacramento CA; United States of America.
- ^p Also at Department of Physics, King's College London, London; United Kingdom.
- ^q Also at Department of Physics, St. Petersburg State Polytechnical University, St. Petersburg; Russia.
- ^r Also at Department of Physics, Stanford University; United States of America.
- ^s Also at Department of Physics, University of Fribourg, Fribourg; Switzerland.
- ^t Also at Department of Physics, University of Michigan, Ann Arbor MI; United States of America.
- ^u Also at Dipartimento di Fisica E. Fermi, Università di Pisa, Pisa; Italy.
- ^v Also at Giresun University, Faculty of Engineering, Giresun; Turkey.
- ^w Also at Graduate School of Science, Osaka University, Osaka; Japan.
- ^x Also at Hellenic Open University, Patras; Greece.
- ^y Also at Horia Hulubei National Institute of Physics and Nuclear Engineering, Bucharest; Romania.
- ^z Also at II. Physikalisch Institut, Georg-August-Universität Göttingen, Göttingen; Germany.
- ^{aa} Also at Institucio Catalana de Recerca i Estudis Avancats, ICREA, Barcelona; Spain.
- ^{ab} Also at Institut für Experimentalphysik, Universität Hamburg, Hamburg; Germany.
- ^{ac} Also at Institute for Mathematics, Astrophysics and Particle Physics, Radboud University Nijmegen/Nikhef, Nijmegen; Netherlands.
- ^{ad} Also at Institute for Particle and Nuclear Physics, Wigner Research Centre for Physics, Budapest; Hungary.
- ^{ae} Also at Institute of Particle Physics (IPP); Canada.
- ^{af} Also at Institute of Physics, Academia Sinica, Taipei; Taiwan.
- ^{ag} Also at Institute of Physics, Azerbaijan Academy of Sciences, Baku; Azerbaijan.
- ^{ah} Also at Institute of Theoretical Physics, Ilia State University, Tbilisi; Georgia.
- ^{ai} Also at Instituto de Física Teórica de la Universidad Autónoma de Madrid; Spain.
- ^{aj} Also at Istanbul University, Dept. of Physics, Istanbul; Turkey.

- ak* Also at LAL, Université Paris-Sud, CNRS/IN2P3, Université Paris-Saclay, Orsay; France.
- al* Also at Louisiana Tech University, Ruston LA; United States of America.
- am* Also at LPNHE, Sorbonne Université, Paris Diderot Sorbonne Paris Cité, CNRS/IN2P3, Paris; France.
- an* Also at Manhattan College, New York NY; United States of America.
- ao* Also at Moscow Institute of Physics and Technology State University, Dolgoprudny; Russia.
- ap* Also at National Research Nuclear University MEPhI, Moscow; Russia.
- aq* Also at Physikalisches Institut, Albert-Ludwigs-Universität Freiburg, Freiburg; Germany.
- ar* Also at School of Physics, Sun Yat-sen University, Guangzhou; China.
- as* Also at The City College of New York, New York NY; United States of America.
- at* Also at The Collaborative Innovation Center of Quantum Matter (CICQM), Beijing; China.
- au* Also at Tomsk State University, Tomsk, and Moscow Institute of Physics and Technology State University, Dolgoprudny; Russia.
- av* Also at TRIUMF, Vancouver BC; Canada.
- aw* Also at Universita di Napoli Parthenope, Napoli; Italy.
- * Deceased